THE INVESTIGATION OF TETHERED SATELLITE SYSTEM DYNAMICS

Contract NAS8-36160

Quarterly Report #7

For the period 15 February 1986 through 14 May 1986

Principal Investigator

Dr. Enrico C. Lorenzini

June 1986

Prepared for
National Aeronautics and Space Administration
Marshall Space Flight Center, Alabama 35812

Smithsonian Institution
Astrophysical Observatory
Cambridge, Massachusetts 02138

The Smithsonian Astrophysical Observatory
is a member of the
Harvard-Smithsonian Center for Astrophysics

THE INVESTIGATION OF TETHERED SATELLITE SYSTEM DYNAMICS

Contract NAS8-36160

Quarterly Report #7

For the period 15 February 1986 through 14 May 1986

Principal Investigator

Dr. Enrico C. Lorenzini

Co-Investigators

Mr. David A. Arnold
Dr. Mario D. Grossi
Dr. Gordon E. Gullahorn

June 1986

Prepared for
National Aeronautics and Space Administration
Marshall Space Flight Center, Alabama 35812

Smithsonian Institution
Astrophysical Observatory
Cambridge, Massachusetts 02138

CONTENTS

		Page
Summary		3
Figure Captions		4
SECTION 1.0	INTRODUCTION	7
2.0	TECHNICAL ACTIVITY DURING REPORTING PERIOD AND PROGRAM STATUS	7
2.1	Subsatellite Rotational Dynamics	7
2.1.1	Initial Conditions For Retrieval With A Wobble Of The Subsatellite	7
2.1.2	Subsatellite Orientation With Respect To The Tether Coordinate System	20
2.1.3	Retrieval With A Wobble Of The Subsatellite	23
2.1.4	Angular Oscillation Amplitude As A Function Of Tether Tension	33
2.1.5	Rotational Energy Dissipated By Wire Damping Forces	55
2.1.6	Attitude Damping Using Active Tension Control	59
2.1.7	Attitude Damping Using A Lever Arm	60
2.1.8	Comparison Of MMC And SAO Simulations Of Retrieval With Rotation Of The Subsatellite	64
2.2	Slack Tether Studies	79
2.2.1	Reel Jam: Dynamics Up To Loss Of Tension	79
2.2.1.1	Pre-Jam Assumptions	80

CONTENTS (Cont.)

		Page
SECTION 2.2.1.2	Problem Parameters And Variables	81
2.2.1.3	Velocity Scales	82
2.2.1.4	Retrieval Law	83
2.2.1.5	Gedanken Experiment $V = V_{rec}$	84
2.2.1.6	Fast Retrieval, $V > V_{rec}$	85
2.2.1.7	Slow Retrieval, $V < V_{rec}$	86
2.2.1.7.1	Jump Conditions	87
2.2.1.7.2	Impulse Reflection And Evolution Past T = L/C	90
2.2.1.7.3	Enumeration Of Final States For Decreasing Reel Velocities	94
2.2.1.8	An Algorithm For The Initial Velocity	98
2.2.2	Separation Of Variables Applied To Reel Jam	99
2.2.3	Implications Of The Control Law For Reel Jam Initial Conditions	102
2.2.4	Satellite Orbit After Reel Jam	104
2.2.5	Implementation Of Reel Jam In SLACK3	107
2.2.6	References To Section 2.2	111
3.0	PROBLEMS ENCOUNTERED DURING REPORTING PERIOD	111
4.0	ACTIVITY PLANNED FOR THE NEXT REPORTING PERIOD	111

Summary

The content of this Quarterly Report can be summarized as follows:

The analysis of the rotational dynamics of the satellite has been focused on the rotational amplitude increase of the satellite, with respect to the tether, during retrieval. The dependence of the rotational amplitude upon the tether tension variation to the power 1/4 has been thoroughly investigated. The damping of rotational oscillations achievable by reel control has also been quantified while an alternative solution that makes use of a lever arm attached with a universal joint to the satellite has been proposed. Comparison simulations between the SAO and the Martin Marietta (MMA) computer code of retrieval maneuvers have also been carried out. The agreement between the two, completely independent, codes has been extremely close, demonstrating the reliability of the models.

The slack tether dynamics during reel jams has been analytically investigated in order to identify the limits of applicability of the SLACK3 computer code to this particular case. Test runs with SLACK3 have also been carried out.

Figure Captions

Figure 1. Wobble of the subsatellite with no initial angular velocity and an angular displacement halfway between the x and y principal axes. Part (a) Motion of the tip of the body z-axis as seen from the wire for the first 25 seconds. Part (b) Motion of the tip of the body z-axis for the first 90 seconds. Part (c) The rotation angle of the body x-axis relative to the inertial y-z plane. Part (d) The component of angular velocity along the body z-axis. Part (e) The kinetic energy vs. time.

Figure 2. The relationship between the inertial axes and the body axes.

Figure 3. A 600 sec test run for retrieval of the subsatellite with the same initial conditions for rotation as Figure 1. Part (a) Tether length vs. time. Part (b) Tension vs. time. Part (c) In-plane angle vs. time. Part (d) Out-of-plane displacement of the tether attachment point vs. time. Part (e) Angular velocity component along the body x-axis. Part (f) Angular velocity component along the body y-axis. Part (g) Angular velocity component along the body z-axis. Part (h) The motion of the body z-axis as seen from the wire. Part (i) The angle θ between the wire and the body z-axis. Part (j) The rotation angle of the subsatellite about the direction of the wire. Part (k) The rotational kinetic energy vs. time.

Figure 4. Retrieval simulation for 10,000 seconds of orbital time with a wobble of the subsatellite. Part (a) Tether length vs. time. Part (b) Tension vs. time. Part (c) In-plane libration angle. Part (d) Angular velocity component along the body z-axis. Part (e) Rotation angle of the subsatellite about the body z-axis. Part (f) The angle between the wire and the radius vector to the attachment point. Part (g) The rotational kinetic energy vs. time.

Figure 5. Simulation of z-axis spin control using program ROTAT with stiffness and damping reduced by a factor of ten in the control algorithm. Part (a) Component of the angular velocity along the body z-axis. Part (b) Rotation angle of the subsatellite about the z-axis. Part (c) The work done by the z-axis attitude control thruster. Part (d) The integrated torque of the z-axis attitude control thruster.

Figure 6. Simulation of a single axis rotation of the subsatellite using program ROTAT with an exponential tension decrease. Part (a) The tension vs. time. Part (b) The angle θ between the wire and the vector to the attachment point vs. time. Part (c) The rotational kinetic energy vs. time. Part (d) The subsatellite rotation angle in inertial coordinates vs. time.

Figure 7. Simulation of a circular wobble using program ROTAT with an exponential tension decrease. Part (a) Tension vs. time. Part (b) The angle θ between the wire and the radius vector to the attachment point vs. time. Part (c) The rotational kinetic energy vs. time. Part (d) The motion of the tip of the body z-axis as seen from the direction of the wire.

Figure 8. Simulation of a single axis rotation with program ROTAT with a sinusoidal tension variation. Part (a) The tension vs. time. Part (b) The angle θ between the wire and the radius vector to the attachment point vs. time. Part (c) The rotational kinetic energy vs. time. Part (d) The subsatellite rotation angle in inertial coordinates vs. time. Part (e) The angular velocity vs. time.

Figure 9. Simulation of a single axis rotation using program ROTAT with a sinusoidal variation of the tether angle. Part (a) Tether angle vs. time. Part (b) Rotation angle of the subsatellite in inertial space. Part (c) Rotation angle with respect to the tether. Part (d) Component of the angular velocity along the body x-axis. Part (e) The rotational kinetic energy vs. time.

Figure 10. Rotation angle vs. time for the first 565 seconds of retrieval starting at 20 km.

Figure 11. Kinetic energy vs. time for rotation of the subsatellite with wire damping included in the model.

Figure 12. Lever arm for damping rotational oscillations of the subsatellite. Part (a) Lever arm remains aligned with the wire. Part (b) Lever arm does not follow the direction of the wire closely.

Figure 13. Retrieval from 20 km with a single axis rotation of the subsatellite and two terms in the tension control law. Part (a) Tether length vs. time. Part (b) In-plane tether angle vs. time. Part (c) Tension vs. time. Part (d) Rotation angle of the subsatellite with respect to the tether vs. time.

Figure 14. Retrieval from 20 km without rotational dynamics and three terms in the tension control law. Part (a) Tether length vs. time. Part (b) In-plane angle of the tether vs. time. Part (c) Tension vs. time.

Figure 15. Retrieval from 20 km with a single axis rotation of the subsatellite and three terms in the tension control law. Part (a) Tether length vs. time. Part (b) In-plane angle vs. time. Part (c) Tension vs. time. Part (d) Rotation angle with respect to the tether vs. time for 10,000 seconds. Part (e) Rotation angle vs. time for the first 500 seconds. Part (f) Rotation angle vs. time for the last 500 seconds. Part (g) The rotational kinetic energy vs. time.

Figure 16. Snapshot of the strain and velocity profiles following a reel jam.

Figure 17. Final tether velocity V_f as a function of reel velocity at the moment of jam, V.

Figure 18. SLACK3 simulation of reel jam. Retrieval angle 45°, 1 km deployed tether at jam.

1.0 INTRODUCTION

This is the seventh Quarterly Report submitted by SAO under contract NAS8-36160, "The Investigation of Tethered Satellite System Dynamics," Dr. Enrico C. Lorenzini, PI and covers the period from 15 February 1986 through 14 May 1986.

2.0 TECHNICAL ACTIVITY DURING REPORTING PERIOD AND PROGRAM STATUS

2.1 Subsatellite Rotational Dynamics

2.1.1 Initial Conditions For Retrieval With A Wobble Of The Subsatellite -

Section 2.2 of Quarterly Report #5 shows simulations of the buildup of angular oscillations during retrieval for a one dimensional rotation with the rotational angular velocity parallel to the orbital angular velocity. The simulations showed that the rotational energy at the end of retrieval was only about 1/6 of the initial energy. The angular amplitude increased by more than a factor of 2. Another retrieval simulation has been done with unequal moments of inertia and a two-dimensional wobble. The wobble alternates between circular and linear motion because of the asymmetry. No exact equations have been derived to calculate initial conditions for a circular wobble with unequal moments of inertia. However, the fact that the motion goes through a linear phase provides an alternate method of setting up initial conditions. If the subsatellite is given an initial rotation about an axis that is half way between x and y axes, this generates an oscillation with both x and y components. Since the frequencies of the components are different the oscillation alternates between linear and circular phases.

A short test run has been done to demonstrate that a circular wobble can be created from an initial displacement having both x and y components. The x and y axes are taken to be the axes of the principal moments of inertia. A rotation about only x or y should not produce a circular wobble. The initial conditions are expressed as Euler angles ϕ, θ, and ψ which are rotations about the body x, z, and x axes respectively. The tether is connected to the tip of the body z-axis. The initial conditions $\phi = 0$, $\theta = 20°$, and $\psi = 45°$ should produce the desired result (the value of ϕ is immaterial since the θ rotation is about the body x-axis). A run has been done for 25 seconds with output every .3 seconds.

Figure 1a shows the motion of the tip of the body z-axis as seen from the wire. The coordinate axes on the graphs are the inertial y and z axes with the wire along the -x axis. The relationship of the axes is shown in Figure 2. The motion starts at the left side of the Figure 1a. The motion has become nearly circular by the end of the run. The run has been extended to 90 seconds and Figure 1b shows the wobble pattern over that time. The plot shows an extremely regular pattern covering a square area. Figure 1c shows the rotation angle of the body x-axis relative to the inertial y-z plane. The motion is small because of the small amplitude of the wobble. Figure 1d shows the component of the angular velocity along the body z-axis. Figure 1e shows the kinetic energy vs. time. The initial value is zero since the initial conditions are for a displacement with no angular velocity. The motion is initially linear with a large exchange between kinetic and potential energy. As the motion circularizes at around 30 seconds the variations decrease. The small variation in rotation angle seen in Figure 1c is an indication of the low coupling between the wobble about the x and y axes and the spin about the z-axis. The body could have a spin about the z-axis in addition to the slight rotation back and forth produced by the wobble.

The initial conditions from the test run with program ROTAT have been put into DUMBEL for a short retrieval test run. The initial conditions for the attitude dynamics are $\theta = 2°$, $\phi = 0$, $\psi = 45°$ and $\dot{\theta} = \dot{\phi} = \dot{\psi} = 0$. The initial conditions for the tether have no initial in-plane or out-of-plane libration and no retrieval velocity. A run has been done for 600 seconds with output every second. Figure 3 gives the results. Parts a, b, c, and d give the tether length (cm), tension (dynes), in-plane tether angle (deg), and out-of-plane tether displacement (cm). The large in-plane tether displacement masks the variations due to the wobble. The effects of the wobble show up clearly in the out-of-plane tether displacement. Parts e, f, and g give the components of the angular velocity along the body x,y, and z axes. The period of the oscillations about the x axis is shorter because of the smaller moment of inertia. The period depends on the tension which is decreasing during the runs. Parts h, i, and j give the motion of the z-axis as seen from the wire, the angle between the z-axis and the wire (θ), and the rotation angle about the wire direction. The z-axis plot is somewhat noisy because the wobble period is on the order of 10 seconds and the output interval is 1 second. The plot of θ shows the periods of linear and circular oscillation. The average value of θ is increasing during the run. The back and forth motion of the spin angle has a small amplitude but a systematic effect is developing. Figure 3k shows the kinetic energy. The dominant feature is the alternation between linear and circular oscillation. There is a slight decrease in the average kinetic energy during the run. No thrusters are used during the run. The initial kinetic energy of rotation is 589.9 ergs. This is due solely to the orbital angular velocity. The body has no initial angular velocity with respect to the tether coordinate system. Subtracting the work done by the wire from the kinetic energy gives a value which is constant to within a range of about 589.6 to 589.9 ergs. The changes in kinetic energy are solely due to the work done by the torque of the wire.

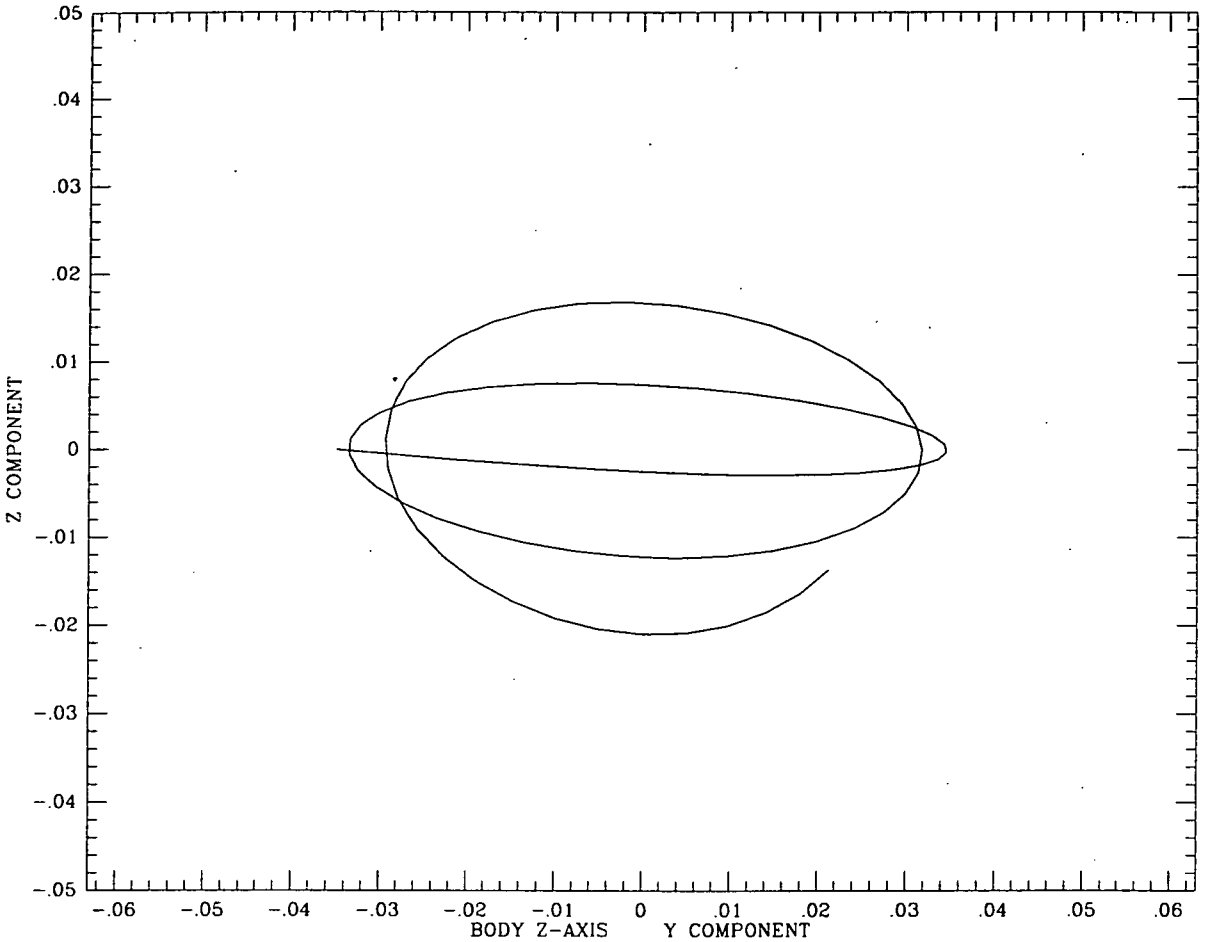

Figure 1a↑

Figure 1b↓

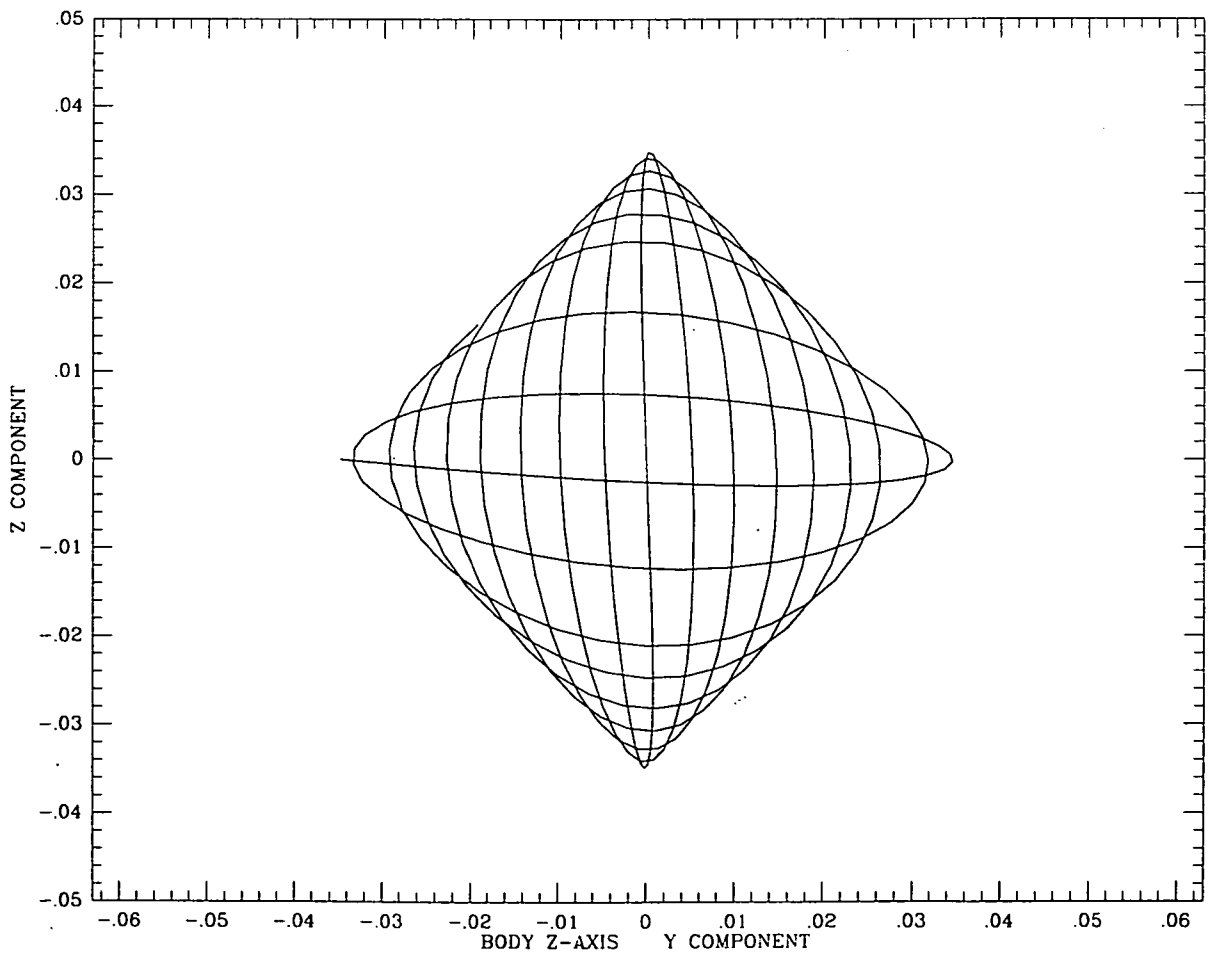

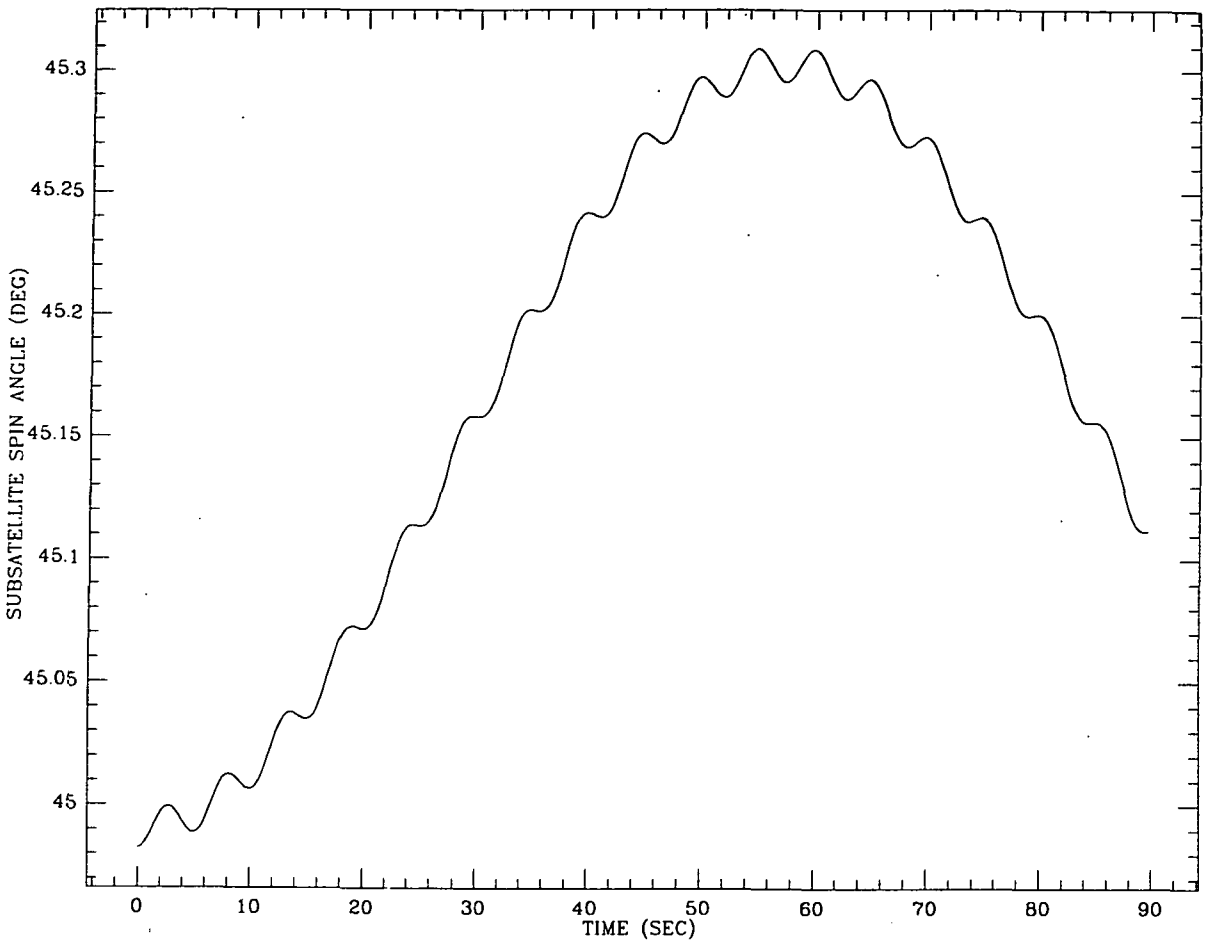

Figure 1c↑

Figure 1d↓

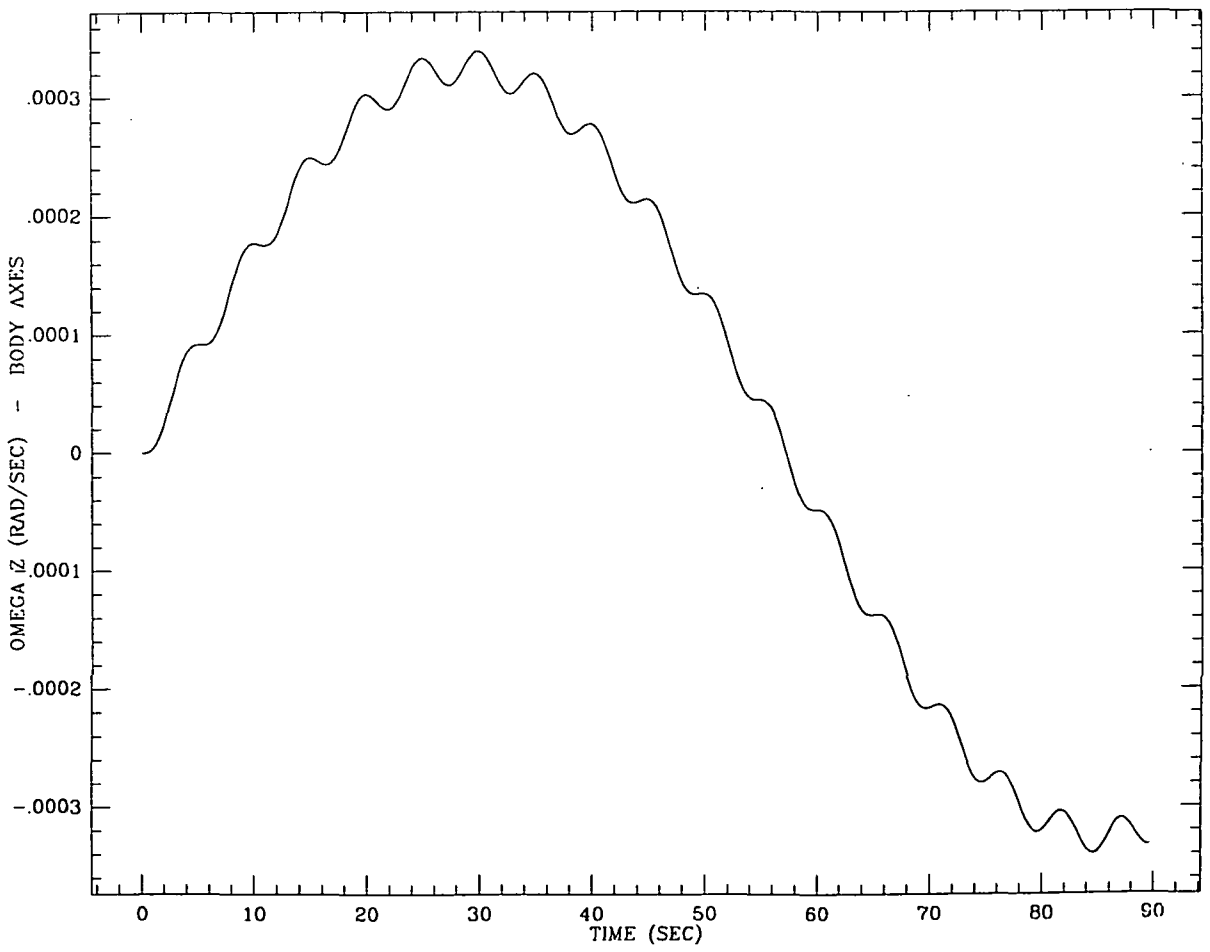

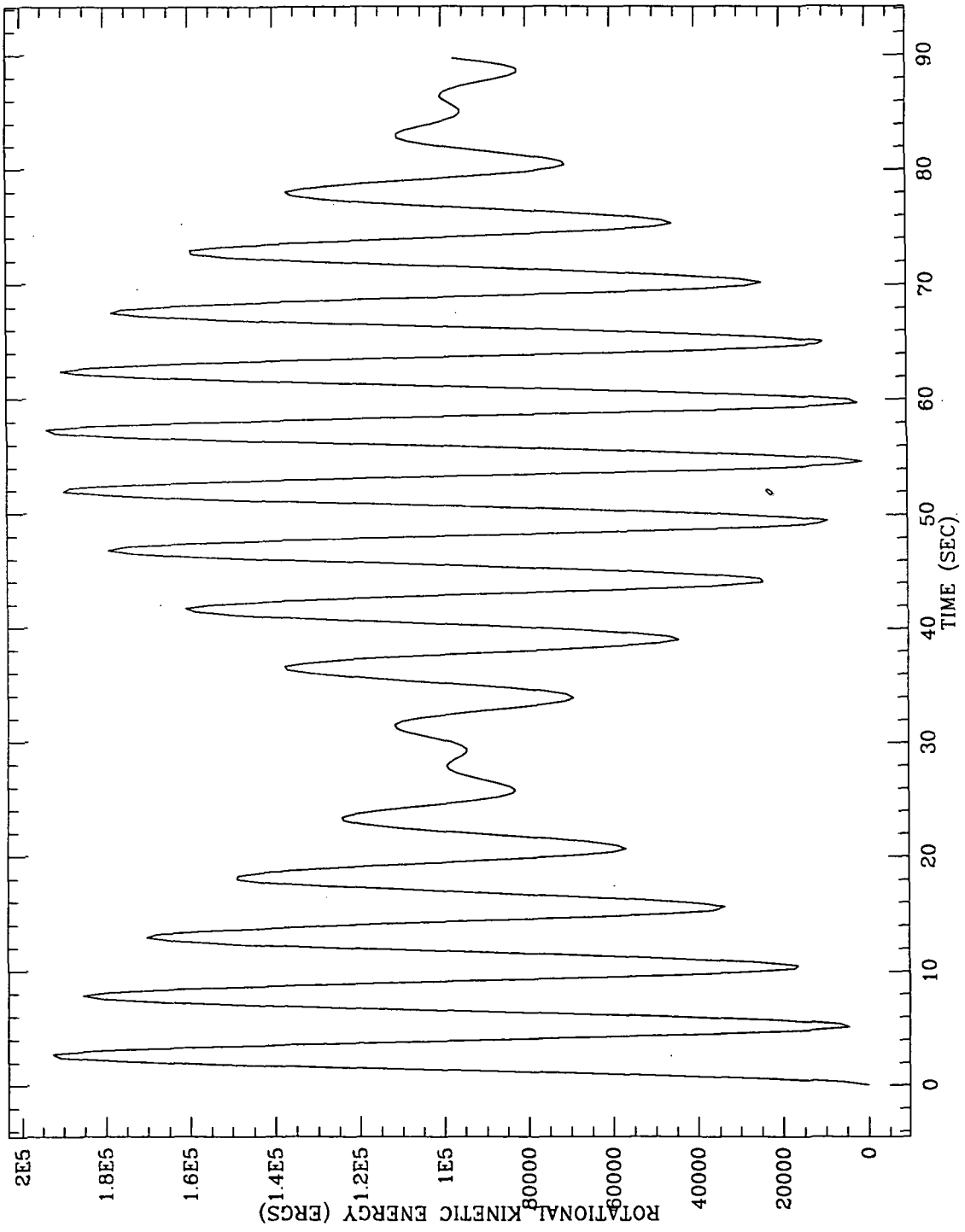
ROTATIONAL KINETIC ENERGY (ERGS)
2E5
1.8E5
1.6E5
1.4E5
1.2E5
1E5
80000
60000
40000
20000
0
0
10
20
30
40
50
60
70
80
90
TIME (SEC)

Figure 1e

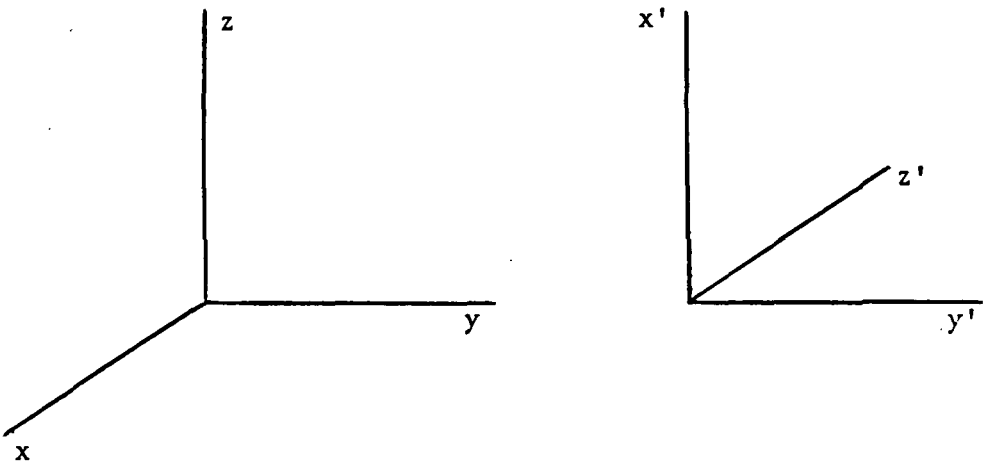

Figure 2

Relationship of the inertial axes x, y, z and the body axes x', y', z'.

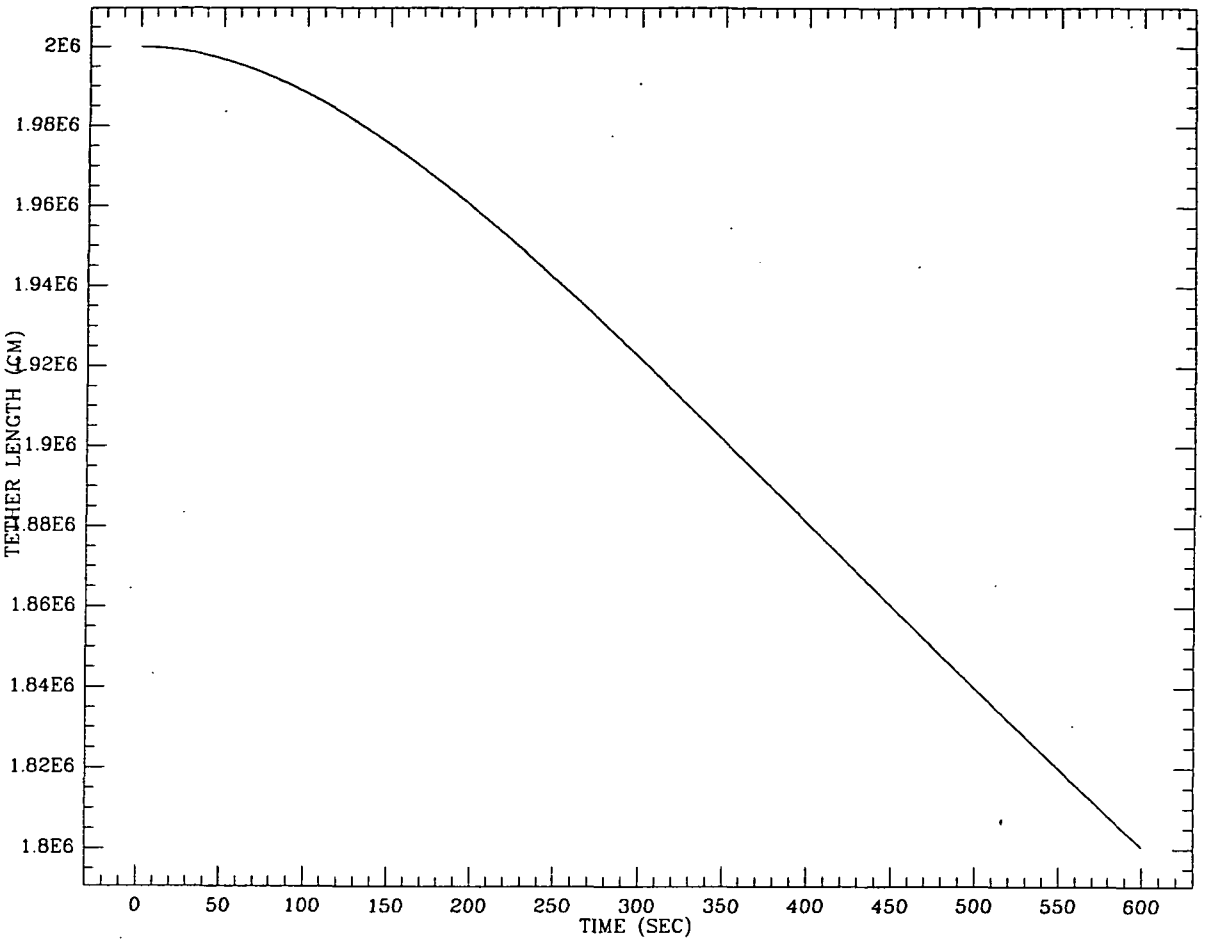

Figure 3a↑

Figure 3b↓

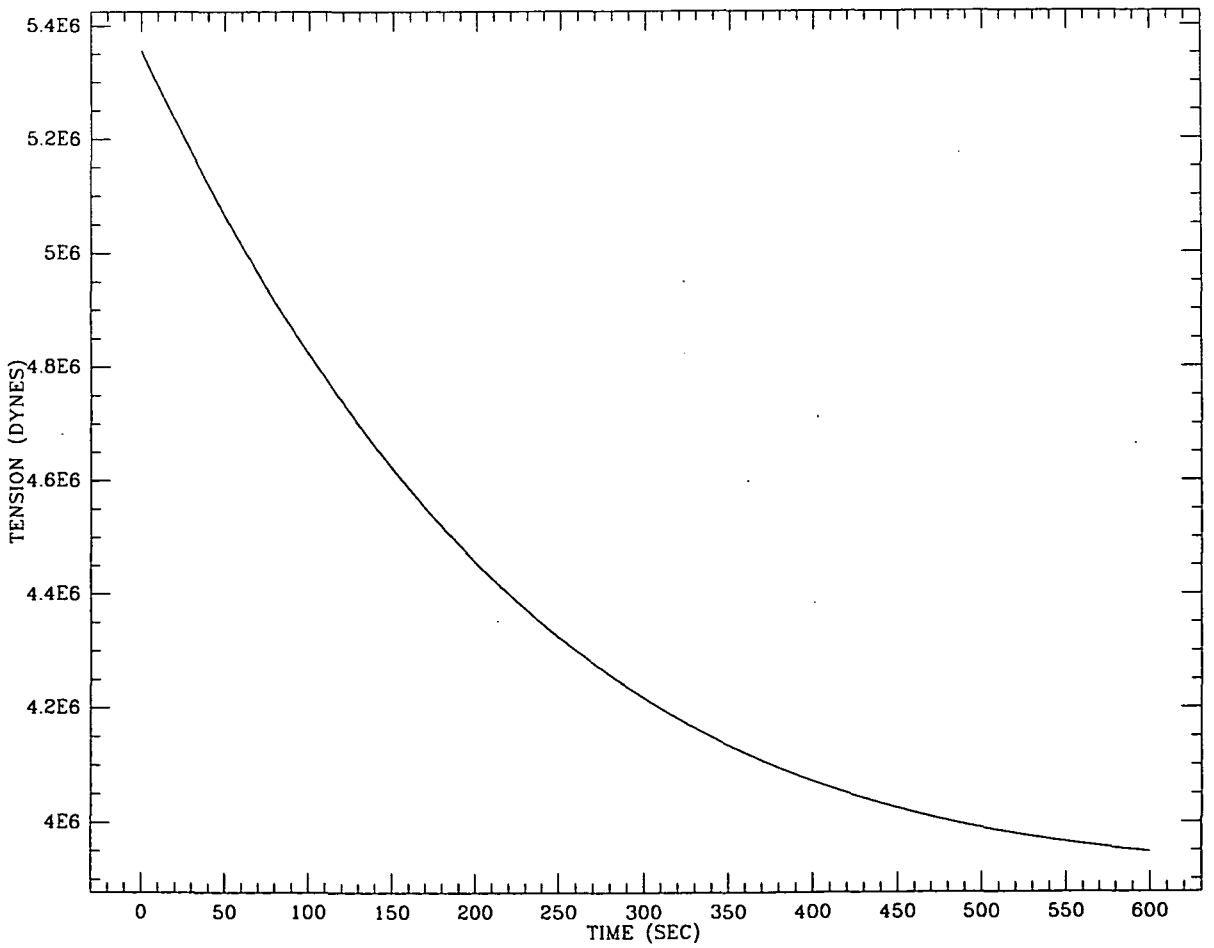

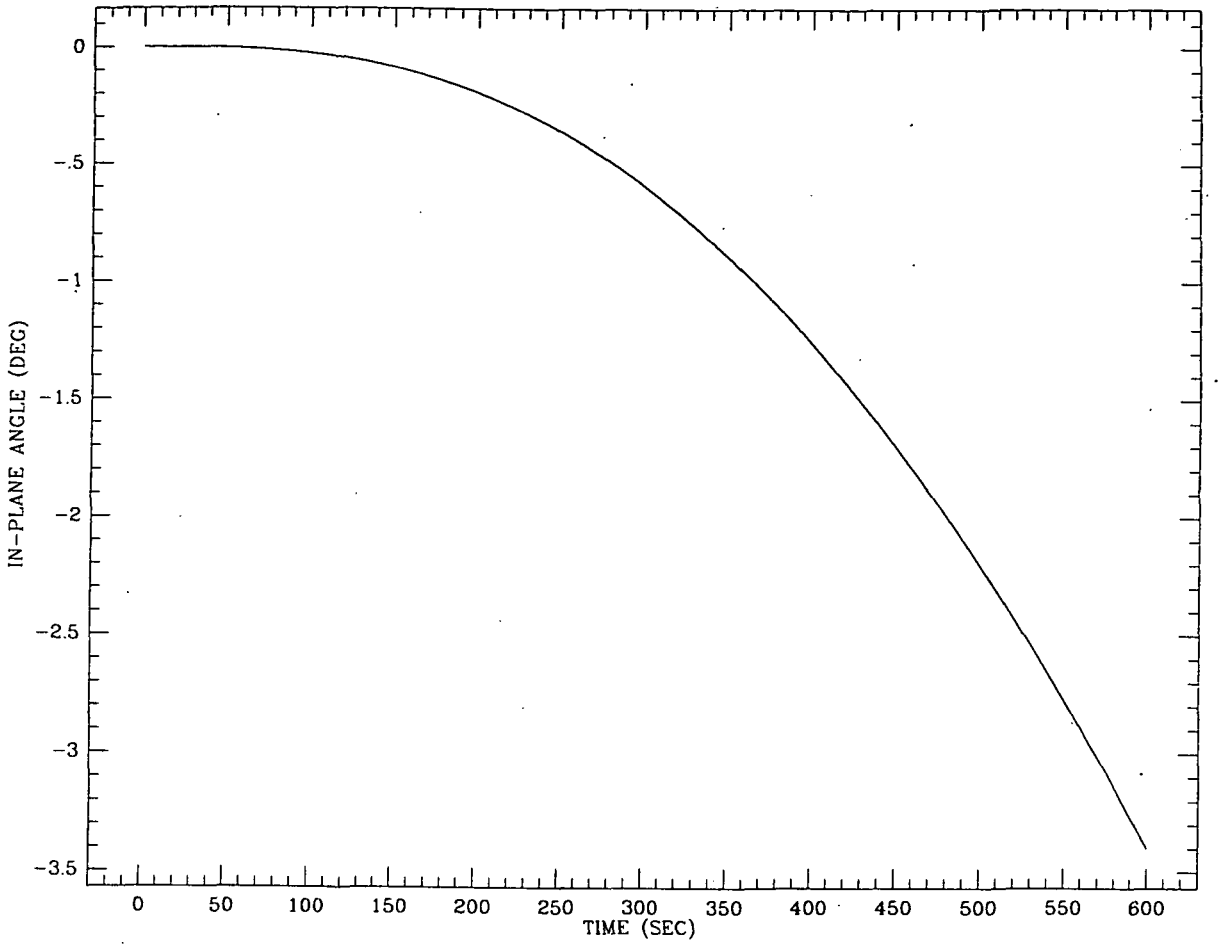

Figure 3c↑

Figure 3d↓

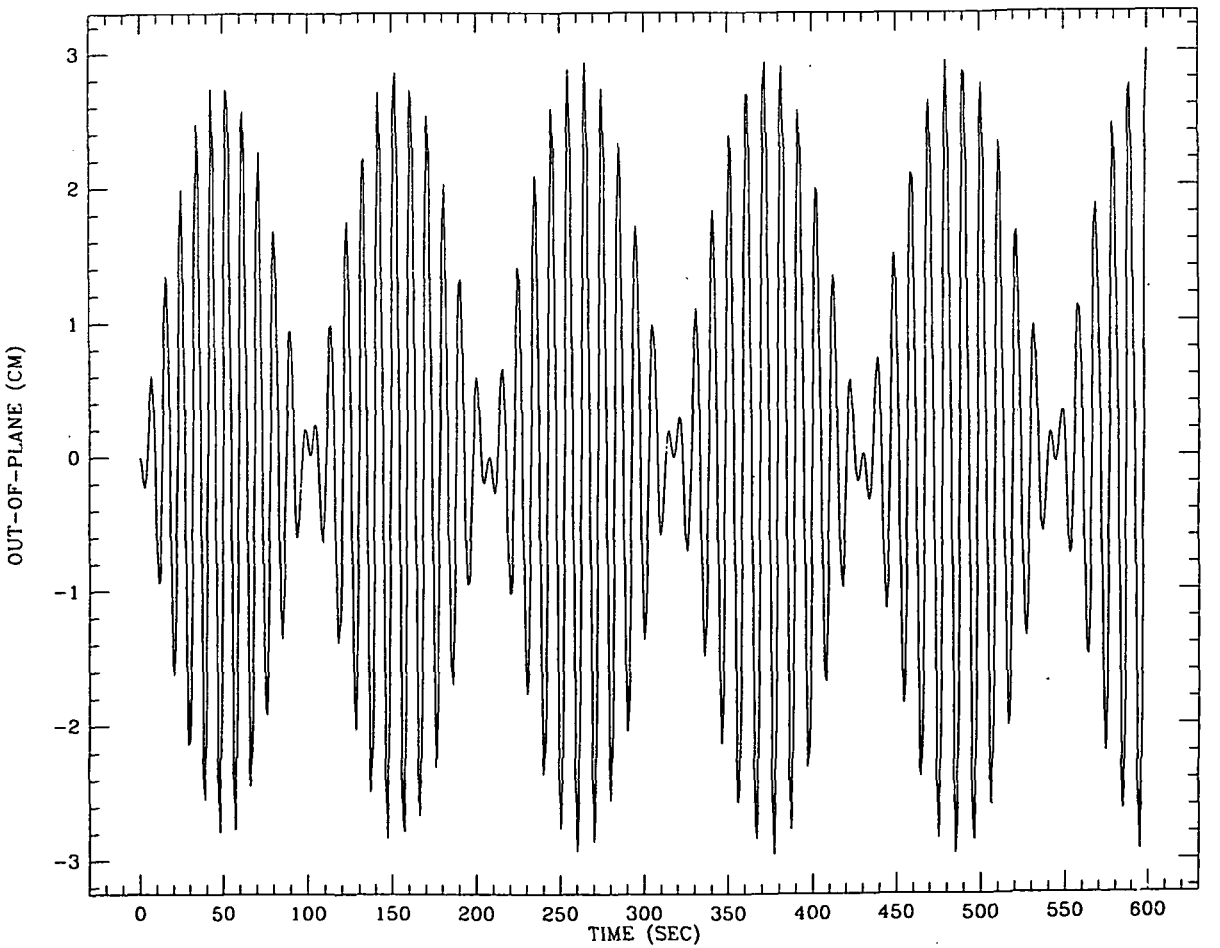

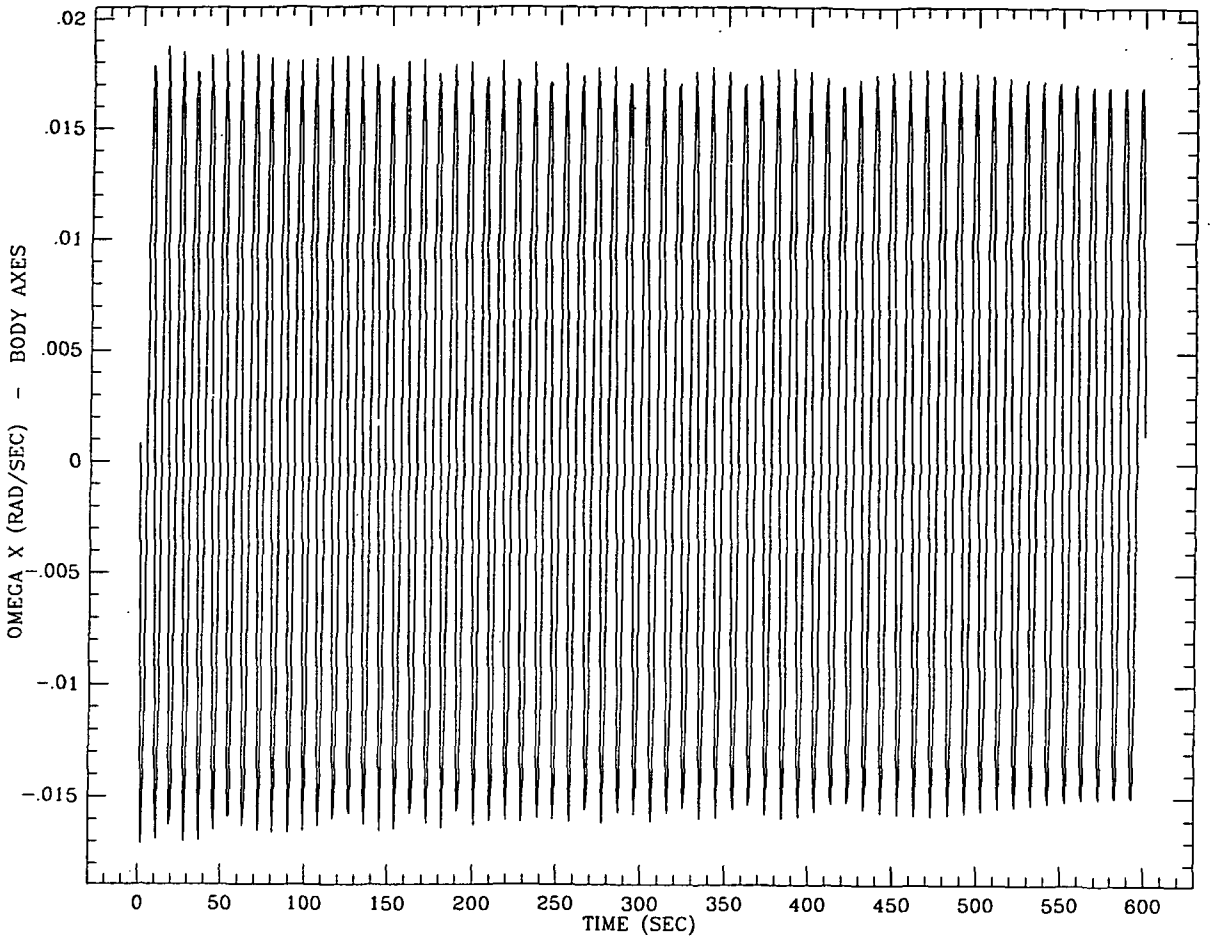

Figure 3e↑

Figure 3f↓

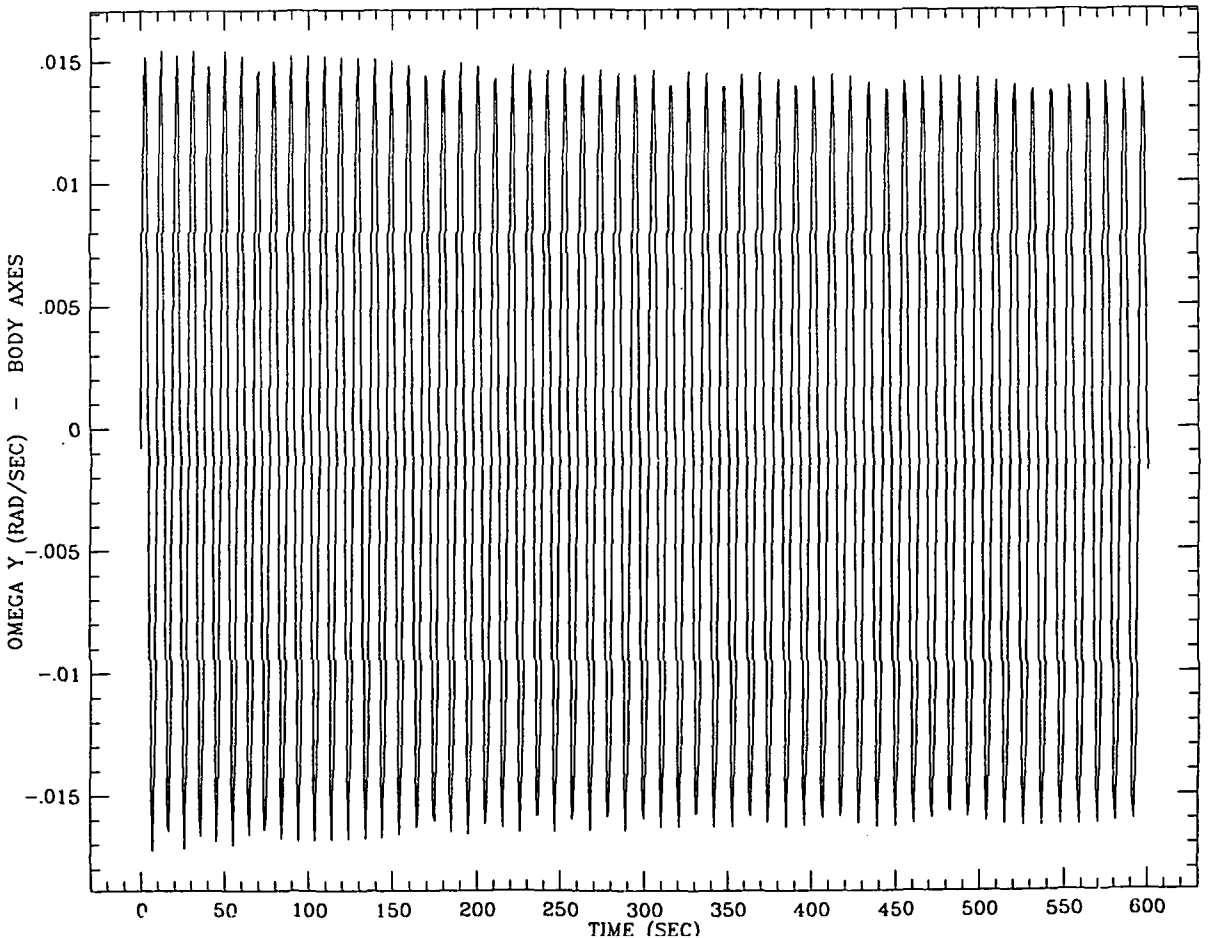

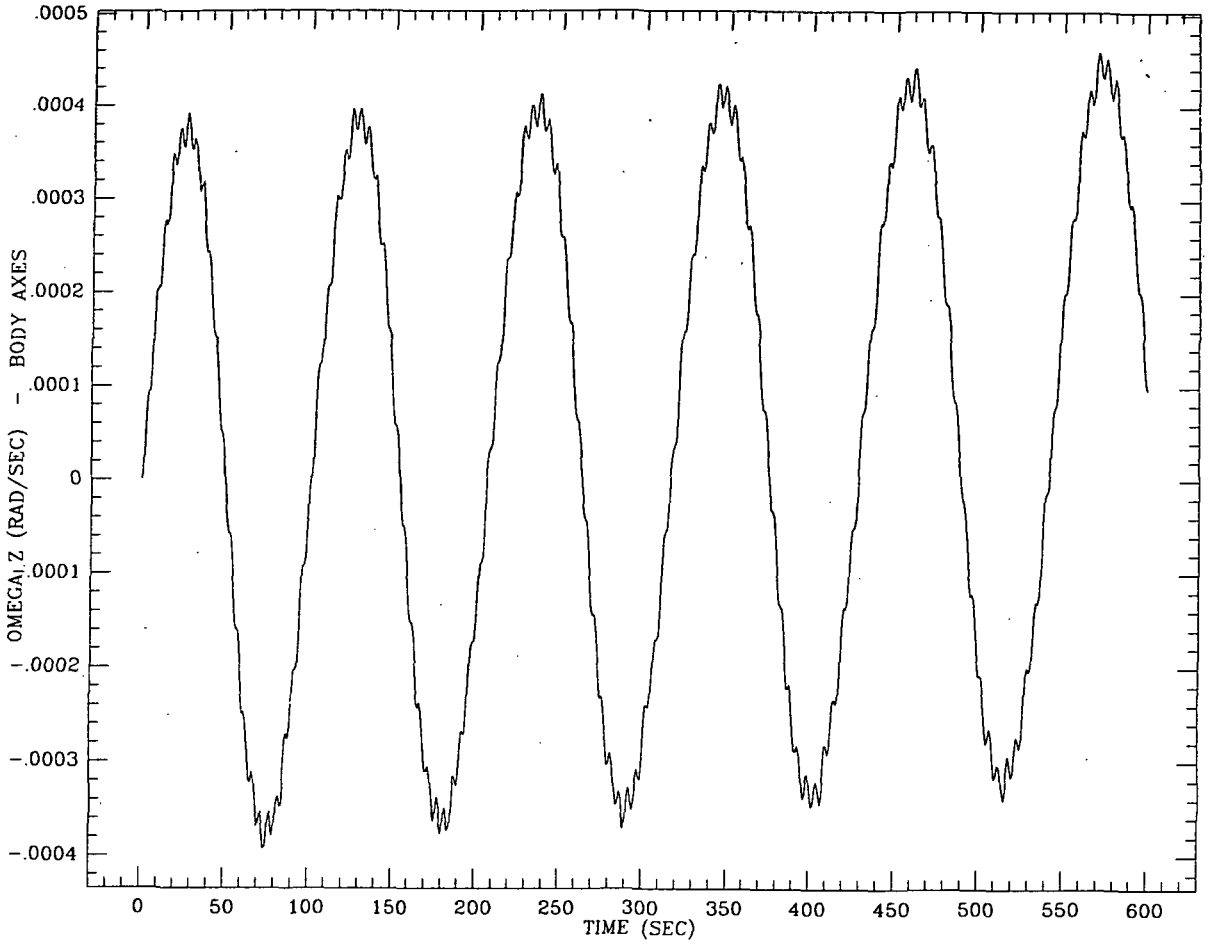

Figure 3g↑

Figure 3h↓

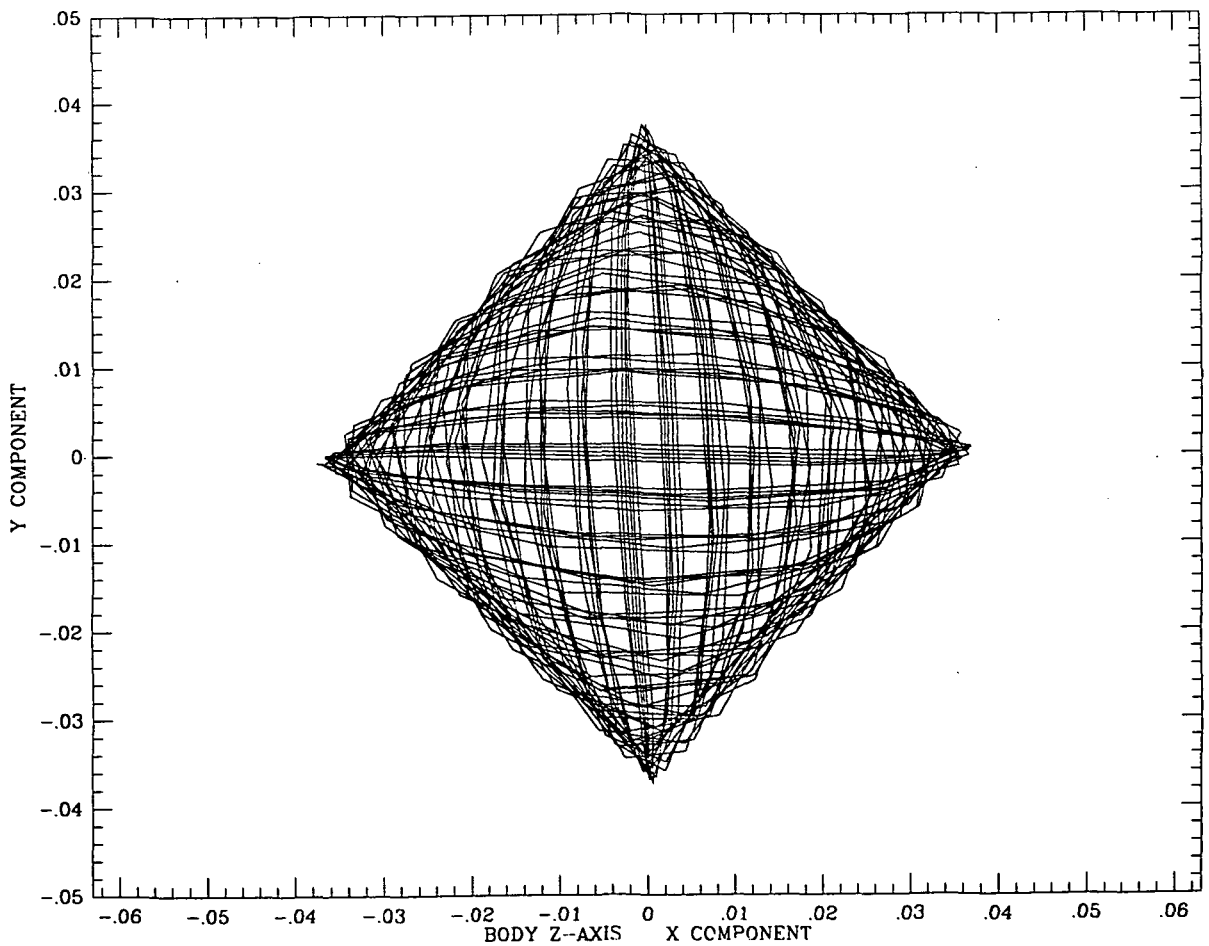

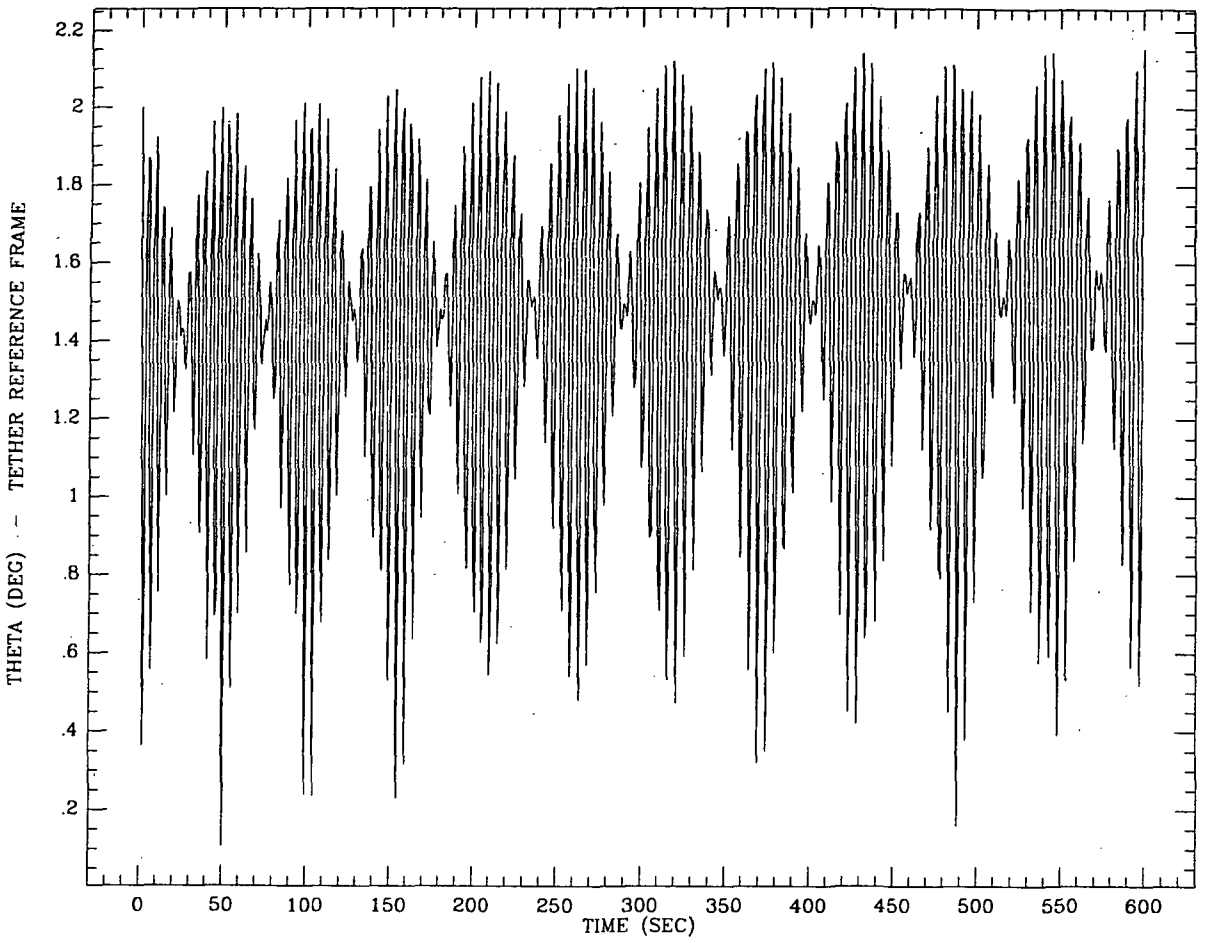

Figure 3i↑

Figure 3j↓

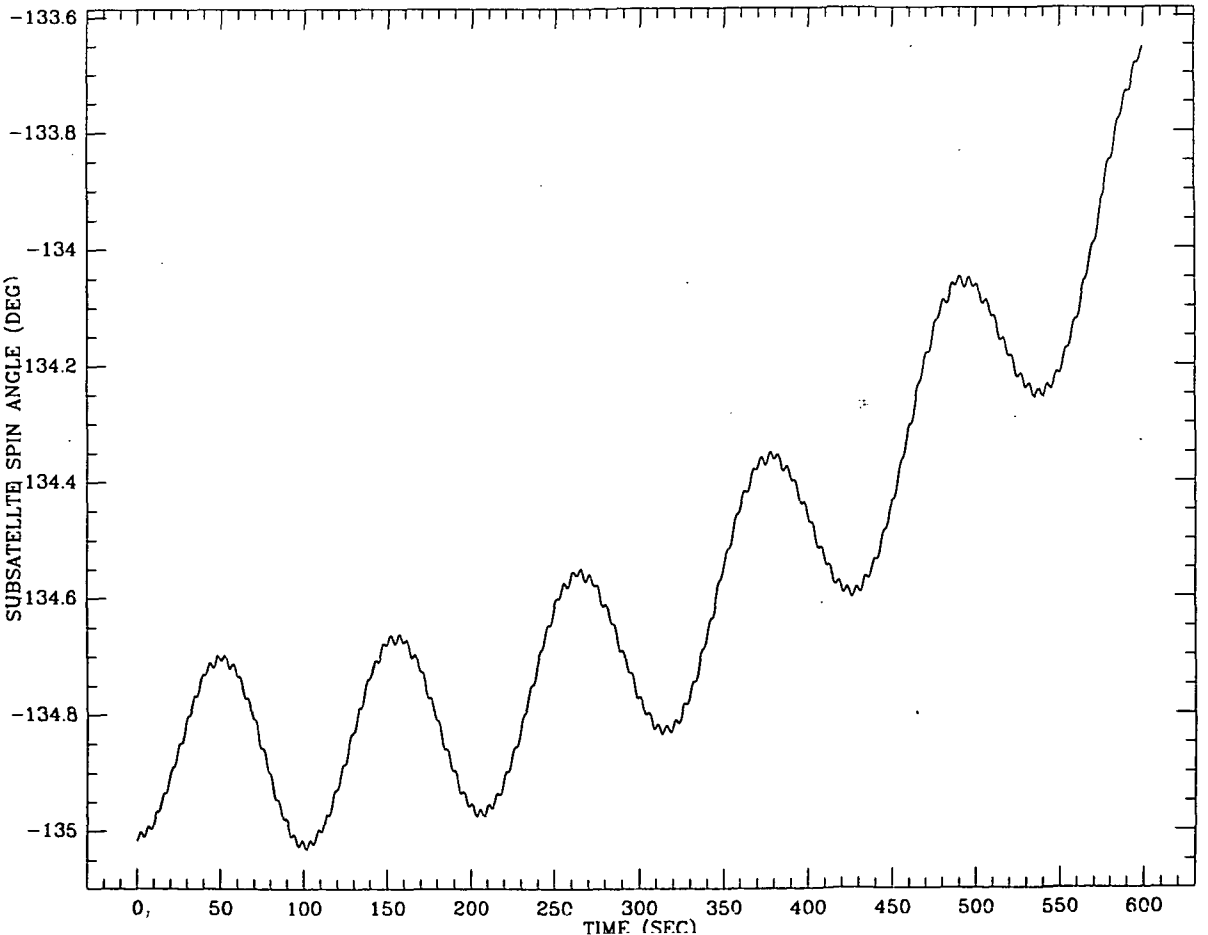

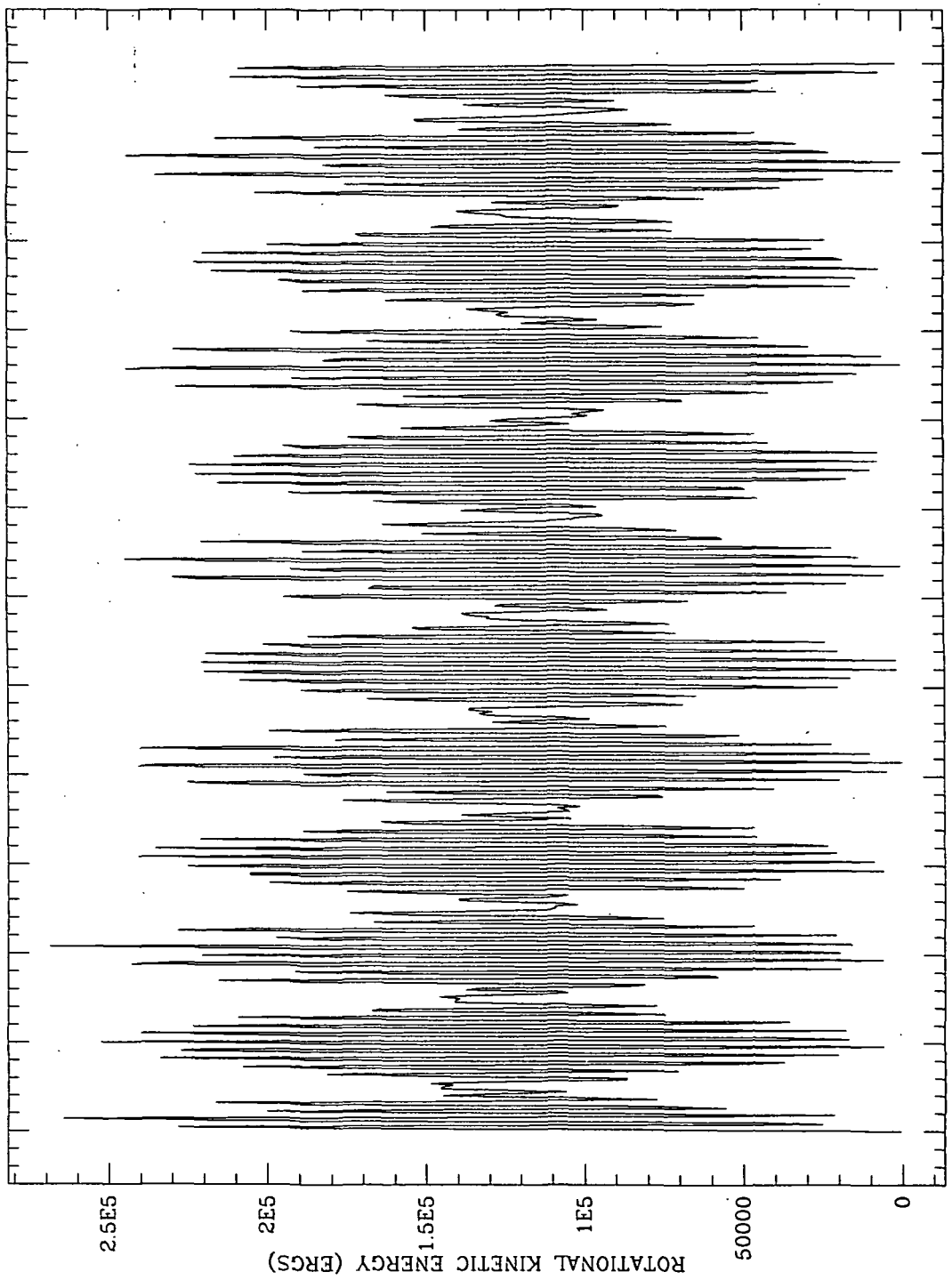
ROTATIONAL KINETIC ENERGY (ERGS)
2.5E5
2E5
1.5E5
1E5
50000
0
TIME (SEC)
0
50
100
150
200
250
300
350
400
450
500
550
600

Figure 3k

2.1.2 Subsatellite Orientation With Respect To The Tether Coordinate System -

There are four coordinate systems that are useful in describing the dynamics of the tethered subsatellite. The equations of motion are integrated in an inertial coordinate system since they have their simplest form in this system. The position and velocity of the Shuttle can be used to define an orbital coordinate system which is useful in describing the libration angles of the tether. The principle axes of the subsatellite form a coordinate system. The relationship of the body axes to the inertial axes are specified by 9 direction cosines which are integrated vs. time to determine the rotational dynamics. The orientation of the subsatellite is influenced primarily by the torque exerted by the tether. It is useful therefore to describe the orientation of the subsatellite with respect to the tether coordinate system.

The tether coordinate system can be defined in terms of the velocity $\vec{v}$ of the Shuttle and the force $\vec{F}$ exerted by the tether on the subsatellite. The z-axis of the tether system is taken to be in the direction of the wire force $\vec{F}$. That is

$$\hat{z} = \vec{F}/|\vec{F}| \tag{1}$$

The x-axis is taken to be in the direction of the vector $\vec{X}$ given by

$$\vec{X} = \hat{z} \times \vec{v} \tag{2}$$

The unit vector for the x-axis is

$$\hat{x} = \vec{X}/|\vec{X}| \tag{3}$$

The unit vector in the direction of the y-axis is

$$\hat{y} = \hat{z} \times \hat{x} \tag{4}$$

A vector $\vec{P}$ in inertial coordinates can be transformed to the tether coordinate system using the equation

$$\vec{P}'' = B\,\vec{P} \tag{5}$$

where $\vec{P}''$ is the vector in the tether system. In the body axis system the vector is $\vec{P}'$ given by

$$\vec{P}' = A\,\vec{P} \tag{6}$$

Premultiplying equation (5) by B^T gives

$$B^T\,\vec{P}'' = \vec{P} \tag{7}$$

Substituting equation (7) into equation (6) gives

$$\vec{P}' = AB^T\,\vec{P}'' \tag{8}$$

Defining

$$C \equiv A\,B^T \tag{9}$$

we have

$$\vec{P}' = C\,\vec{P}'' \tag{10}$$

The matrix C defines the orientation of the body with respect to the tether coordinate system. The Euler angles ϕ, θ and ψ can be computed from the elements of the matrix C. The matrix B^T is

$$\begin{pmatrix} x_1 & y_1 & z_1 \\ x_2 & y_2 & z_2 \\ x_3 & y_3 & z_3 \end{pmatrix} \tag{11}$$

where x_i, y_i, and z_i are the components of the unit vectors $\hat{x}$, $\hat{y}$, and $\hat{z}$ respectively. The validity of equation (11) is obvious from equation (7). For example if

$$\vec{P}'' = \begin{pmatrix} 1 \\ 0 \\ 0 \end{pmatrix} \tag{12}$$

Then

$$\vec{P} = \begin{pmatrix} x_1 \\ x_2 \\ x_3 \end{pmatrix} = \hat{x} \tag{13}$$

Similar relations hold for $\hat{y}$ and $\hat{z}$.

A subroutine called ROTANG has been written using the methods developed in equations (1-4) (9), and (11). This subroutine has as input the state vectors of the Shuttle and subsatellite and the matrix A of direction cosines. The output is the matrix C and the Euler angles ϕ, θ, and ψ. This subroutine has been added to program RSTAVEC which processes the file of state vectors created by the numerical integration programs such as DUMBEL. Figures 3h, 3i, and 3j

were produced using the output of subroutine ROTANG.

The format of the output for program DUMBEL has been changed to eliminate various quantities which were not generally useful and add some new output. All rotational dynamics quantities given in the inertial coordinate system have been eliminated. At each output point the Euler angles of the subsatellite are printed with respect to both the orbital coordinate system and the tether coordinate system (using the new subroutine ANGROT). File FOR011 has been changed to contain the Euler angle θ in the tether system rather than in the orbital system. As a test, the case of Figure 3 has been rerun for 250 seconds with the new version of DUMBEL. The results agree with the previous runs of DUMBEL and postprocessing by RSTAVEC.

2.1.3 Retrieval With A Wobble Of The Subsatellite -

The run of Figure 3 has been done for 10,000 seconds of orbital time with output at 1.0 second intervals. The Shuttle of mass 100 metric tons is at 296 km with a 500 kg subsatellite deployed upward on a 20 km, 2.54 mm diameter tether. The initial Euler angles of the subsatellite in the tether coordinate system are $\theta = 2°$, $\phi = 0$, and $\psi = 45°$. The satellite radius is 80 cm and the moments of inertia are 80, 96, and 99 kg-m^2 for the x, y, and z axes respectively. The tether is initially aligned with the local vertical. The tension is regulated by the retrieval tension control algorithm according to equation (2.1.16) of Quarterly Report #3.

Figure 4 shows the results of the retrieval simulation. Parts (a), (b), and (c) give the tether length, tension, and in-plane libration angle. The control law damps out the in-plane librations during the retrieval. Parts (d)

and (e) show the z component of angular velocity and the spin angle about the z-axis. The wobble introduces a small spin but the spin rate is very small and the satellite does not do a full revolution even without any spin control. Figure 4f shows the angle between the wire and the radius vector to the attachment point. The amplitude of the wobble goes from 2° in the beginning to about 4.8° at 10,000 seconds. The motion alternates between linear and circular oscillation because of beats between the x and y components of the wobble. Figure 4g shows the kinetic energy as a function of time. The maximum kinetic energy goes from about 2.7×10^5 ergs at the beginning to about 4.8×10^4 ergs at the end. It is difficult to determine exact values from the plot because the 1.0 second output interval does not give very good resolution.

The period of the wobble lengthens as the tension decreases. The frequency ω of the wobble is, for small amplitudes,

$$\omega = \sqrt{rF/I} \tag{14}$$

The initial value of the tension is 5.35×10^6 dynes. With I_x = 80 kg-m^2 and I_y = 96 kg-m^2, and r = 80 cm, equation (14) gives a period of 8.59 seconds for the x-component. The average observed periods are about 8.56 and 9.40 seconds respectively. The motion is complex with unequal moments of inertia so that the periods of the motions are not exactly constant. The average period of the wobble computed with I = 88 kg-m^2 is about 9 seconds. Table 1 lists the tension, and average computed wobble period at 1000 second intervals during the run.

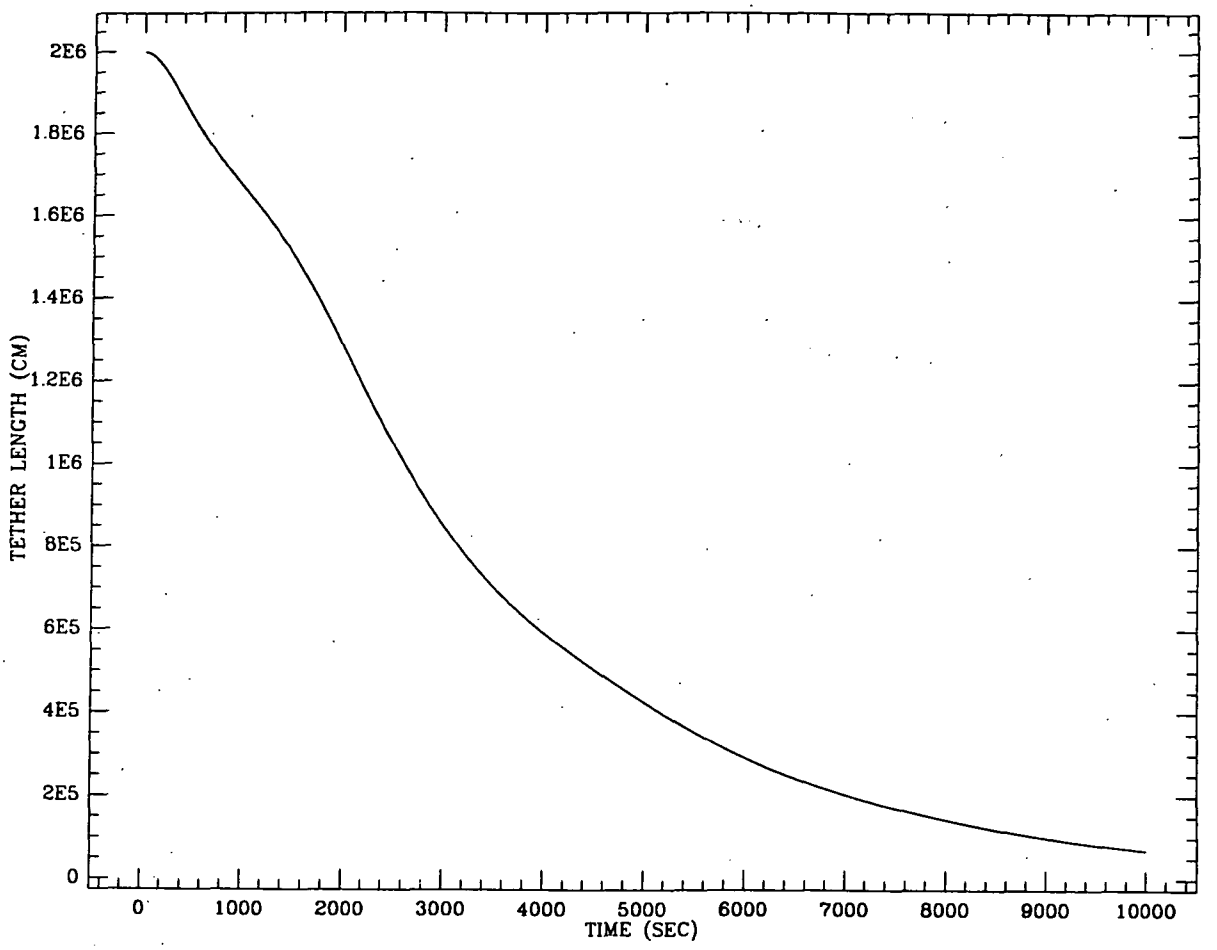

Figure 4a↑

Figure 4b↓

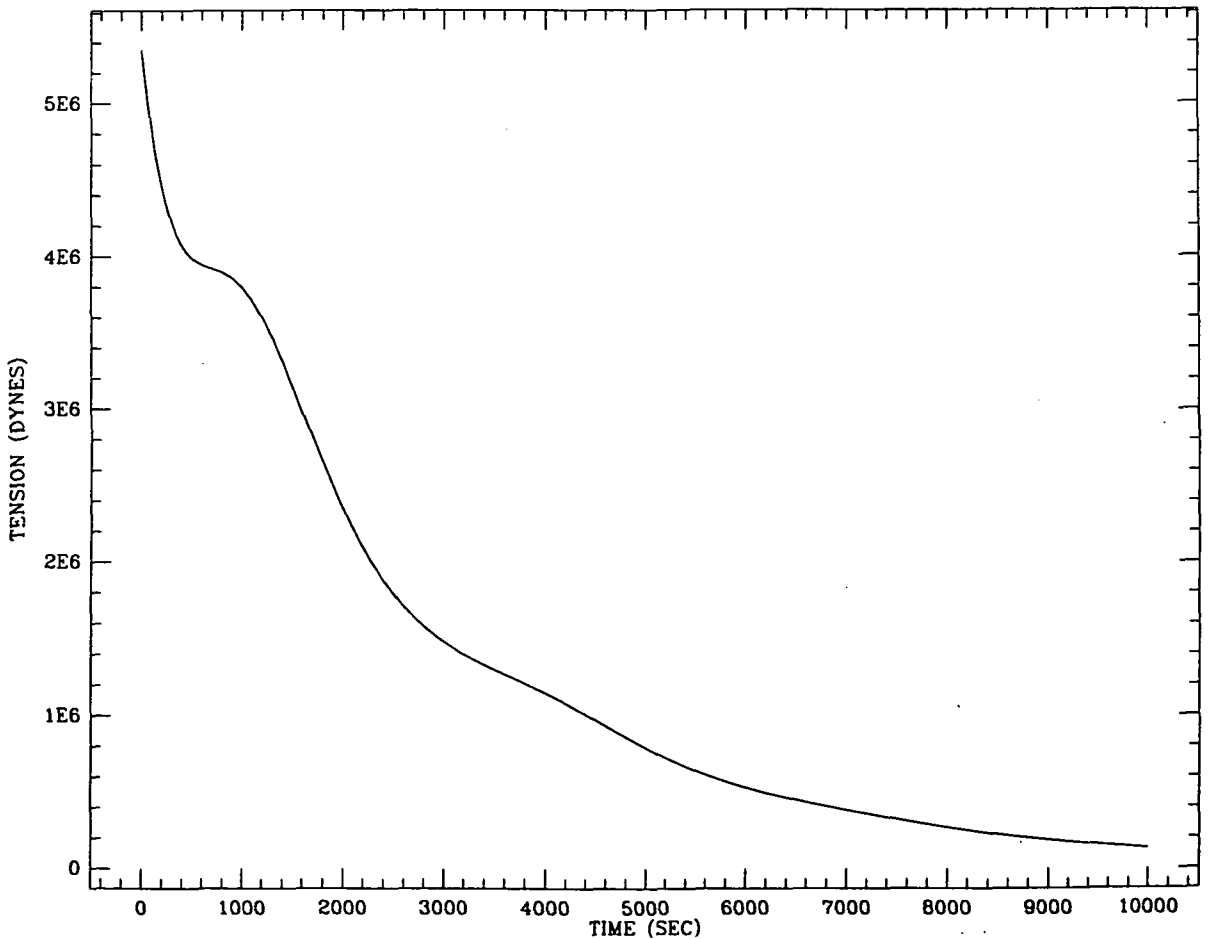

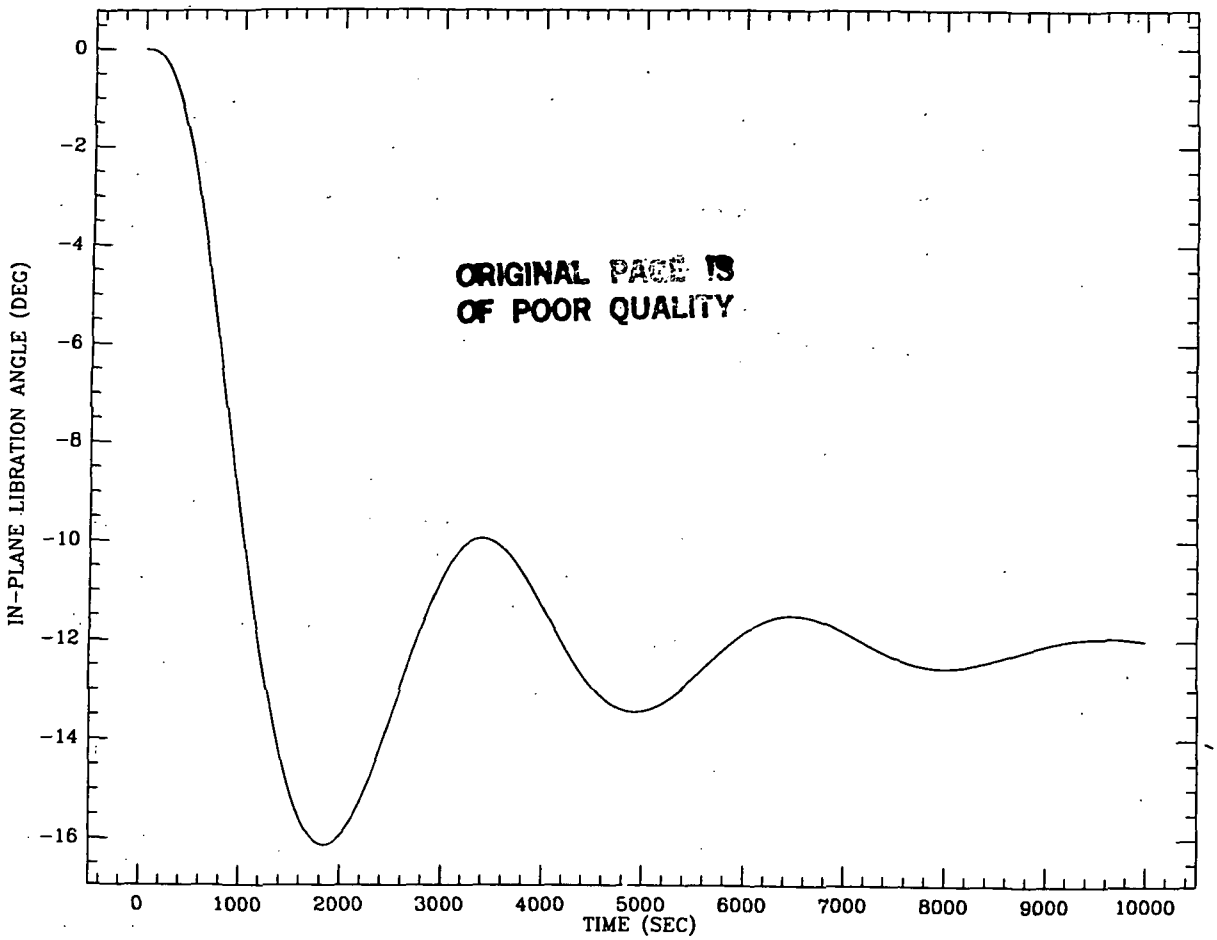

Figure 4c↑

Figure 4d↓

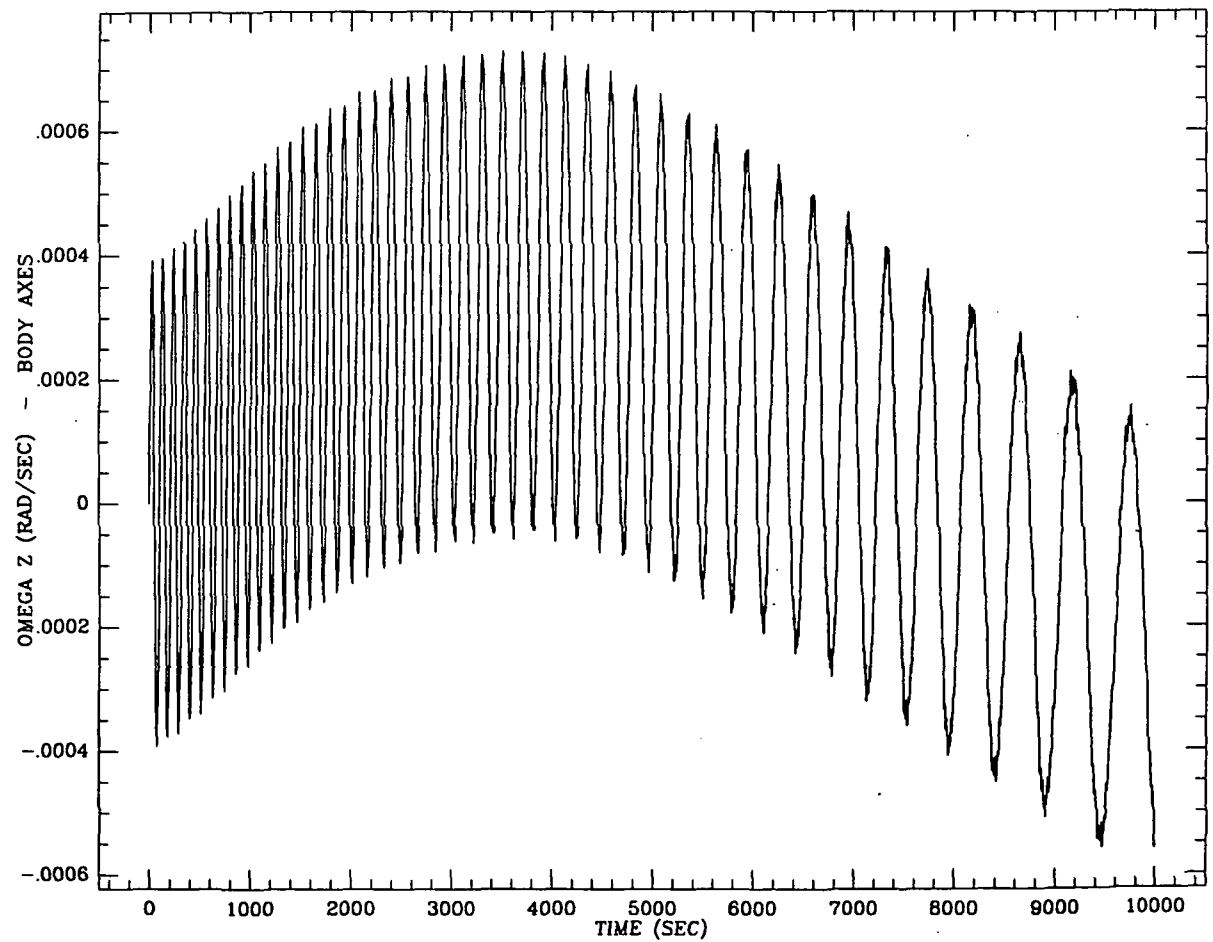

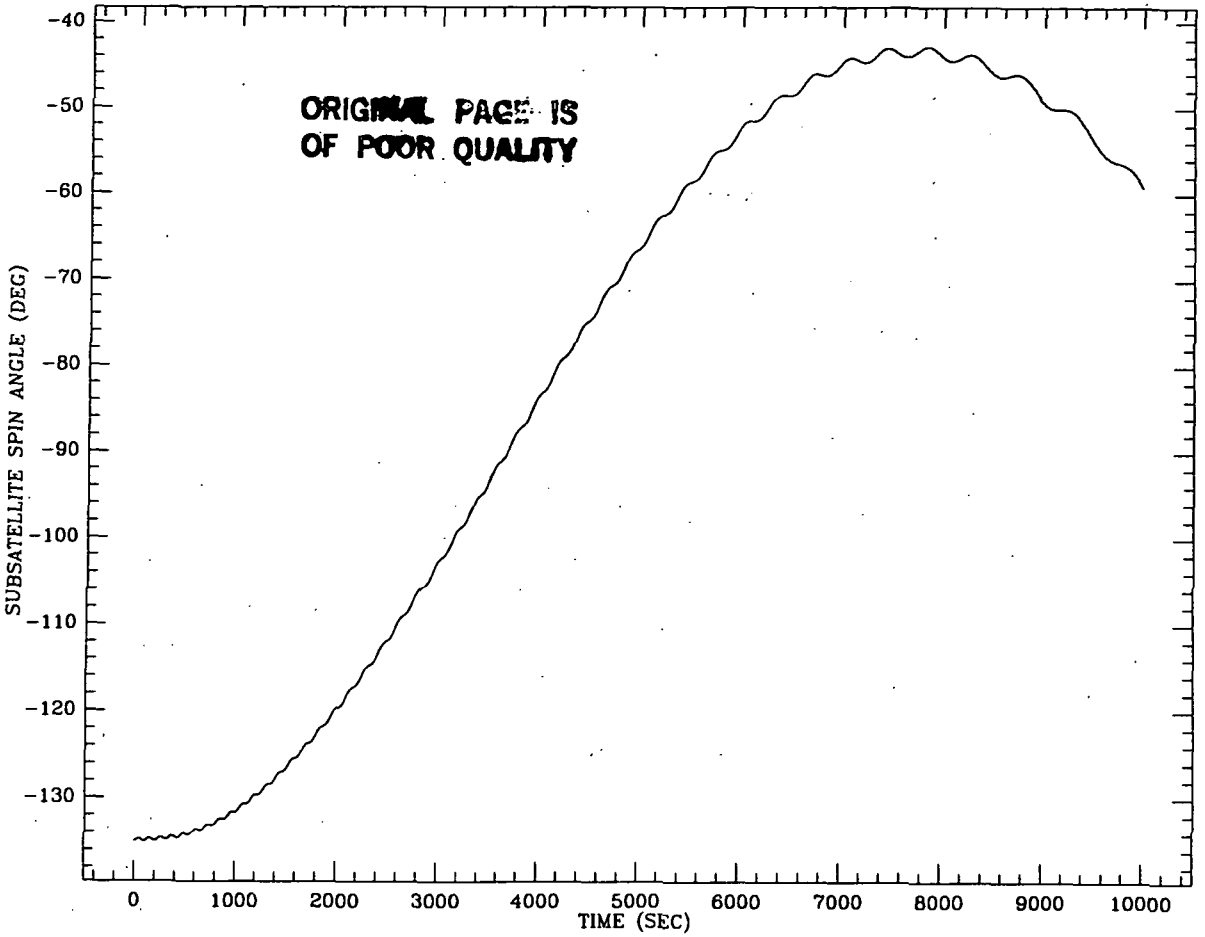

Figure 4e↑

Figure 4f↓

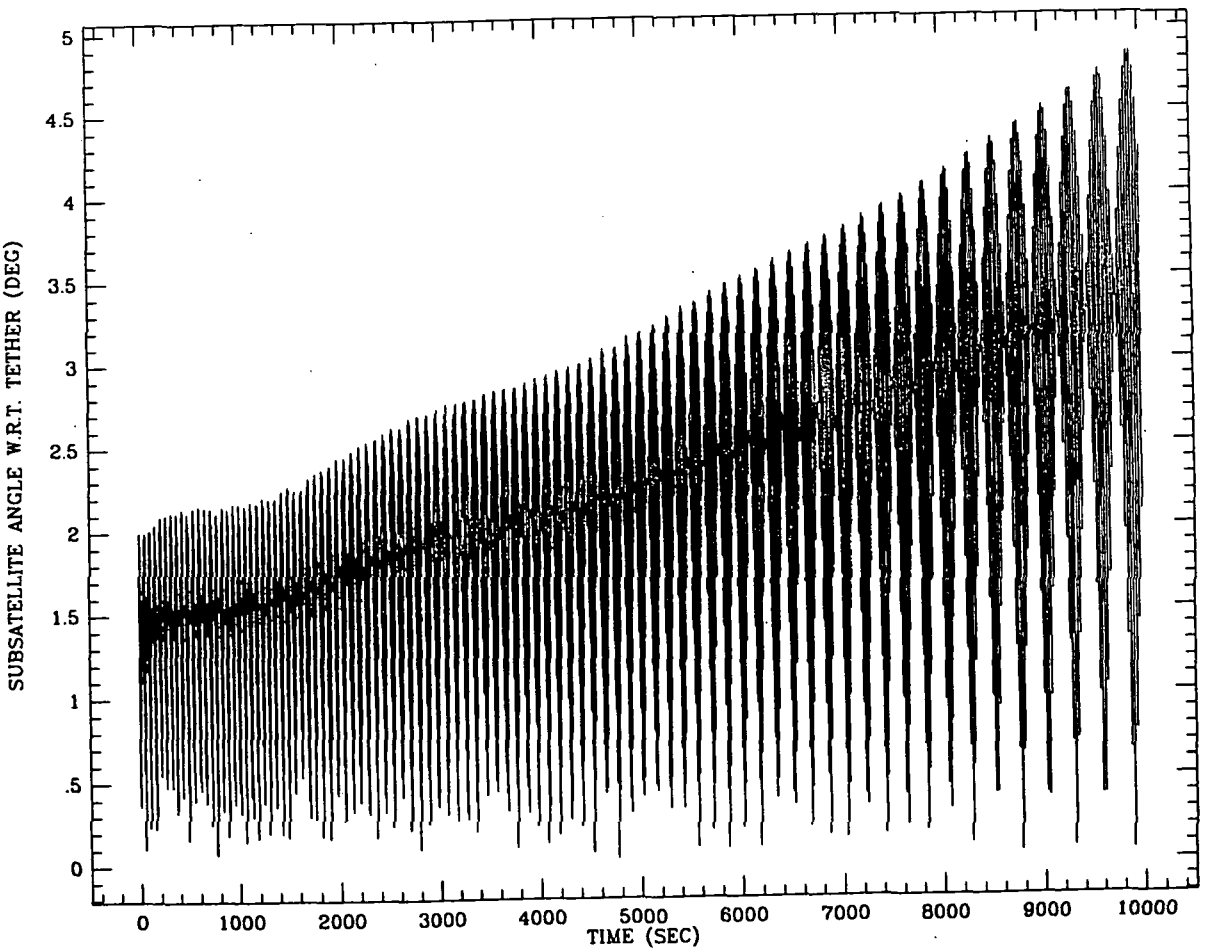

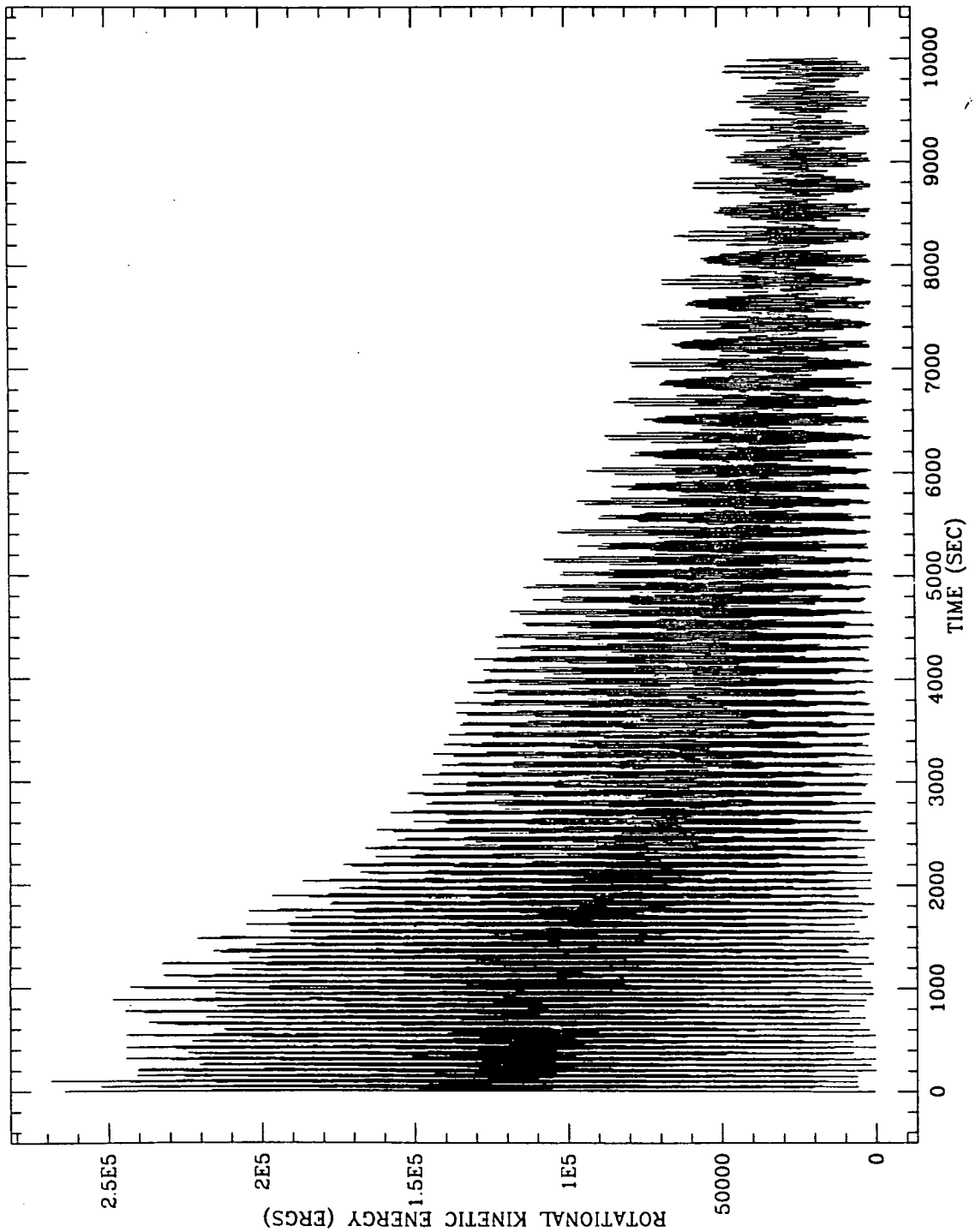
ROTATIONAL KINETIC ENERGY (ERGS)
2.5E5
2E5
1.5E5
1E5
50000
0
0
1000
2000
3000
4000
5000
6000
7000
8000
9000
10000
TIME (SEC)

Figure 4g

Table 1

Time (sec)	Tension (dynes x 10^6)	Wobble Period (sec)
0	5.35	9.0
1000	3.80	10.7
2000	2.35	13.6
3000	1.48	17.1
4000	1.15	19.5
5000	.79	23.5
6000	.53	28.6
7000	.38	33.7
8000	.27	40.3
9000	.18	48.6
10,000	.13	57.8

The numerical integration of the retrieval run took about one hour of computer time. Processing of the output files took anywhere from 5 minutes for shorter files to 20 minutes for the state vector file processed by RSTAVEC.

Since the spin of the subsatellite induced by the wobble is very small it should be possible to maintain the orientation of the subsatellite using the z-axis attitude thruster. A simulation has been done using program ROTAT with both a restoring term and a damping term in the thruster control algorithm. The restoring stiffness is 1/10 that of the wire and the damping coefficient is 1/10 of the value for critical damping of a wobble under the restoring torque of the wire. The initial conditions are $\theta = 2°$, $\dot{\phi} = .6025040423$ rad/sec and $\dot{\psi} = -.6021370130$ rad/sec. Figure 5 shows the results of a 25 second run with output every .3 seconds. Parts (a) and (b) are the z-component of the angular velocity and the spin angle about the z-axis. The maximum angular excursion is about .16 degrees. Parts (c) and (d) show the work done by the thruster, and the integrated torque of the thruster. The work done is positive because the thruster is being used in a spring mode, but the amount of fuel used is small because the wobble has a low coupling with spin about the z-axis for a 2° wobble amplitude.

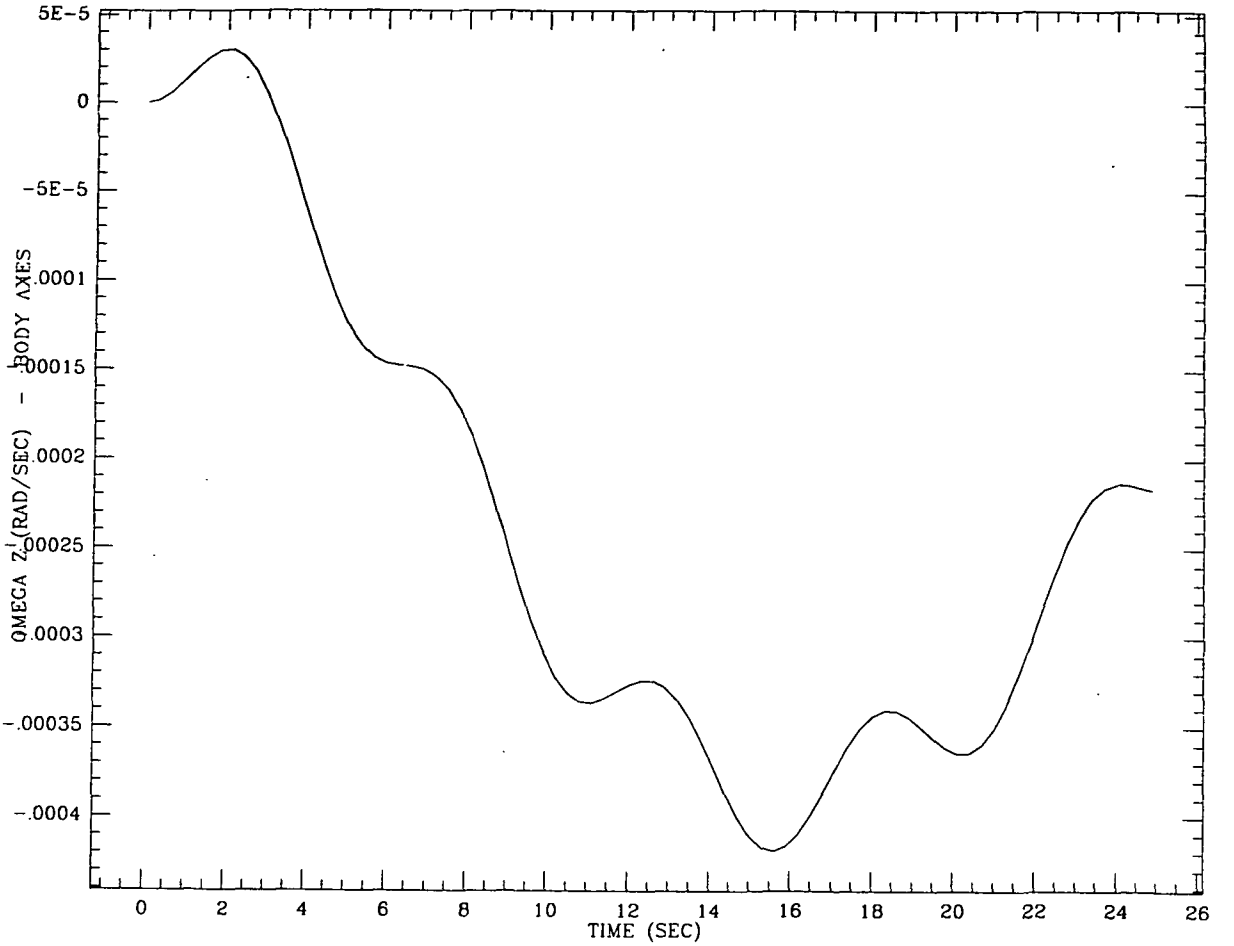

Figure 5a↑

Figure 5b↓

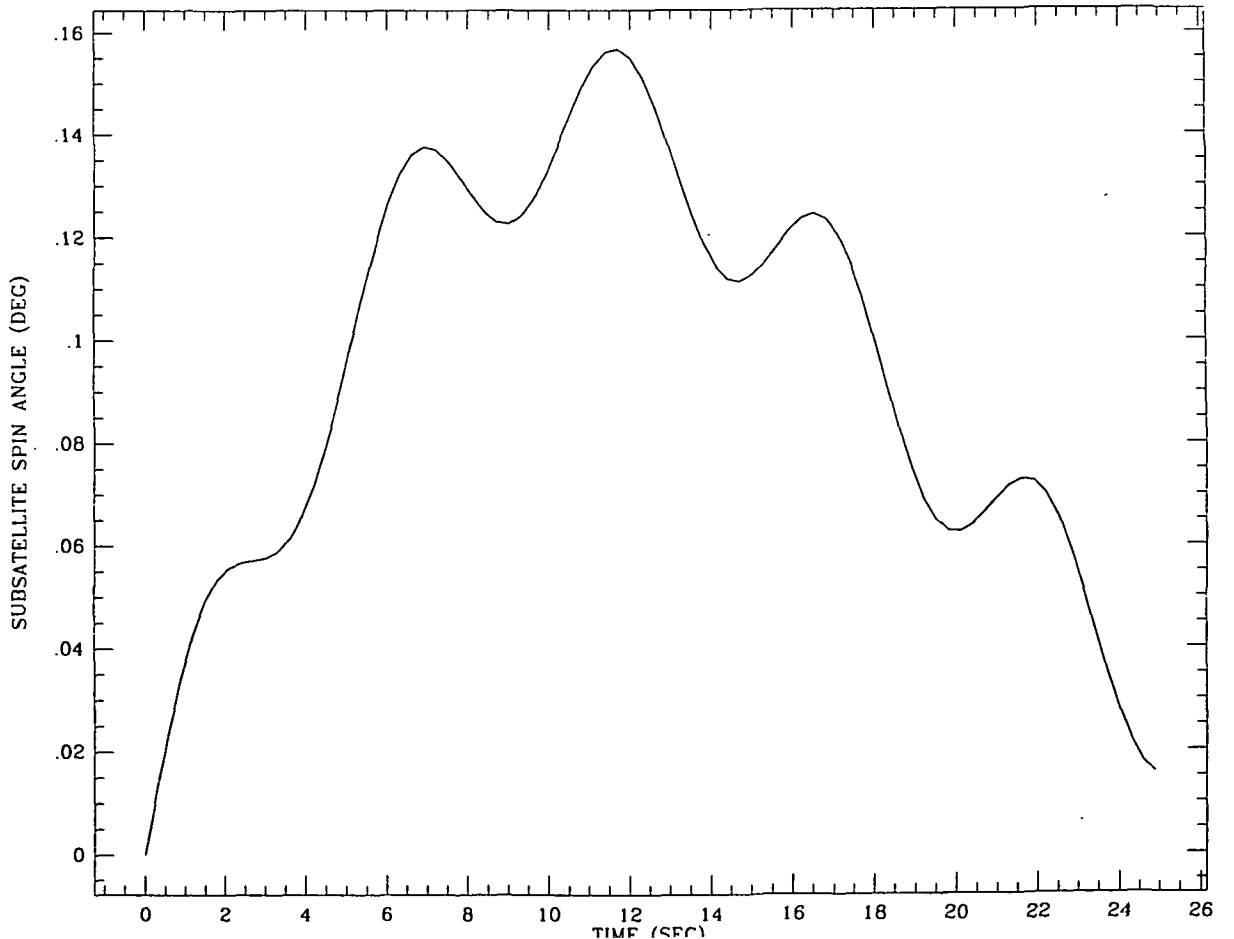

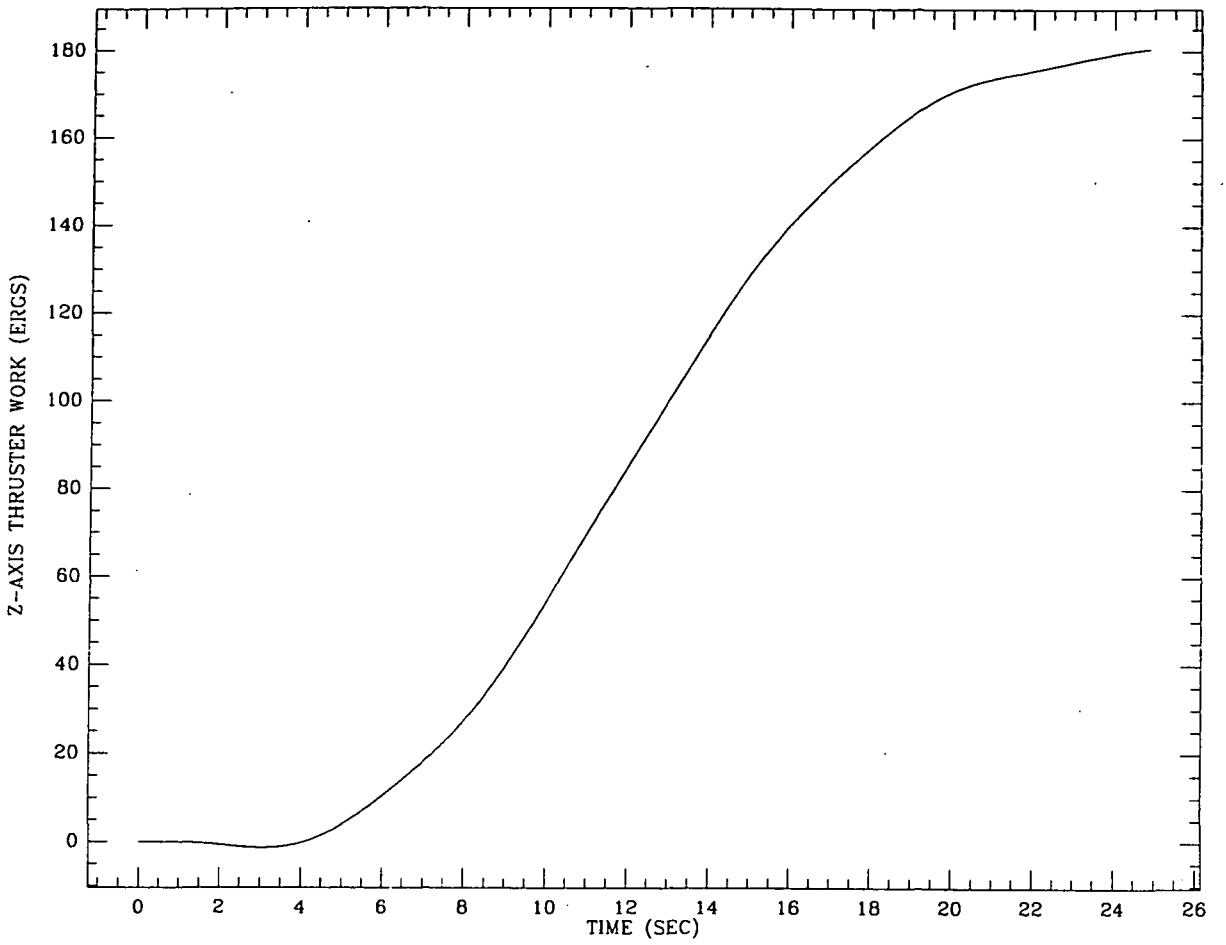

Figure 5c↑

Figure 5d↓

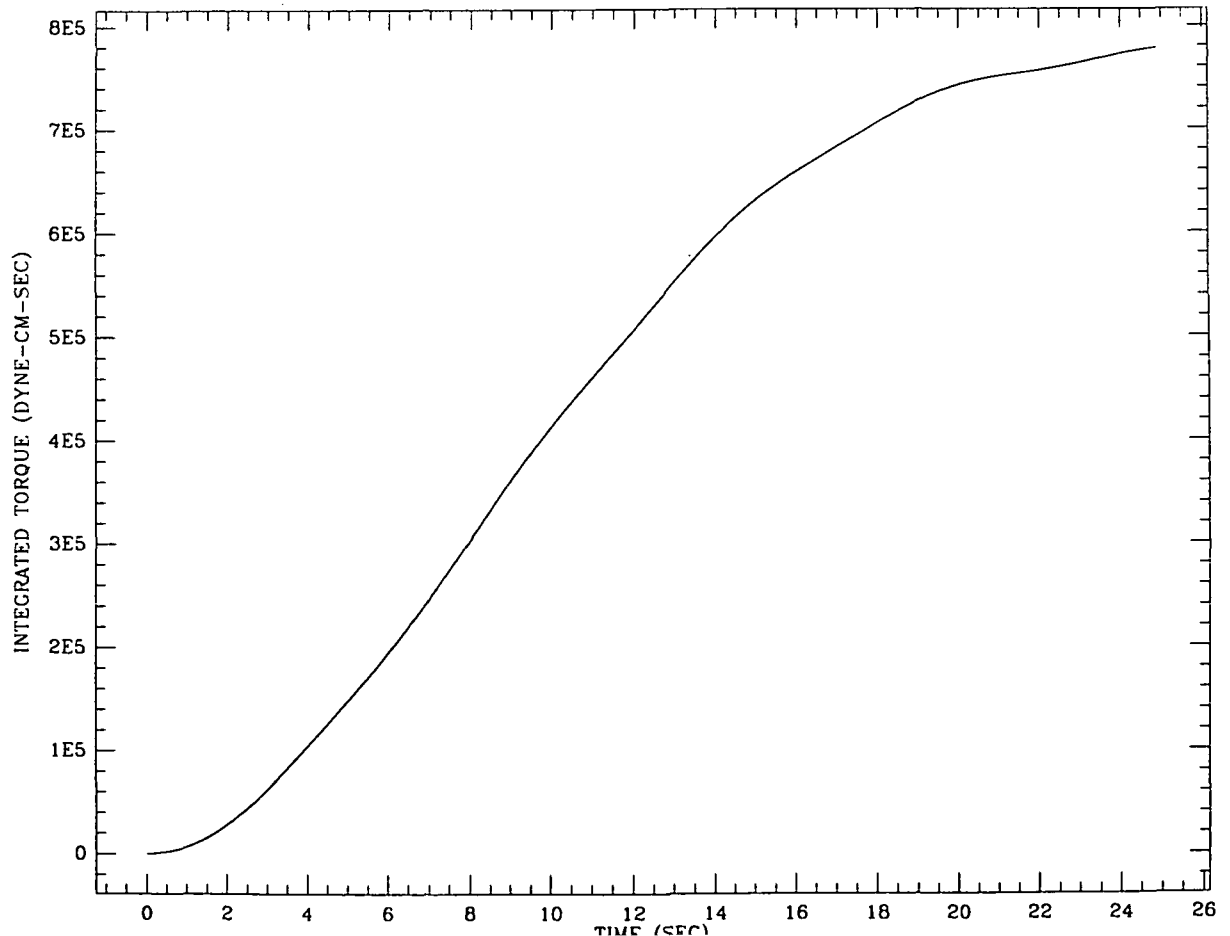

The decrease in rotational energy during retrieval shown in Figure 4g is due solely to the work done by the wire. Subtracting the work done by the wire from the rotational kinetic energy gives a constant value. The only damping in the model is the damping term in the tension control law used for retrieval. The damping term F_D in the algorithm is

$$F_D = 4m\Omega\ (\dot{\ell} - \dot{\ell}_c) \tag{15}$$

where m is the subsatellite mass (500 kg), Ω is the orbital angular velocity (.001158 rad/sec), $\dot{\ell}$ is the reeling velocity and $\dot{\ell}_c$ is the "commanded" reeling velocity. For the given values of m and Ω, the retrieval damping coefficient b_r is

$$b_r = 4\ m\ \Omega = 2316 \text{ dynes/(cm/sec)} \tag{16}$$

If the retrieval is following the commanded profile, F_D is zero. A wobble of the subsatellite with a 2° amplitude produces a maximum wire stretching $d\ell$ of

$$d\ell = r\ (1 - \cos 2°) = .049 \text{ cm} \tag{17}$$

This occurs in a quarter of a cycle, or about 2.5 seconds for a 10 second period. The average velocity is .02 cm/sec. The damping force is therefore about 45 dynes and the power about .9 ergs/second. The rotational kinetic energy decreased by about 2.2×10^5 ergs in 10,000 seconds, or an average of 22 ergs/second. From this crude analysis it appears that the damping in the control law is more than an order of magnitude too small to account for the loss of rotational energy observed during the retrieval run.

The energy integrals show clearly that the loss of rotational energy during retrieval is due solely to the work done by the wire. In general, the wire can do either positive or negative work on the subsatellite depending on how the tension varies with time. Any asymmetry of the tension during one wobble cycle can alter the rotational energy. The principle term in the retrieval algorithm is proportional to the length of the wire and should not produce the type of asymmetry that would alter the energy.

The next section describes a mechanism whereby the rotational energy can change as a result of slowly varying changes in the tension.

2.1.4 Angular Oscillation Amplitude As A Function Of Tether Tension -

Suppose a spherically symmetrical subsatellite is executing a perfect wobble such that the attachment point of the wire moves in a circle perpendicular to the mean direction of the wire. If the tension slowly decreases, the radius of rotation of the attachment point will increase. In the process, the body does work against the restoring torque of the wire. Let us assume that the tension changes are slow enough that the attachment point continues to rotate in a circle whose radius varies as the tension changes. Under these assumptions it is possible to derive an analytic expression for the angle of the wobble as a function of the tether tension using the principle that the decrease in rotational kinetic energy is equal to the work done against the torque of the wire.

The final equation obtained from the derivation is

$$\theta \sim F^{-1/4} \qquad (18)$$

where θ is the angular amplitude of circular wobble and F is the wire tension. The complete details of the derivation are contained in Section 1.0 of Technical Note TP86-002, January 1986. This technical note is included as Appendix B of Quarterly Report #6, March 1986 for this contract.

Equation (18) has been used to analyze the case of Figure 4. Table 2 shows as a function of time the wire tension F, the wobble amplitude θ, and the predicted wobble angle $\theta_o(F_o/F)^{1/4}$. The last column is the percentage error in the observed wobble amplitude. The percentage error is increasing with time, but in general the data agrees quite well with equation (18). The discrepancies observed could be due to the effect of the damping in the retrieval control law. As a check on this, the rotational kinetic energy E of the last entry has been computed using the formula

$$E = r\ F\ \theta^2/2 \qquad (19)$$

where r is the radius of the subsatellite. Using this equation, the actual energy of the last entry is 38,100 ergs and the predicted value is 41,300 ergs. The discrepancy is about 3200 ergs which is .3 ergs/sec. This is well within the estimate of .9 ergs/sec for the damping in the retrieval law. The damping should be greatest at the beginning when the frequency is highest.

Table 2

t (sec)	F (dynes x 10^6)	θ (deg)	$\theta_o(F_o/F)^{1/4}$	%Error
0	5.356	2.000	2.000	.0
101	4.817	2.044	2.054	.5
208	4.434	2.096	2.097	.0
485	4.000	2.145	2.151	.3
1008	3.795	2.172	2.180	.4
2045	2.288	2.463	2.474	.4
3074	1.445	2.760	2.775	.5
4086	1.119	2.931	2.958	.9
5025	.780	3.194	3.238	1.4
6020	.526	3.520	3.573	1.5
7047	.376	3.808	3.885	2.0
8054	.261	4.153	4.255	2.5
9033	.182	4.520	4.658	3.1
9912	.134	4.831	5.029	4.1

Equation (18) was derived under very specialized conditions. In the retrieval run of Figure 4, there are various factors that differ from the conditions under which the equation was derived. The damping in the control law is probably the principal factor causing the observed discrepancies. The retrieval included both linear and circular wobble of the subsatellite as a result of the unequal moments of inertia. The relative success of the formula suggests that it is valid for a linear as well as a circular wobble of the subsatellite.

As noted earlier the long retrieval run used to create the data of Figure 4 required about a hour or computer time. In addition, some of the postprocessing runs took as much as 20 minutes. Almost all of the information needed for plotting is available during the integration. In order to save time, it has been decided to add extra output files to the integration program which contain various data ready for plotting. A file FOR012 has been added containing the time, Euler angle θ in the tether coordinate system, the rotational kinetic energy E_k, and the "total energy" obtained by subtracting the work done by the wire from the kinetic energy. Another file FOR013 has been created containing

the time, and the components of the body x and z axes in the tether coordinate system. This file is used to plot the motion of the axes, and can be used to compute the spin angle of the subsatellite. A new program called PLOTMO has been created for generating printer page plots of any of the quantities on the new output files.

Since the retrieval run involved various effects that differ from the conditions under which equation (18) was derived it was decided to run some tests under more controlled conditions using program ROTAT. In the first of these tests the tension F instead of being computed from the stretch of the wire is varied according to the equation

$$F = F_o\, e^{-ct} \tag{20}$$

where F_o is the initial tension and c is the time constant. A test run has been done with the parameters $\theta = 2°$, $\phi = \psi = 0$, and $c = .01$. The integration was done for 200 seconds. Figure 6 shows the results of the run. Part (a) is the tension vs. time, part (b) is the Euler angle θ, part (c) is the rotational kinetic energy and part (d) is the spin angle of the subsatellite. The Euler angle in part (b) is the absolute value of the spin angle in part (d) for this case. The tension in part (a) shows more noise than expected. The problem turned out to be an error in the call to the subroutine that computes the values of various parameters at each output time. The subroutine was given the integration time instead of the output time. The tension in this case is an explicit function of the time rather than being a function of the state vector (which was correctly interpolated and passed to the subroutine).

Table 3 shows a comparison of the observed oscillation amplitudes with equation (18).

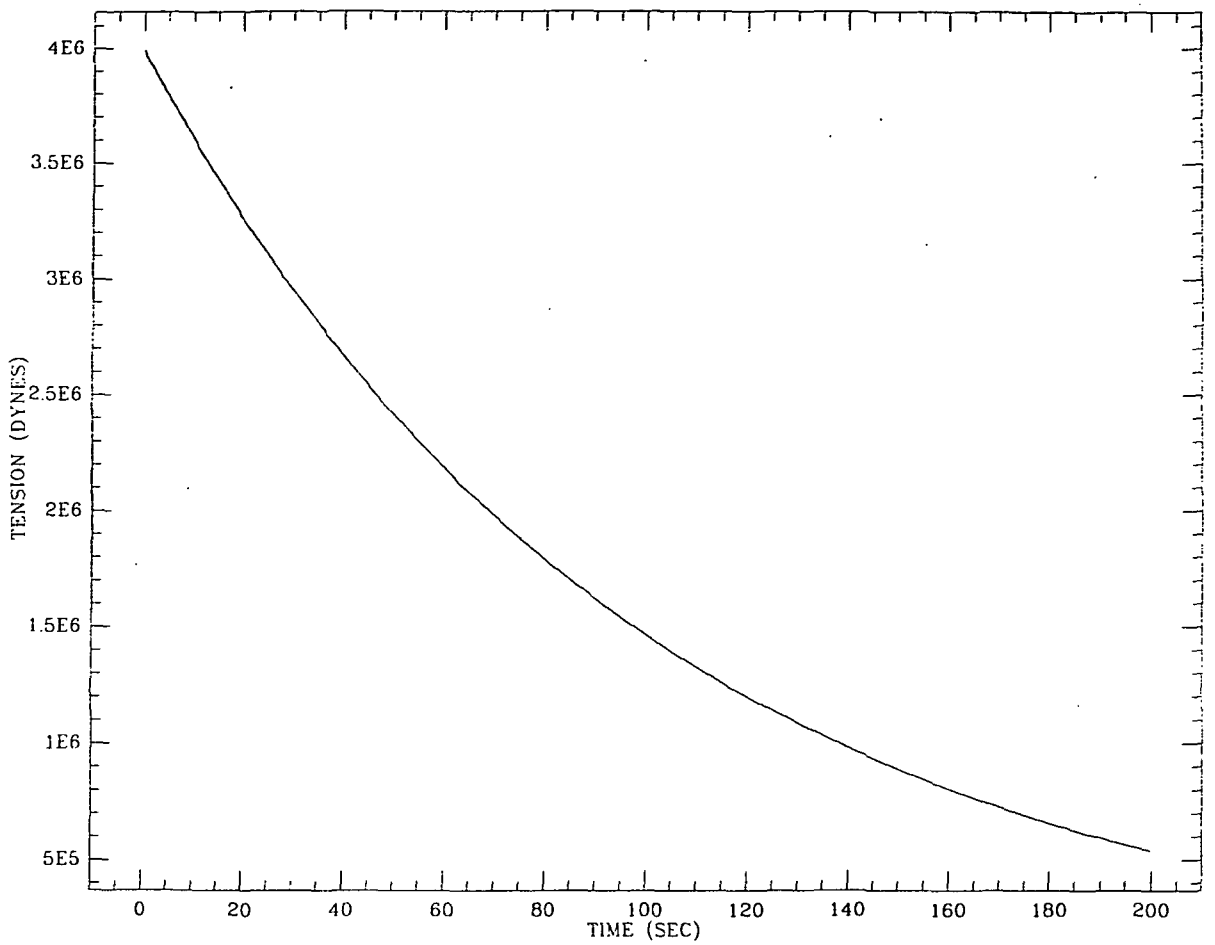

Figure 6a↑

Figure 6b↓

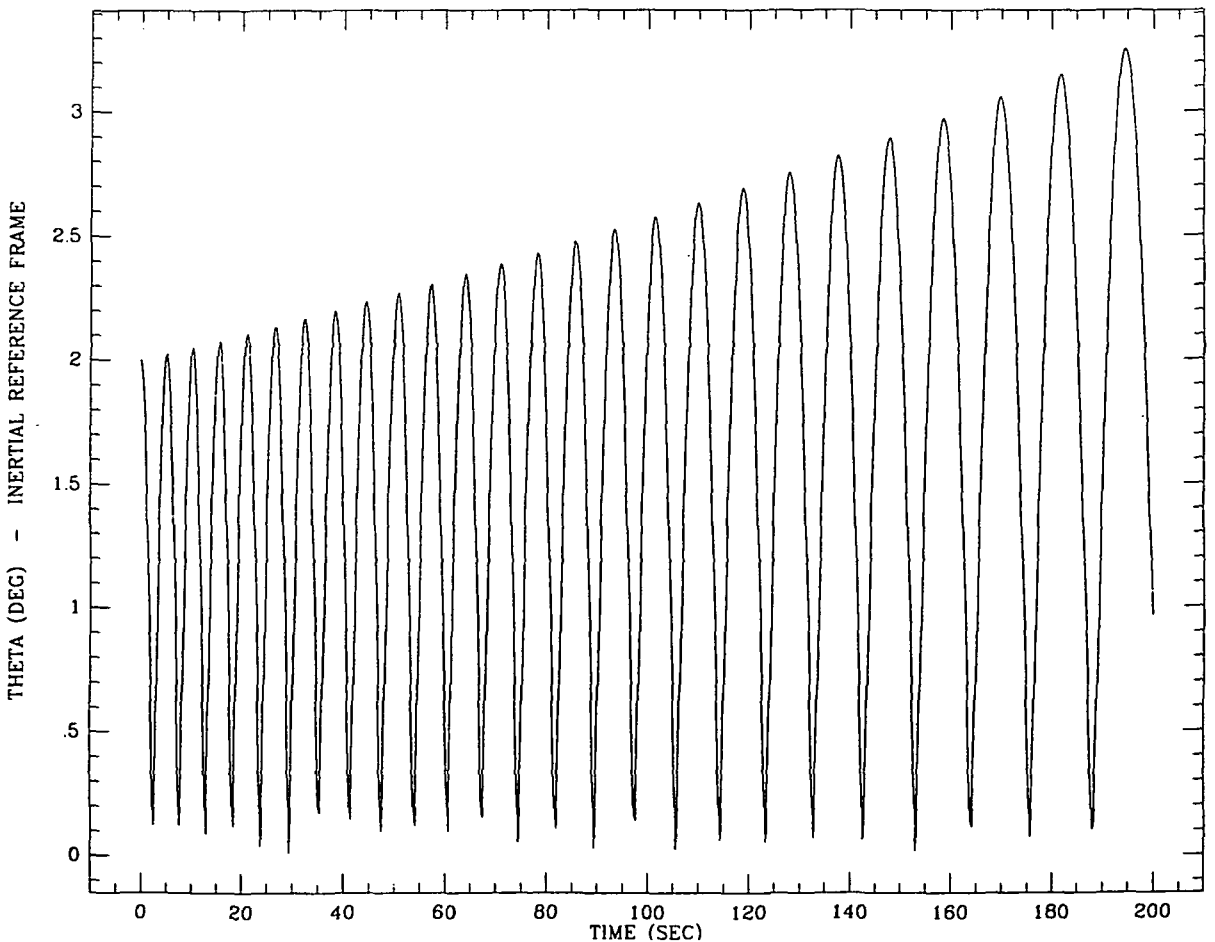

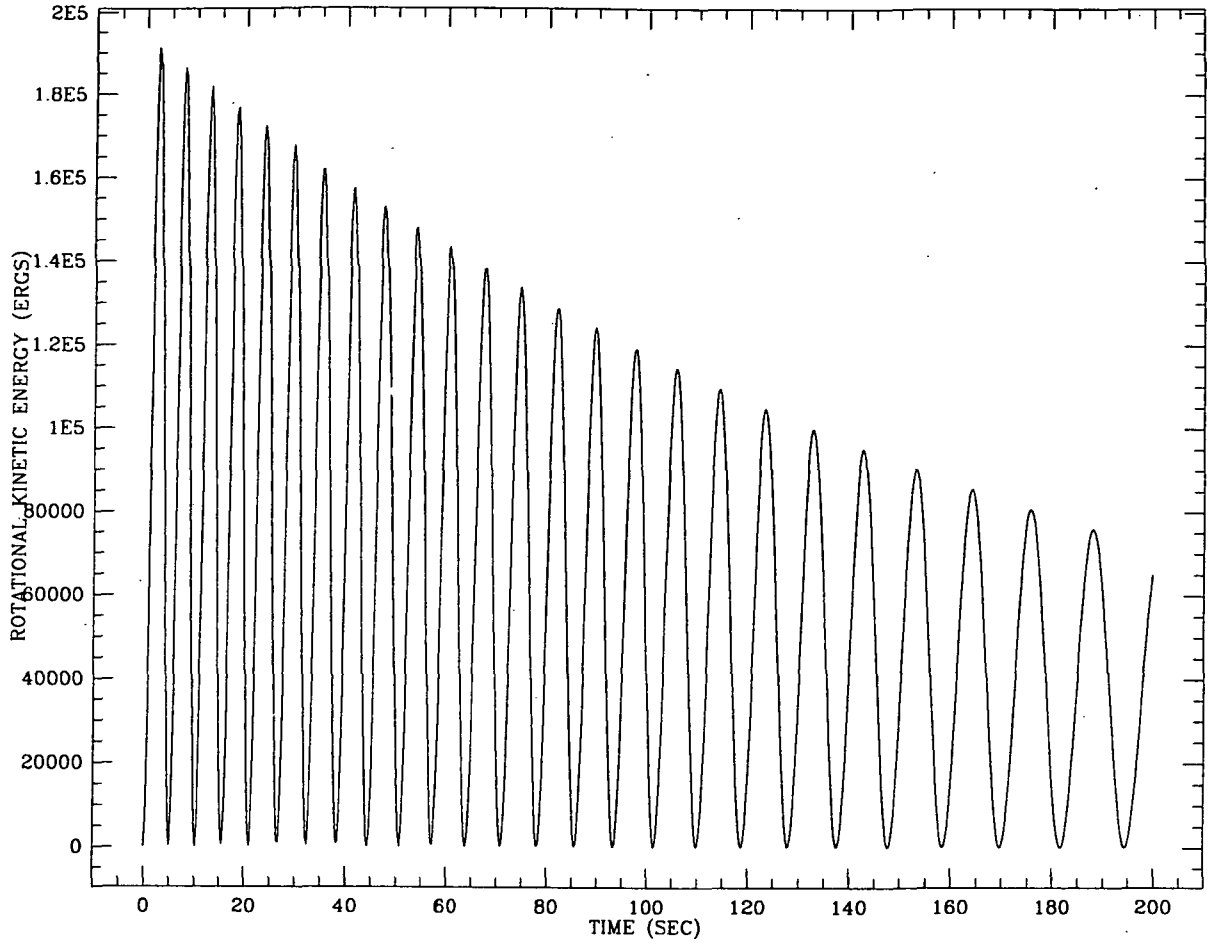

Figure 6c↑

Figure 6d↓

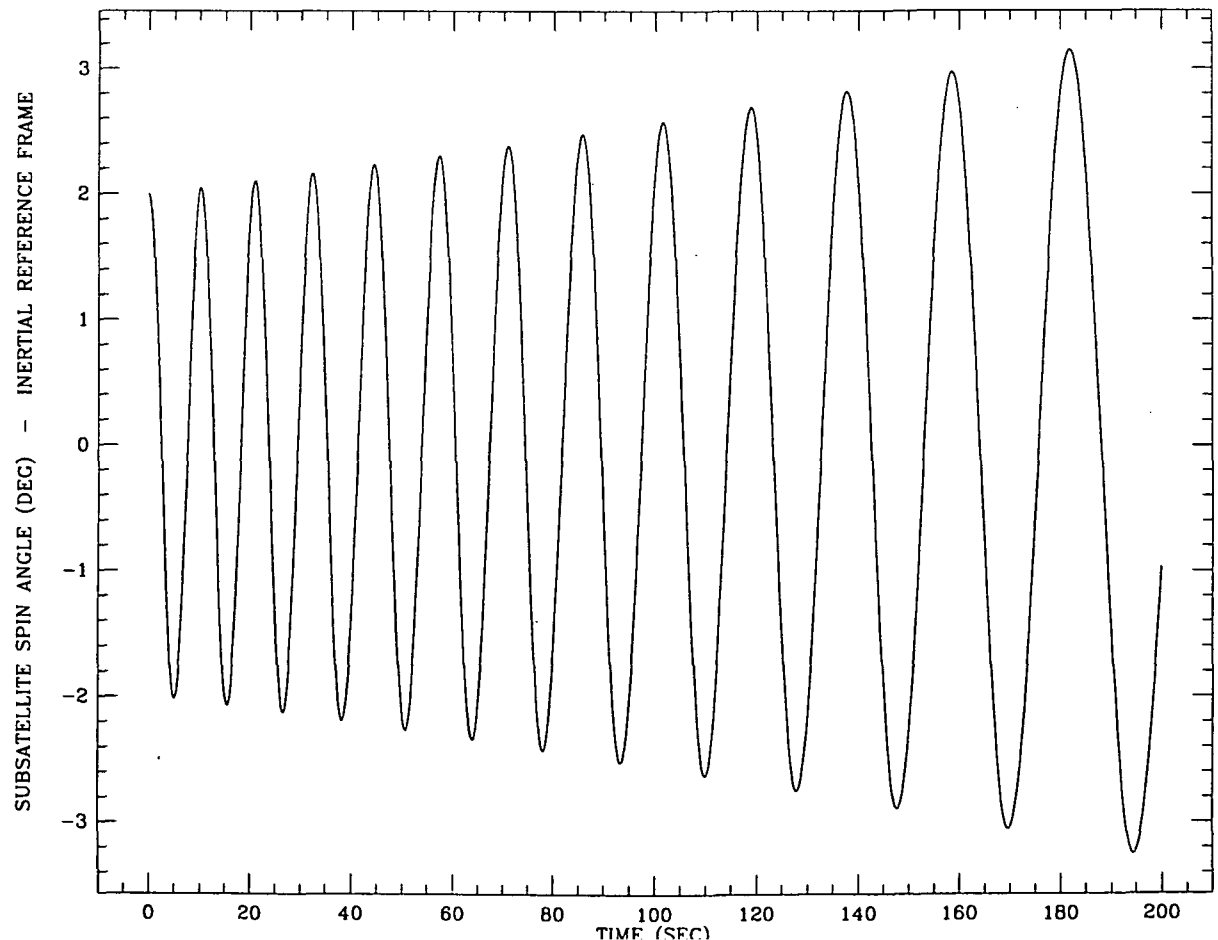

Table 3

t (sec)	F (dynes x 10^7)	θ (deg)	$\theta_o(F_o/F)^{1/4}$	%Error
0.000000	.3990530	2.000000	2.000000	
15.506974	.3417312	2.079027	2.079057	.0014
32.317990	.2888520	2.168278	2.168297	.0009
50.673044	.2404143	2.270112	2.270113	.0001
70.884693	.1964185	2.387769	2.387768	-.0001
93.371668	.1568638	2.525848	2.525847	-.0001
118.711907	.1217507	2.691027	2.691038	.0004
147.736041	.0910796	2.893544	2.893559	.0005
181.701447	.0648502	3.149947	3.149995	.0015

The time in the first column is the time of a maximum in the plot of the angle θ or the spin angle. These times are obtained by quadratic interpolation of the output points at .3 second intervals. The wire tension F in the second column is calculated from the time t using equation (20). The values of θ in the third column are computed by quadratic interpolation from the output at .3 second intervals. The fourth column is the angle θ computed from equation (18). The last column is the percentage error in the computed value of θ. The agreement of the observed values of θ with equation (18) is virtually exact in this simulation. The observed residuals may be interpolation error. The close agreement indicates that equation (18) can be applied to the case of a linear oscillation.

A second test has been run applying equation (20) to a circular wobble. The initial conditions are $\theta = 2°$, $\dot{\phi} = .5680462585788$ rad/sec and $\dot{\psi} = -.5677002201461$ rad/sec and the moments of inertia are 99 kg-m^2 for all axes in order to give a perfect circular wobble initially. The run was done with and without the error in the time passed to the output subroutine. The output value of F was the only quantity affected by the error. Figure 7 shows the results of the run. Part (a) is the tension vs. time. The plot is free of the slight noise observed in Figure 6a. Part (b) is the angle θ vs. time, part (c) is the rotational kinetic energy, and part (d) is the motion of the body z'-axis as

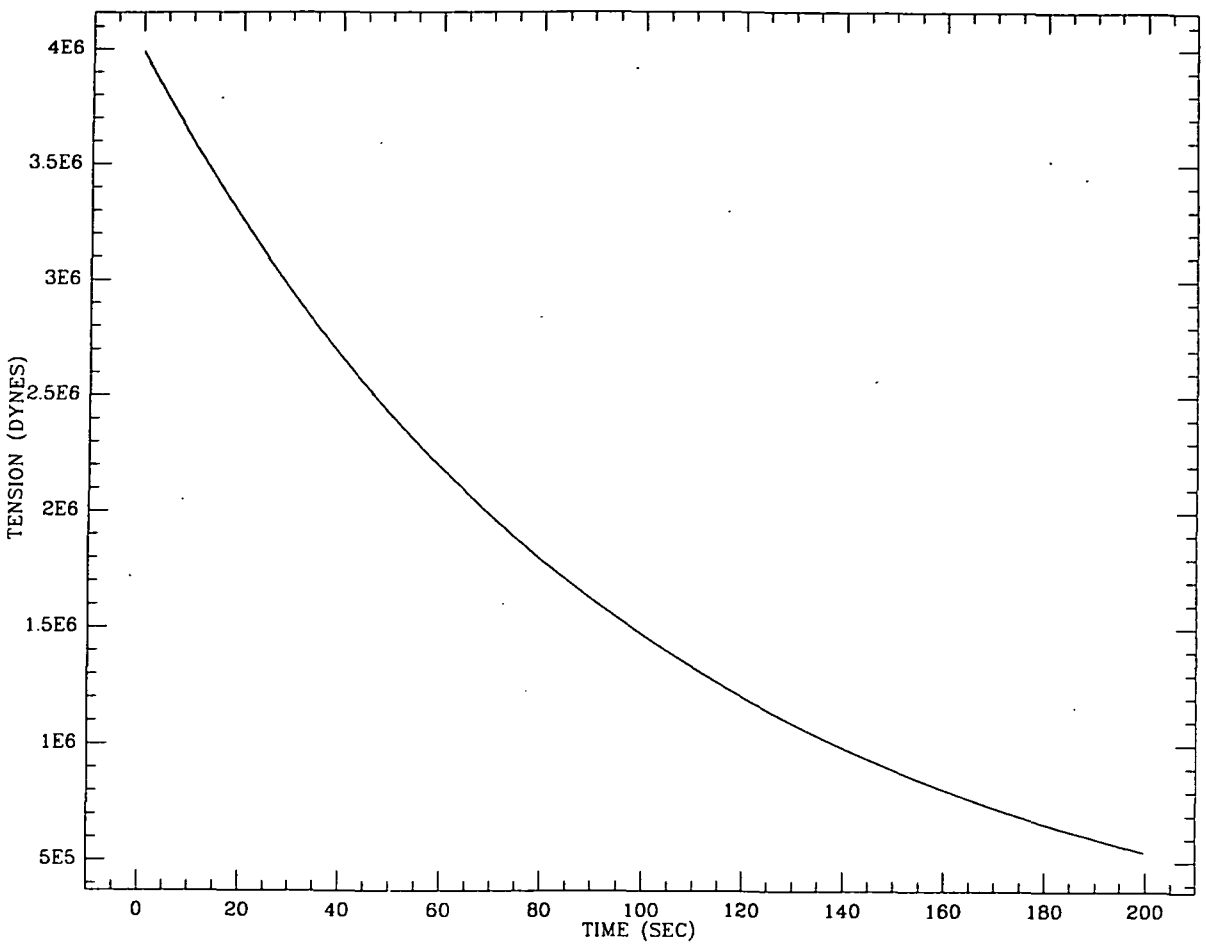

Figure 7a↑

Figure 7b↓

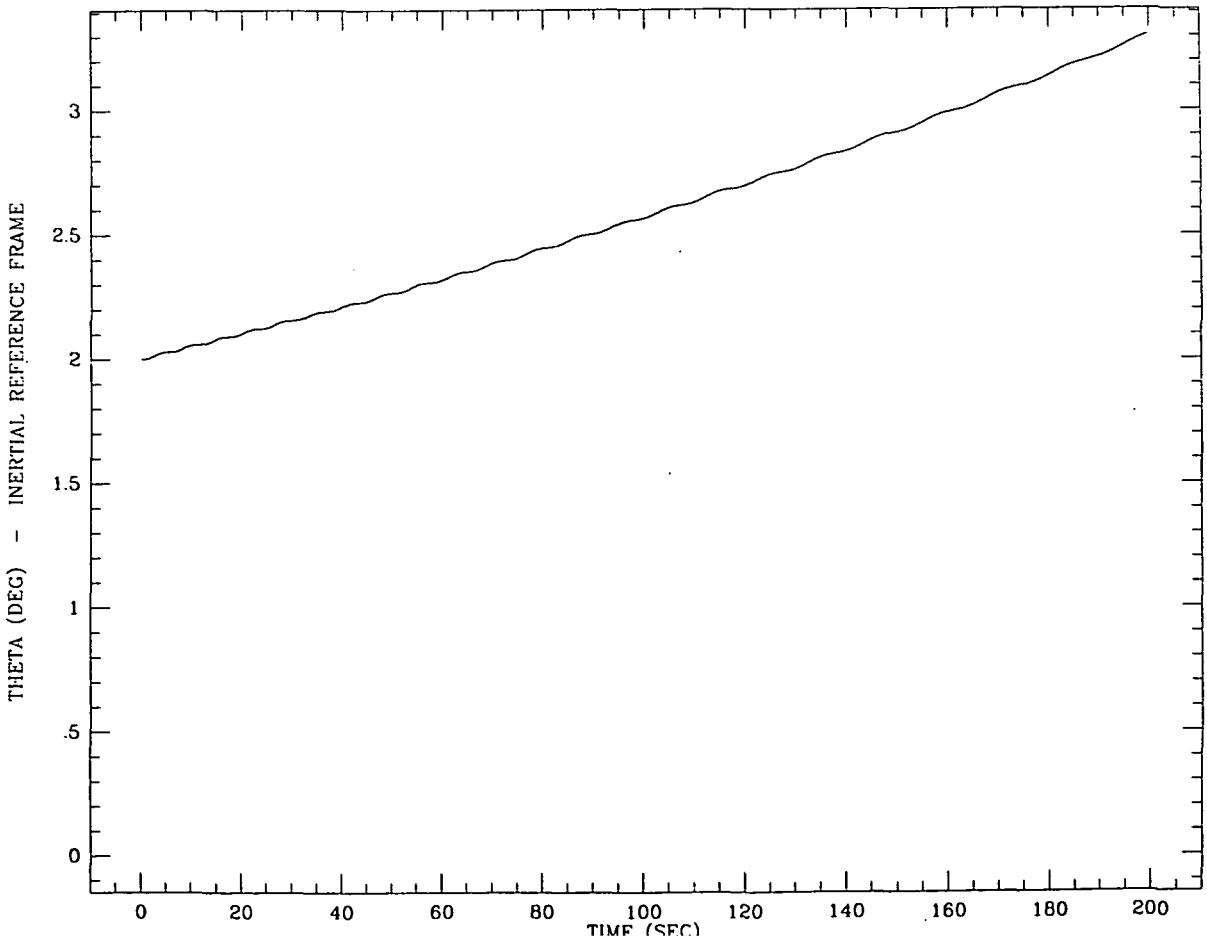

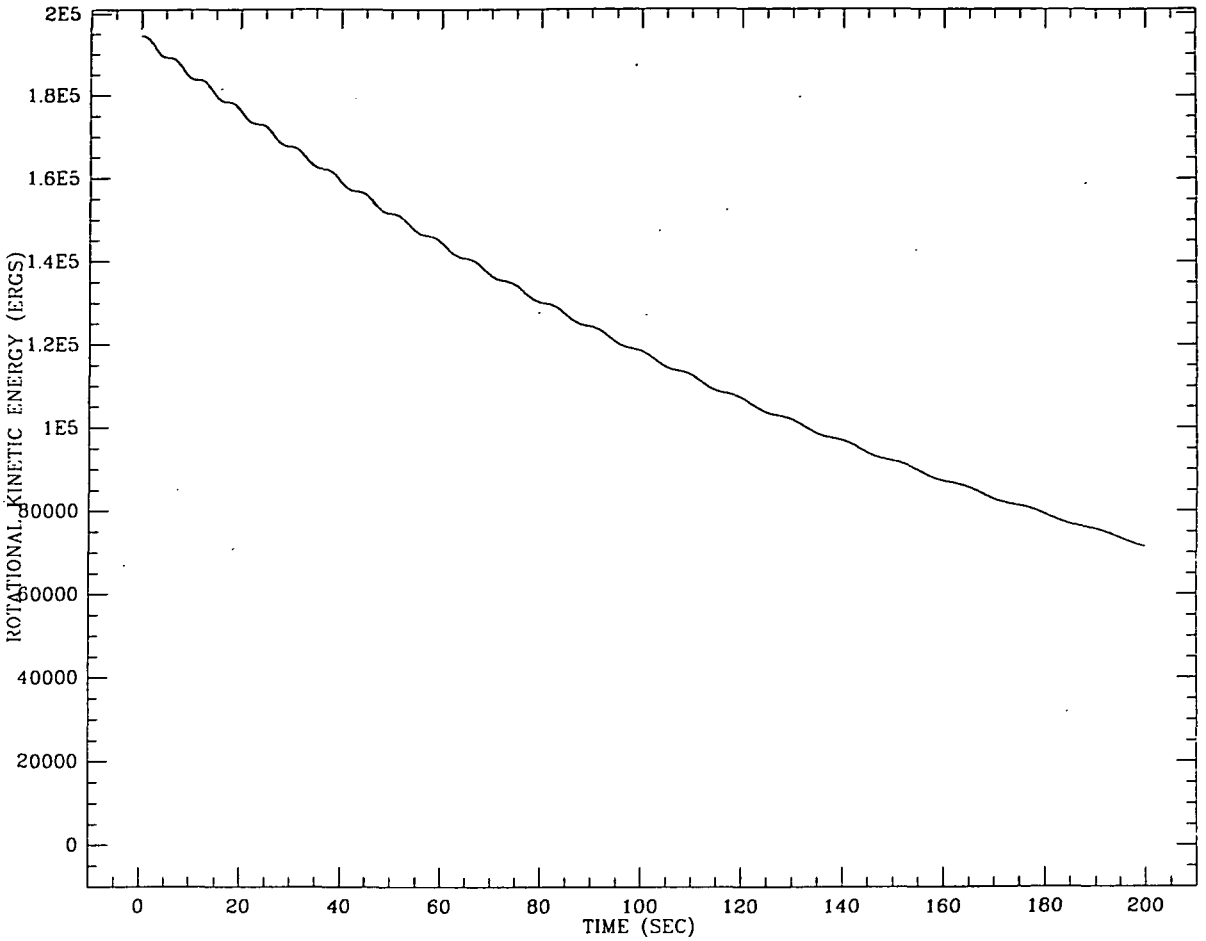

Figure 7c↑

Figure 7d↓

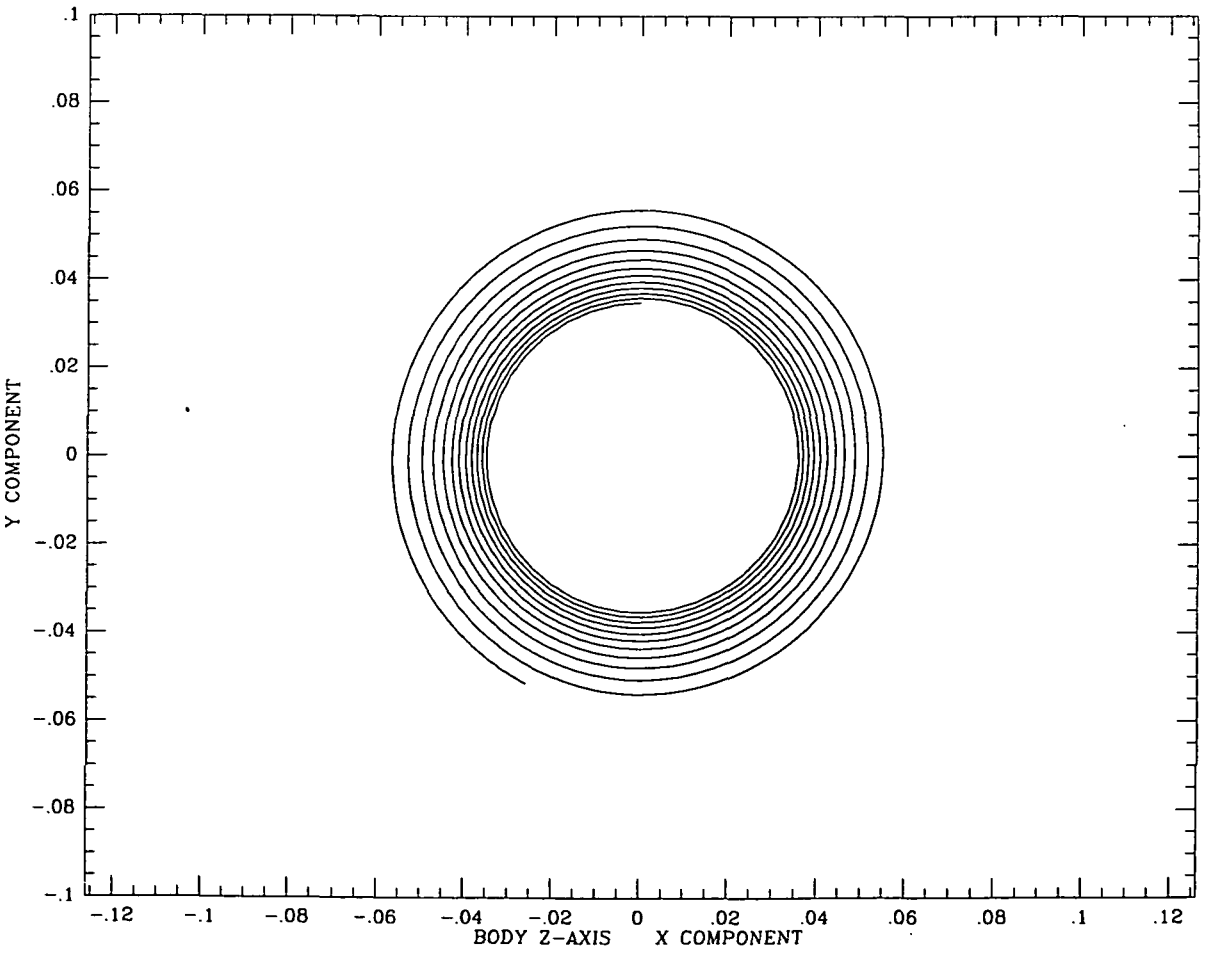

seen from the wire.

The plot of the angle θ shows an oscillation superimposed on the secular change. In order to determine the phases of the oscillation, program PLOTMO has been modified to compute and plot the derivative as well as the value of each quantity being displayed. This facility has been used to locate the maxima and minima of the slope of the θ plot. If we assume the fluctuation in θ is sinusoidal, a maximum or minimum of $\dot{\theta}$ should correspond to a mean value of θ. The point 1/4 cycle after a maximum of $\dot{\theta}$ should be a maximum value of θ and a point 1/4 cycle after a minimum of $\dot{\theta}$ should be a minimum of θ. The data of Figure 7 covers a 200 second interval with output every .3 seconds. A set of points near the end at various phases of the θ oscillation has been compared to equation (18). The results are shown in Table 4

Table 4

t (sec)	Phase of θ	F (dynes x 10^6)	θ (deg)	$\theta_o(F_o/F)^{1/4}$ (deg)	%Error
0.0		3.9905303	2.00000		
167.4	AV	.7482068	3.03923	3.03936	.004
170.7	MAX	.7239189	3.07142	3.06454	-.224
174.0	AV	.7004195	3.09000	3.08993	-.002
177.3	MIN	.6776828	3.10881	3.11552	.216
180.6	AV	.6556843	3.14119	3.14133	.004
183.9	MAX	.6343998	3.17444	3.16736	-.223
187.5	AV	.6119676	3.19660	3.19599	-.019

The results show that the average value of θ agrees well with equation (18). The peak values of θ are higher than the calculated value and the minimum values are lower. Table 5 shows a comparison with equation (18) of various average values of θ selected from the extrema of $\dot{\theta}$.

Table 5

t (sec)	F (dynes x 10^6)	θ (deg)	$\theta_o(F_o/F)^{1/4}$	%Error
0.0	3.9905303	2.00000		
20.4	3.2541273	2.10480	2.10465	-.007
33.0	2.8688869	2.17195	2.17200	.002
46.5	2.5065921	2.24653	2.24655	.001
64.8	2.0874101	2.35164	2.35172	.003
80.7	1.7805532	2.44709	2.44708	.000
102.6	1.4303571	2.58505	2.58480	-.010
143.4	.9511572	2.86241	2.86236	-.002
174.0	.7004195	3.09000	3.08993	-.002

The agreement is quite good over the whole range. The errors observed may be due to the lack of interpolation to obtain the values at the extrema of $\dot{\theta}$. The times can be in error by up to .05 seconds.

In the next test of equation (18), the tension F is varied according to the equation

$$F = F_o\,[1 - .9 \sin(.01\pi t)] \tag{21}$$

For convenience in plotting, two extra quantities have been added to the output file FOR012. They are the wire tension and wire length making a total of 6 quantities in all. The initial conditions for the run are $\theta = 2°$, $\phi = \psi = 0$, so that the oscillation is linear with no wobble. Figure 8 shows the results of the 200 second simulation. Part (a) is the tension vs. time, part (b) is the Euler angle θ, part (c) is the rotational kinetic energy, part (d) is the rotation angle, and part (e) is the angular velocity. The angle θ in part (b) is the absolute value of the rotation angle in part (d). The angular velocity about the body y and z axes is zero since the rotation is one dimensional. Table 6 shows a comparison of the peak values of θ with equation (18). The first column is the time in seconds, the second is the tension calculated from

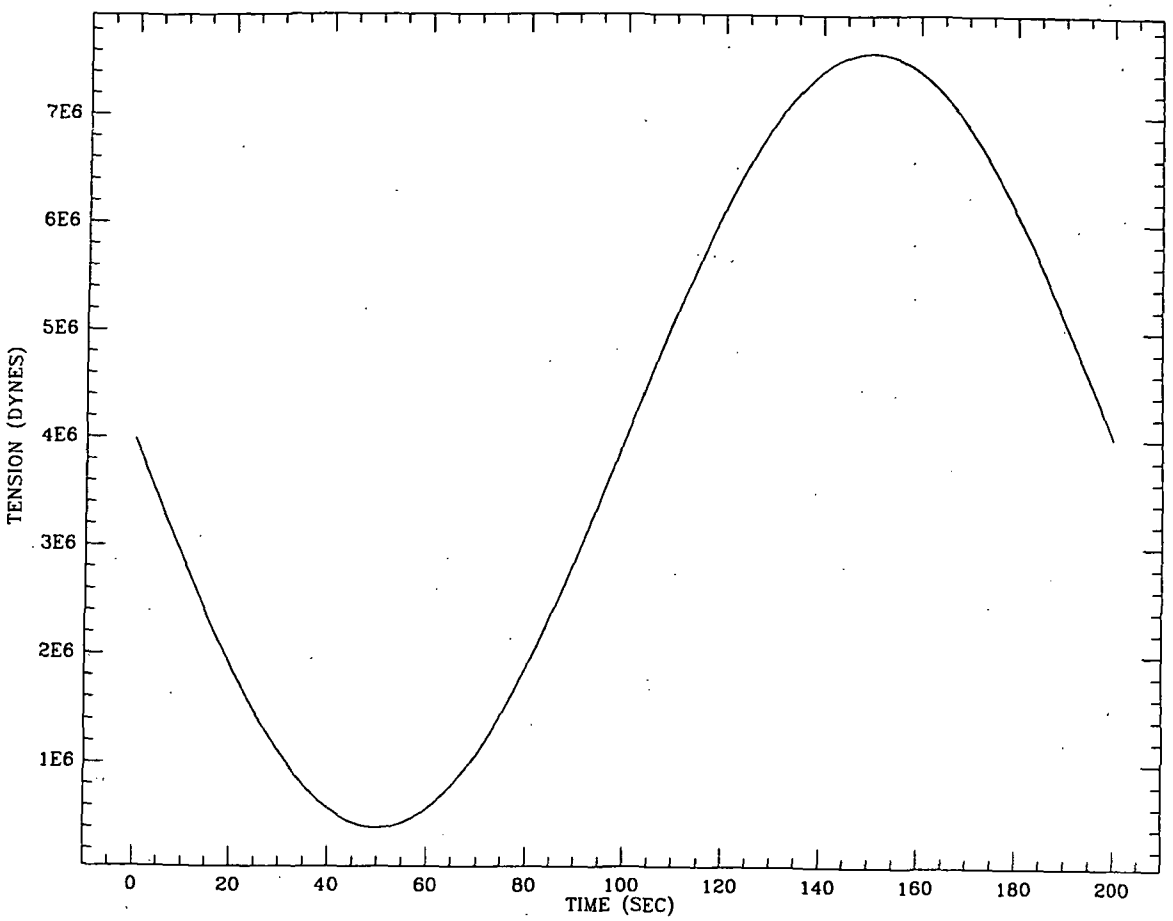

Figure 8a↑

Figure 8b↓

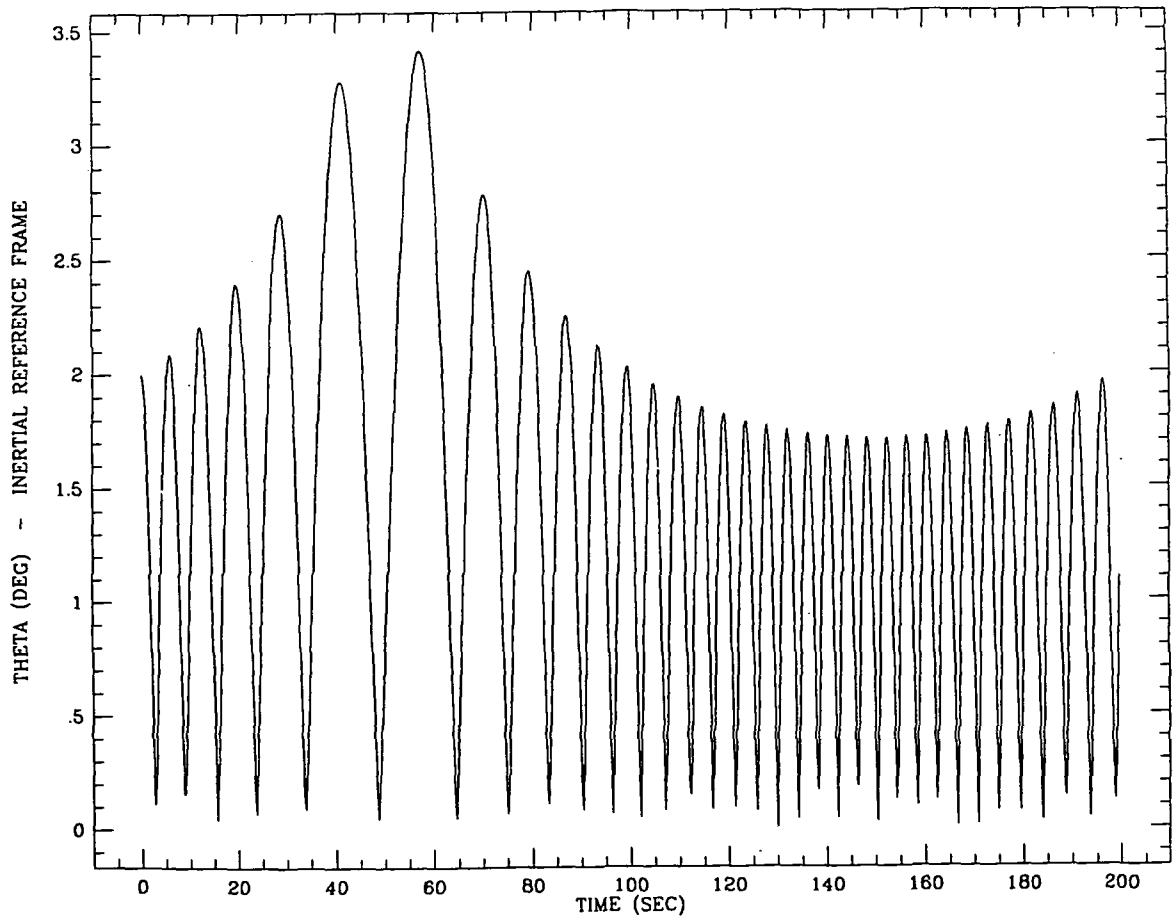

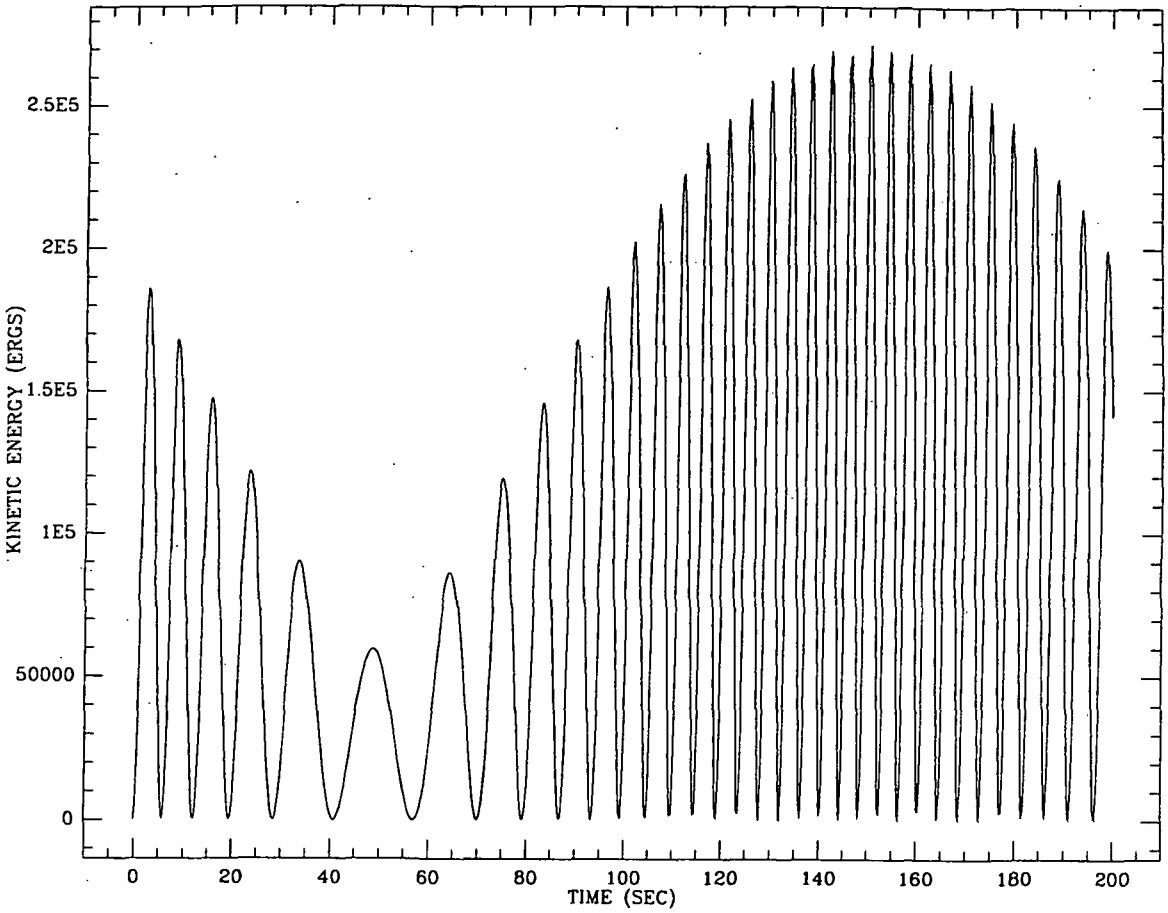

Figure 8c↑

Figure 8d↓

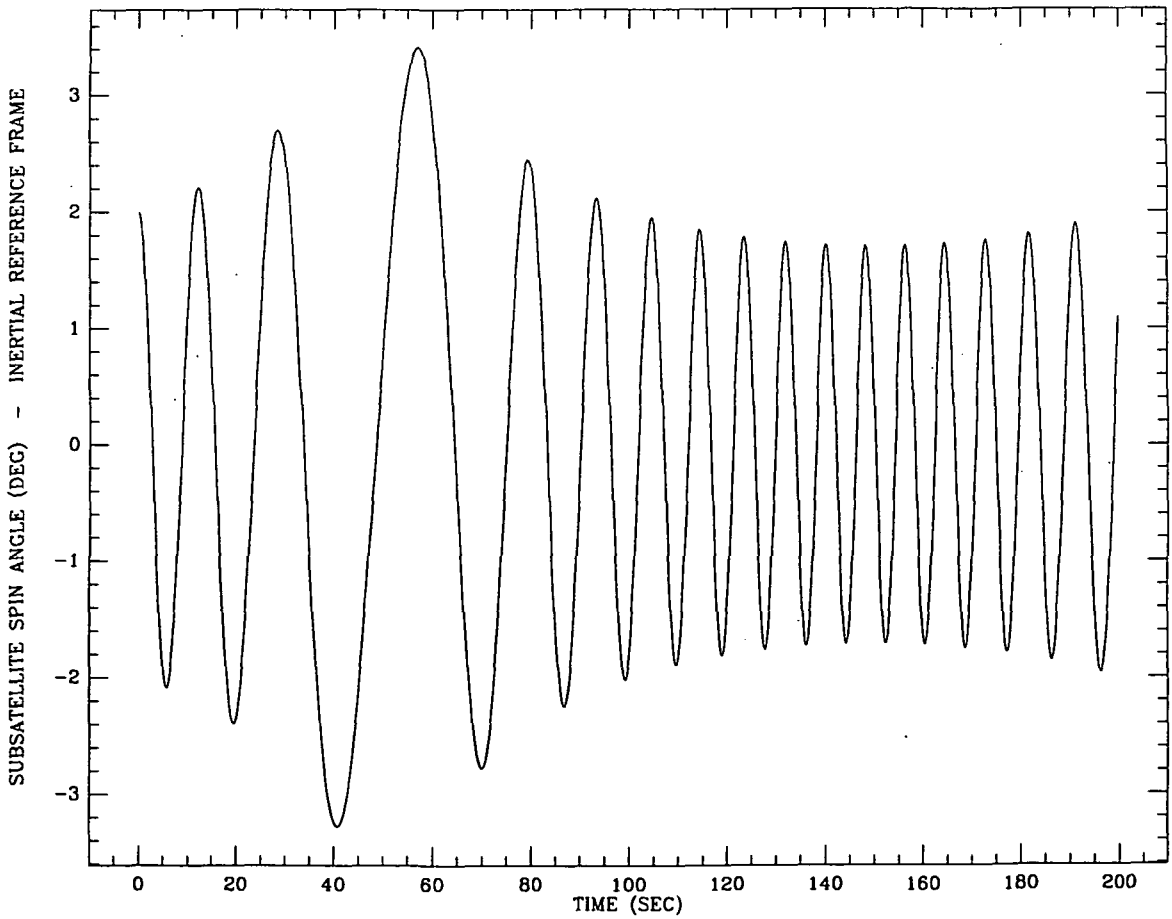

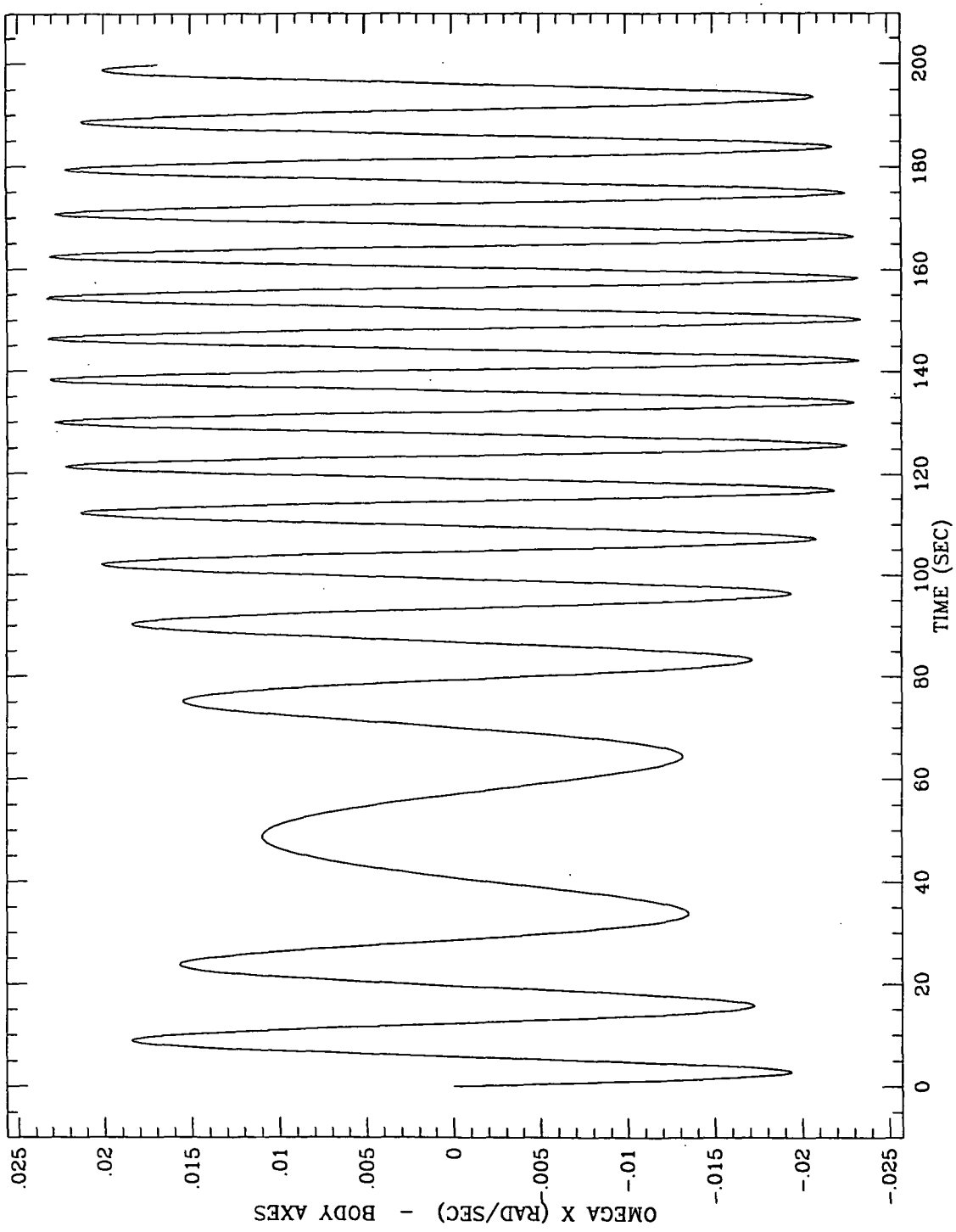
OMEGA X (RAD/SEC) - BODY AXES
.025
.02
.015
.01
.005
0
-.005
-.01
-.015
-.02
-.025
0
20
40
60
80
100
120
140
160
180
200
TIME (SEC)

Figure 8e

equation (21) using the time in the first column, the third column is the peak value of θ, the fourth column is the value of θ calculated from equation (18), and the last column is the percentage error in the calculated value.

Table 6

t (sec)	F (dynes x 10^6)	θ (deg)	$\theta_o(F_o/F)^{1/4}$ (deg)	%Error
0.00000	3.99053	2.00000		
28.47810	1.18918	2.70097	2.70692	.22
57.00310	.48562	3.41381	3.38620	-.81
70.01141	1.08572	2.78049	2.76922	-.41
99.19274	3.89946	2.02477	2.01158	-.65
123.46641	6.40483	1.78884	1.77689	-.67
148.27146	7.57671	1.71533	1.70380	-.67
177.14195	6.35358	1.79243	1.78046	-.67
196.14038	4.42494	1.96189	1.94899	-.66

The tension in Figure 8a has its lowest value at 50 seconds. The period of the oscillations is longest at this time. Equation (18) was derived under the assumption that the tension varies slowly over one cycle. This condition is probably not well satisfied in the interval around 50 seconds. In Table 6 the greatest percentage errors occur in the range around 50 seconds. From 100 seconds on, the percentage error remains nearly constant. The period of the oscillations is shortest in the range 100 to 200 seconds because the tension is largest. The amplitude of the oscillation varies according to equation (18), becoming larger as the tension decreases, and becoming smaller as the tension increases.

A factor that can affect the rotational energy of the subsatellite is changes in angle of the tether. This occurs during retrieval as a result of Coriolis forces on the subsatellite. A test run has been done using program ROTAT in order to see the effect on the oscillation amplitude and rotational kinetic energy of the subsatellite as a result of changes in the angle of the

tether. In this run the angle α of the tether has been varied according to the equation

$$\alpha = .2 \sin (.01 \pi t) \text{ radians} \qquad (22)$$

The amplitude of .2 radians is equal to 11.46 degrees which is on the order of the retrieval angle. The run has been done for 200 seconds with output every .3 seconds. The initial conditions are $\theta = 2°$, $\phi = \psi = 0$. Figure 9 gives the results of the run. Part (a) is the tether angle vs. time, part (b) is the spin angle of the subsatellite in inertial space, part (c) is the spin angle with respect to the tether, part (d) is the angular velocity along the body x'-axis, and part (e) is the rotational kinetic energy. The energy in part (e) is proportional to the square of the angular velocity in part (d). The angle of the subsatellite follows the angle of the tether. The amplitude of the oscillation with respect to the tether in part (c) is nearly constant. Table 7 gives some peak values of the rotational angle θ at around 0, 50, 100, 150, and 200 seconds.

Table 7

t (sec)	θ (deg)
.5407	2.0981
6.0765	-2.1053
44.8041	2.0639
50.3374	-2.1338
55.8702	2.0641
94.5978	-2.1046
100.1341	2.0988
105.6633	-2.0924
144.3947	2.1333
149.9275	-2.0635
155.4597	2.1333
188.6554	2.1109
194.1911	-2.0923

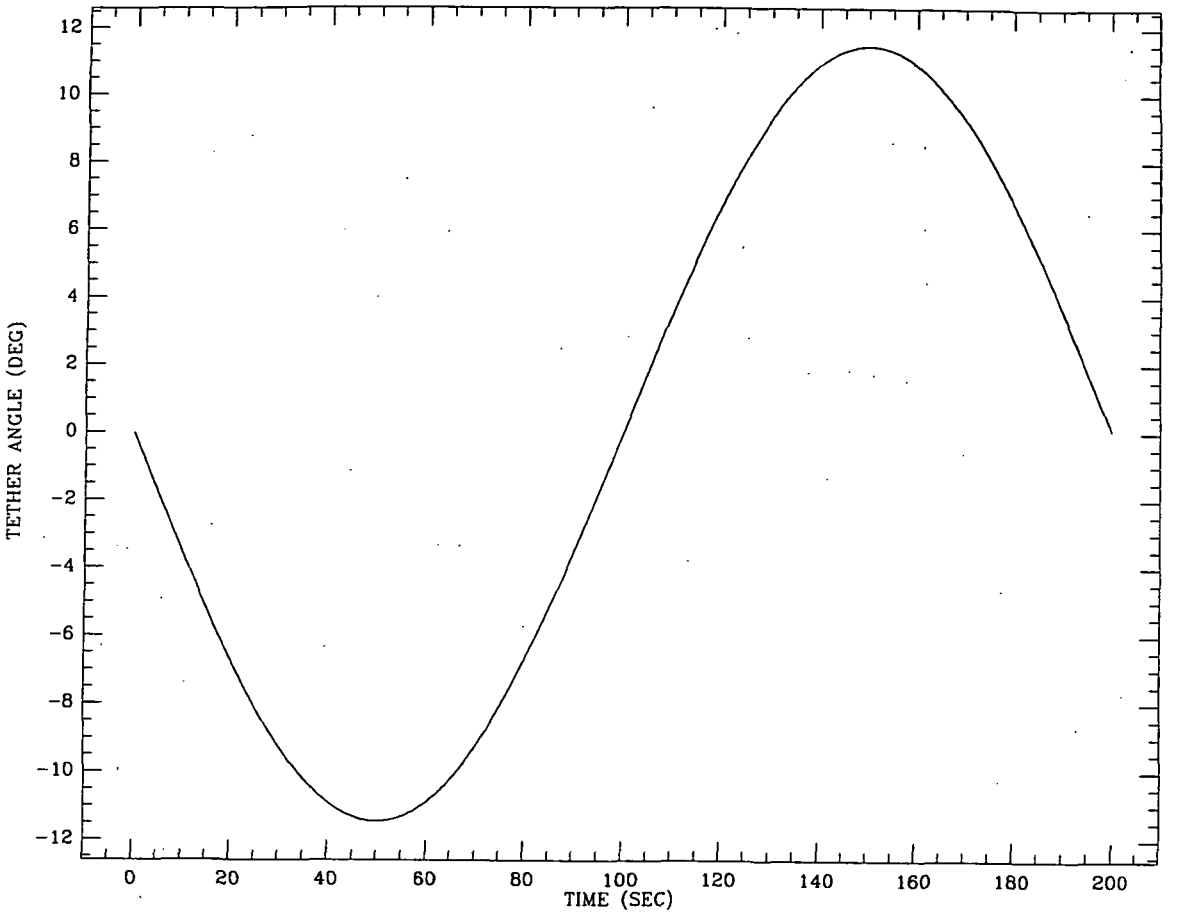

Figure 9a↑

Figure 9b↓

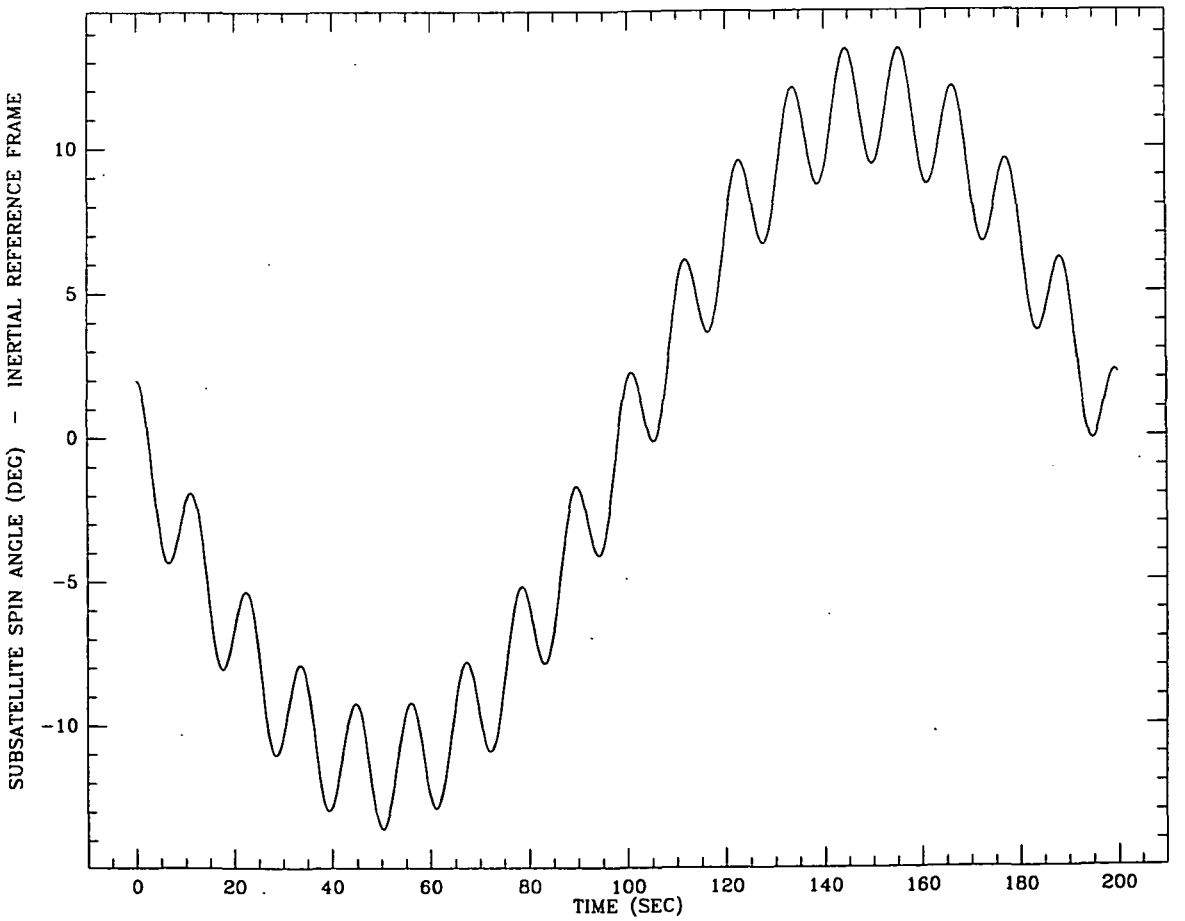

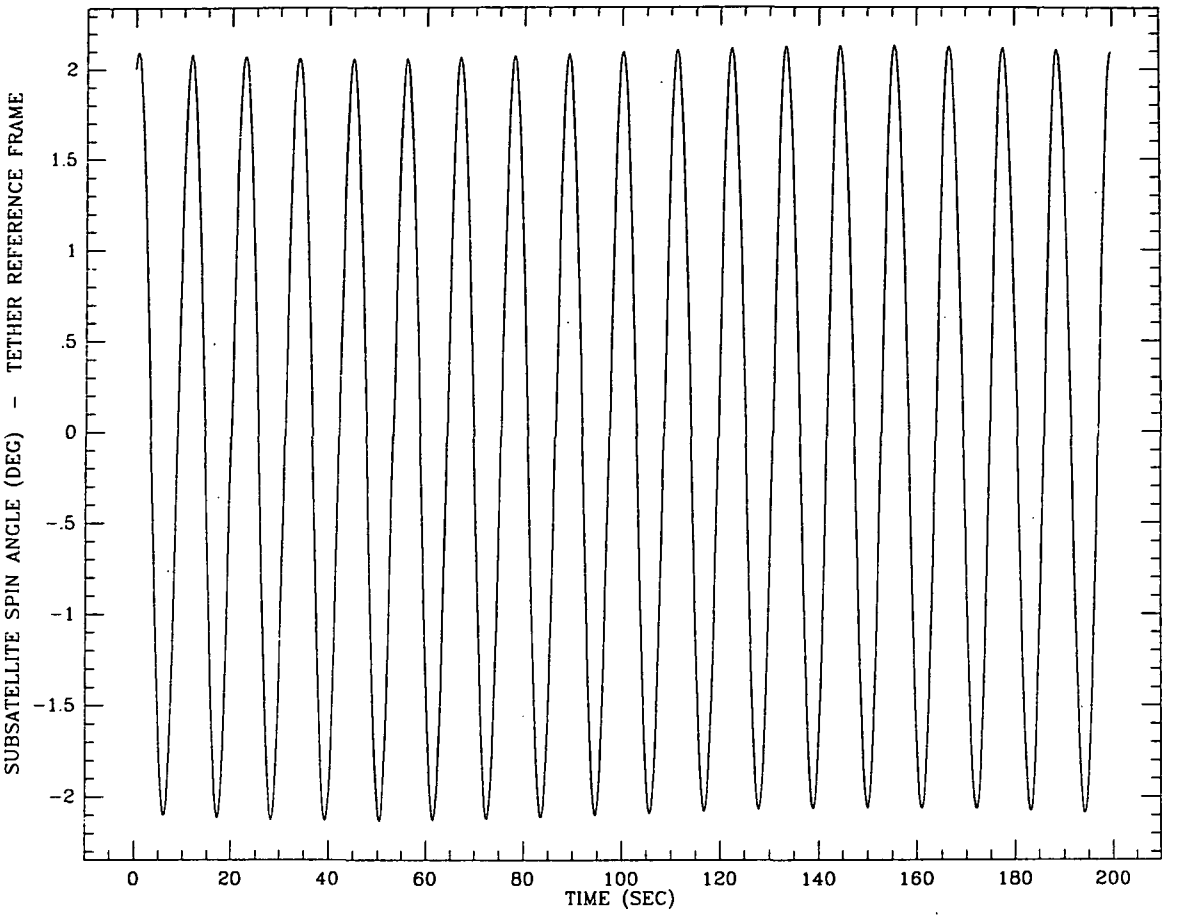

Figure 9c↑

Figure 9d↓

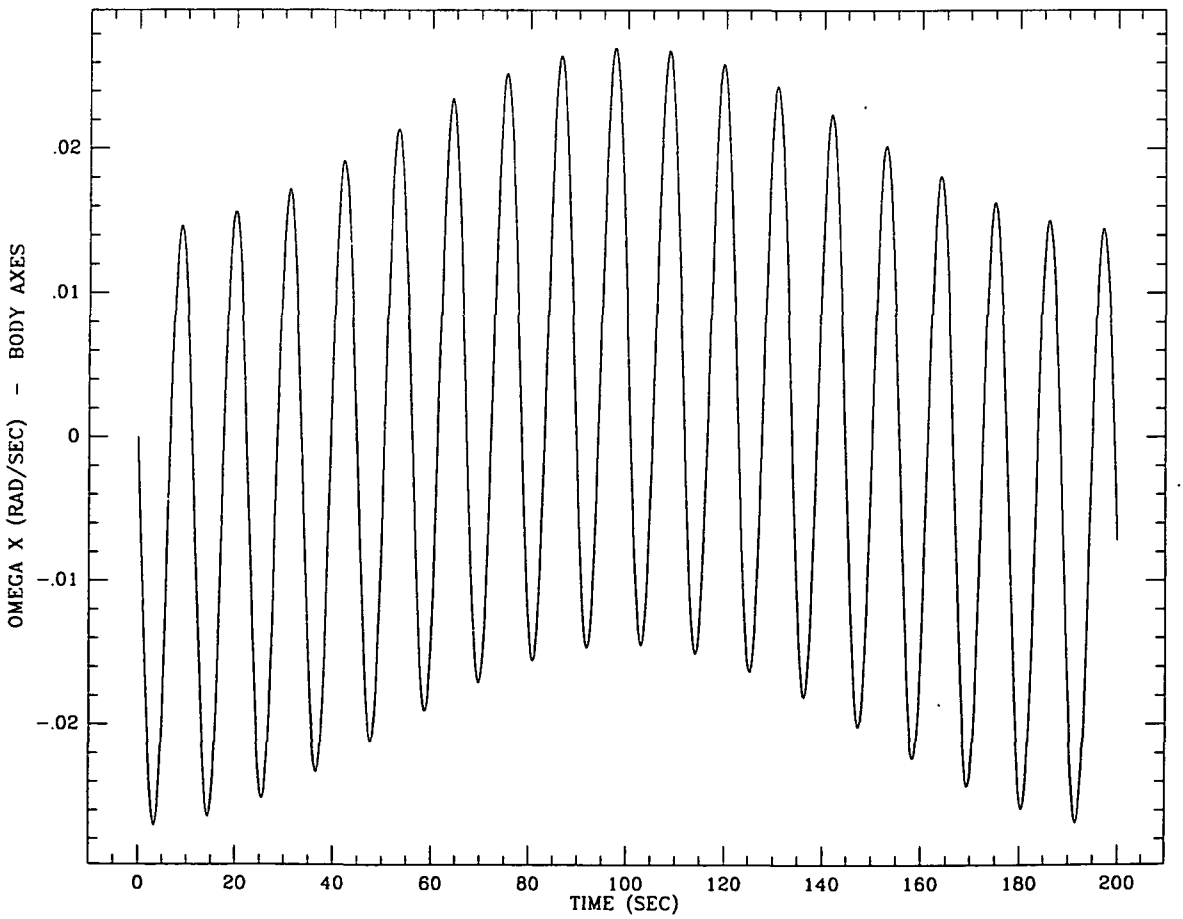

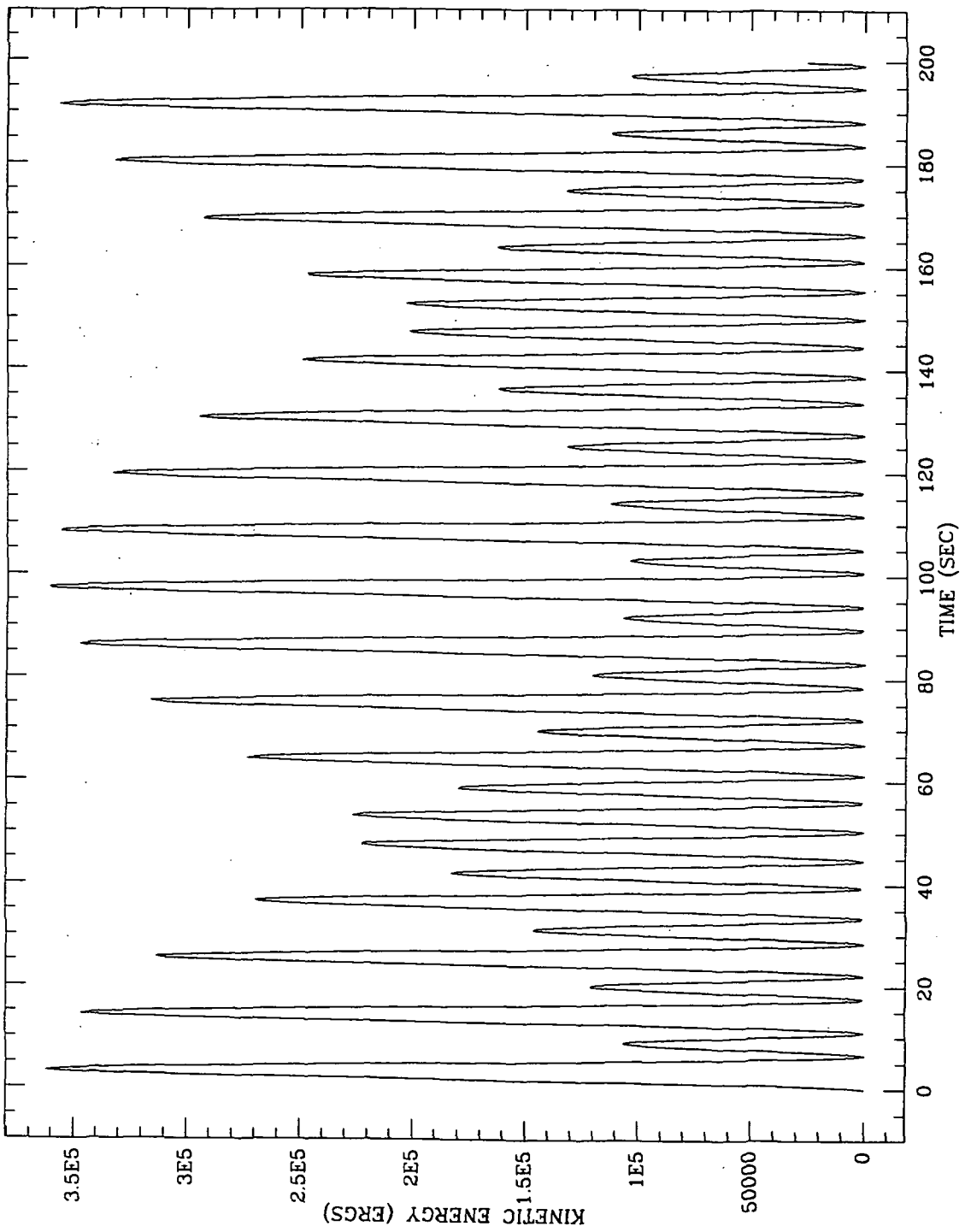
KINETIC ENERGY (ERGS)
3.5E5
3E5
2.5E5
2E5
1.5E5
1E5
50000
0
0
20
40
60
80
100
120
140
160
180
200
TIME (SEC)

Figure 9e

The average value of the peak amplitudes is 2.0995 deg ± .0251 deg. The change in angle of the tether clearly has an effect on the amplitude of the rotation. The rate of change of the tether angle is much greater in this test case than the rates during retrieval.

Equation (18) has been used to analyze the data from two 10,000 second retrieval runs described in Quarterly Report #5, December 1985. These runs are described beginning at the bottom of page 15 and the results are plotted in Figures 7 and 8. It was noted at that time that there was a significant energy loss which was assumed due to the damping in the control law. Figure 7 of the referenced report shows results of a retrieval run starting with equilibrium initial conditions for retrieval at a tether length of 2 km. The oscillation of the subsatellite is one-dimensional with no coning motion. The initial angle of rotation of the subsatellite is 8 deg and the initial angle of the tether is 12.1846 deg so that the angle of the subsatellite with respect to the tether is 4.1846 deg. Since the subsatellite oscillates about the angle of the tether it should oscillate between about 8 deg and 16.3692 deg as measured in the orbiting reference frame. Table 8 of the present report shows a comparison of the oscillation angle with equation (18). The equation agrees very well with the actual oscillation angles. The values of the oscillation amplitude are obtained by quadratic interpolation to find the peaks and the times given in the first column are the times of the peaks. The output values of the tension F are printed at 3 second intervals and the values listed are a rough interpolation. The lack of accurate interpolation probably contributes to the errors listed. There does not appear to be any systematic loss of amplitude such as observed in Table 2. The rotation frequency is much lower for the case of Table 8 since the run was started at 2 km. This reduces the effect of the damping term in the control algorithm.

Table 8

t (sec)	F (dynes x 10^5)	θ (deg)	$\theta_o(F_o/F)^{1/4}$ (deg)	%Error
42.2	4.042	4.2229		
993.0	2.853	4.6047	4.6071	.05
2019.4	1.985	5.0499	5.0446	-.10
2987.3	1.401	5.5020	5.0357	.03
3987.5	.9804	6.0153	6.0173	.03
5000.2	.6850	6.5786	6.5816	.05
5989.9	.4820	7.1786	7.1861	.10
7044.0	.3325	7.8779	7.8851	.09
7986.7	.2391	8.5528	8.5627	.11
8911.4	.1737	9.2686	9.2748	.07
9774.9	.1293	9.9799	9.9851	.05

Figure 8 of Quarterly Report #5 gives the results of a retrieval run started at 20 km. Part (d) of the Figure shows the amplitude of the rotation of the subsatellite as measured in the tether coordinate system. This amplitude has been compared to the amplitude predicted by equation (18) as a function of the tension. The comparison showed errors of 5.8, 14.1, 13.3 and 13.7 percent at 1005, 2502, 4995, and 9941 seconds, respectively. The damping in the control law is not large enough to account for the results. The discrepancies appear to be due primarily to the bug described on page 34 of the same report. Due to an error in variable names, the torque applied to the subsatellite contained only the ℓ and not the $(\dot{\ell}-\dot{\ell}_c)$ term in the control law. Since the retrieval was not started in equilibrium, the $(\dot{\ell}-\dot{\ell}_c)$ term is significant. In the 2 km retrieval the $(\dot{\ell}-\dot{\ell}_c)$ term is negligible since the run uses equilibrium initial conditions for retrieval. Since the erroneous torque is proportional to ℓ, the amplitudes of Figure 8d have been compared to equation (18) with F replaced by ℓ. This gives percentage errors of 1.2, 2.5, 3.7, and 4.1 at 1005, 2502, 4995, and 9941 seconds respectively, which are more reasonable.

A short rerun has been done for the case of Figure 8 in Quarterly Report #5 using the current version of the computer program. Table 9 shows a comparison of the oscillation amplitude with equation (18). The results agree very well with the formula. For the original run the percentage errors were 2.0, 4.0, 5.2, 5.9 and 6.0 at 98.3, 203.5, 296.5, 403.8 and 498.9 seconds respectively because of the mistake in the torque calculation. Figure 10 shows a plot of the rotation angle vs. time during the 565 second rerun. The angle is increasing because of the rapid decrease in tension as the subsatellite accelerates.

Table 9

t (sec)	F (dynes x 10^6)	θ (deg)	$\theta_o(F_o/F)^{1/4}$ (deg)	%Error
16.36	5.78	2.0078		
106.22	5.26	2.0552	2.0557	.02
200.01	4.87	2.0965	2.0957	-.04
297.05	4.58	2.1274	2.1281	.03
396.64	4.394	2.1491	2.1502	.05
498.02	4.267	2.1649	2.1661	.05

In summary, equation (18) agrees well with the observed changes in oscillation amplitude for slow variations in tension and no damping. The energy losses seen in the retrieval runs are within that expected from the damping term in the retrieval tension control law. In the next section a more accurate expression is presented for calculating the energy losses from wire stretch damping.

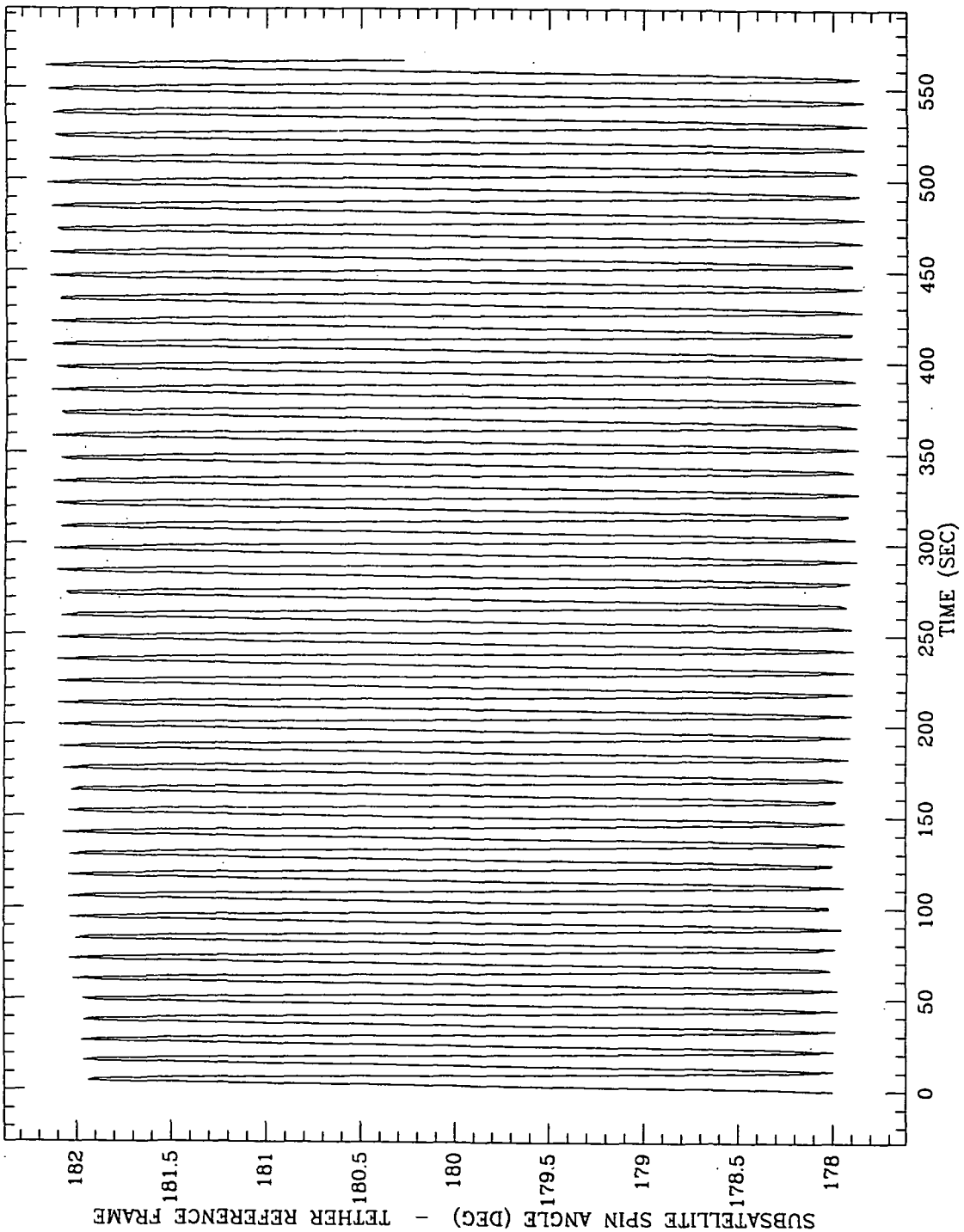
SUBSATELLITE SPIN ANGLE (DEG) - TETHER REFERENCE FRAME
182
181.5
181
180.5
180
179.5
179
178.5
178
0
50
100
150
200
250
300
350
400
450
500
550
TIME (SEC)

Figure 10

2.1.5 Rotational Energy Dissipated By Wire Damping Forces -

Rotation of the subsatellite will cause stretching of the wire except in the case of a perfect circular wobble. For an oscillation about an axis perpendicular to the wire, we can calculate the work done against wire stretch damping forces under the assumption that the center of mass remains fixed. The result of the derivation is

$$W = b\ r^2\ A^4\ \omega^2 \left[\frac{t}{8} - \frac{\sin 4\omega t}{32\omega}\right] \qquad (23)$$

where W is the work done, b is the damping coefficient, A is the amplitude of the oscillation in radians, ω is the frequency, and t is the time. The amplitude will, of course decrease with time so that the equation is valid only for small damping and short intervals of time. The average work $\bar{W}$ as a function of time is

$$\bar{W} = \frac{1}{8}\ b\ r^2\ A^4\ \omega^2\ t \qquad (24)$$

Equation (24) would have to be used in a further integration to obtain the amplitude A as a function of time by setting the rate of loss of rotational energy equal to $\bar{W}/t$.

The details of the derivation of equation (23) are given in Section 2.0 of Technical Note TP86-002, January 1986 which is included as Appendix B of Quarterly Report #6 for this contract.

A simulation has been run using program ROTAT in order to verify equation (24). In program ROTAT, the motion of the center of mass is not integrated so that the assumption used in the derivation is satisfied. The initial conditions

for the run are $\theta = 2°$, $\phi = \psi = 0$. The other parameters are moment of inertia I = 99 kg-m^2, wire damping coefficient b = 326177 dynes/(cm/sec), wire tension F = 3,990,530 dynes, and subsatellite radius r = 80 cm. The frequency ω of the oscillation is

$$\omega = \sqrt{\frac{rF}{I}} = .567862 \text{ rad/sec}$$

The amplitude A of the oscillation is .0349066 rad/sec. Putting all these parameters into equation (24) gives

$$\overline{W} = 124.9\ t$$

Figure 11 shows a plot of the kinetic energy as a function of time during the 12.5 second test run. Table 10 shows the kinetic energy at the two peaks.

Table 10

t (sec)	Energy (ergs)	ΔE	ΔT	$\Delta E/\Delta T$
2.768548	194072.79			
8.301609	193386.87	-685.92	5.53306	-123.97

This agrees with the calculated energy loss to an accuracy of .7 percent.

Equation (24) can be used to make a more accurate estimate of the energy absorbed by the damping term in the retrieval control law. The damping term is given by equation (15) and the value of the coefficient is given in equation (16). Using equation (17) with a 10 second period (ω = .62832 rad/sec), and 2° amplitude (A = .0349066), the energy loss was estimated at .9 ergs/sec on the

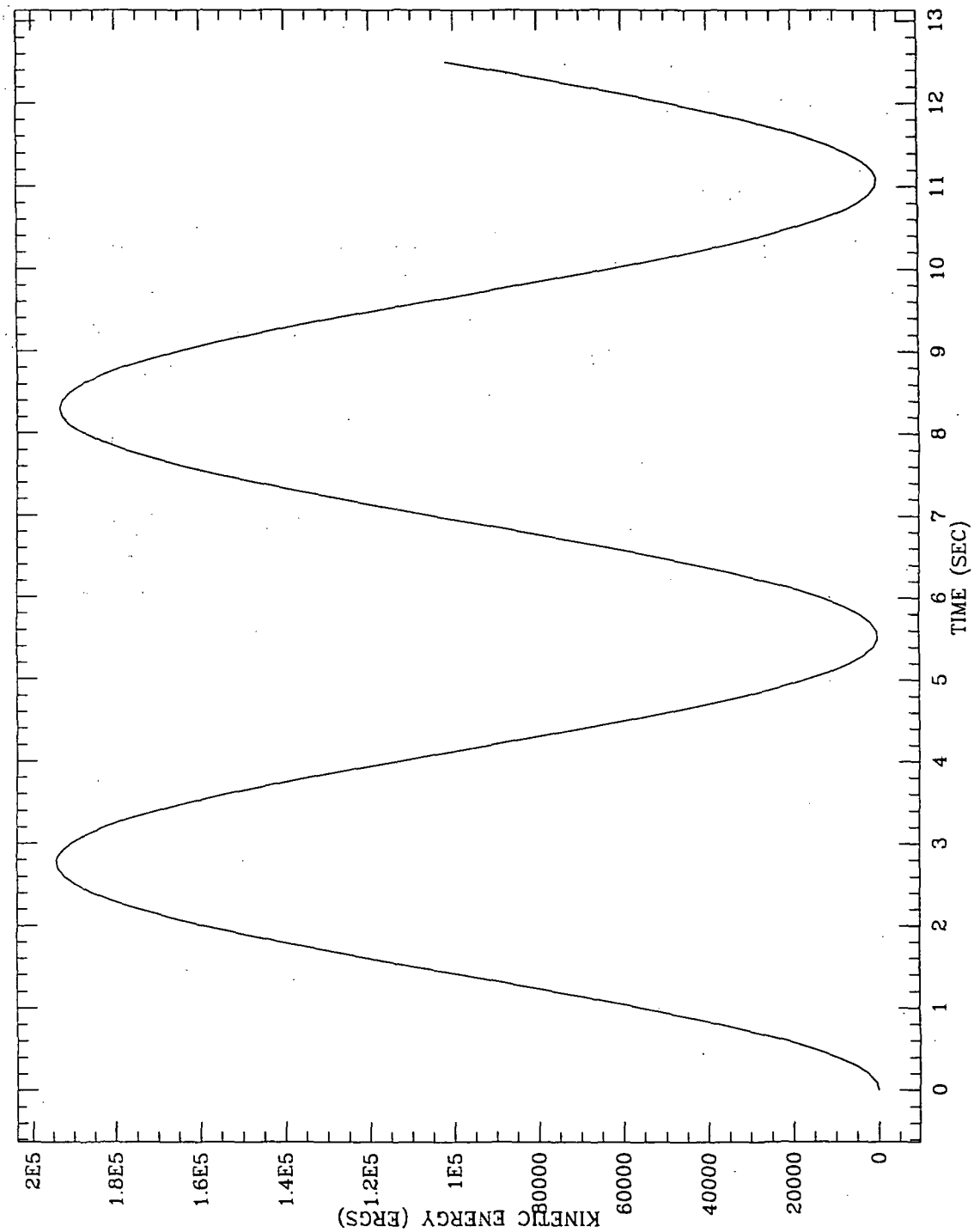
KINETIC ENERGY (ERGS)
2E5
1.8E5
1.6E5
1.4E5
1.2E5
1E5
80000
60000
40000
20000
0
0
1
2
3
4
5
6
7
8
9
10
11
12
13
TIME (SEC)

Figure 11

basis of a crude analysis. Using equation (24) for the same parameters gives 1.086 ergs/sec. In order to calculate the energy absorbed during the retrieval it would be necessary to integrate equation (24) over the whole retrieval. This has not been done for any of the cases. The assumption that the center of mass does not move would contribute some degree of error to the calculation. The major energy loss during retrieval is described by equation (18). Equation (24) could be used to estimate the effectiveness of a reel control algorithm used to damp rotations of the subsatellite.

2.1.6 Attitude Damping Using Active Tension Control -

Extensive analysis has shown that the z-axis attitude control thruster on the tethered subsatellite cannot control small amplitude oscillations about the x and y axes. Since the coupling with these motions increases with amplitude, some control can be achieved at large amplitudes. Wire stretch damping is more directly coupled to the rotation but is also ineffective against small amplitude oscillations. It is possible in principle to use either tension control or the in-line thruster to control the torque on the subsatellite in a way which is effective against small amplitude oscillations. Both techniques require active control based on knowledge of the attitude of the subsatellite. Tension control using the reel motor on board the Shuttle would have to take into account the propagation delay of tension signals along the wire in order to insure that the control is properly phased with the rotation. With the in-line thruster there is also a phasing problem since the subsatellite must move enough to stretch the wire and alter the torque applied by the wire. The thruster itself applies no torque since the line of action is through the center of mass of the subsatellite. For short tether lengths either method should work well. For thruster

control the delay time depends on the longitudinal oscillation period of the subsatellite at the end of the tether. There would be some immediate change in tension as a result of the inertial mass of the tether. This effect depends on the mass per unit length and propagation velocity for tension waves along the tether.

A detailed analysis of the technique of attitude damping using tension control is presented in Section 3.0 of Technical Note TP96-002, which is included as Appendix B of Quarterly Report #6 for this contract.

2.1.7 Attitude Damping Using A Lever Arm -

Figure 12 shows a subsatellite with a lever arm between the wire and the subsatellite. In this analysis the lever arm is assumed to be long enough that it remains aligned with the wire (Figure 12a). The lever arm could be attached to the subsatellite by a ball and socket joint or a universal joint having two perpendicular rotation axes. It is assumed that the joint is capable of applying a damping torque that is proportional to the angular velocity of rotation of the joint. This arrangement is capable of damping any oscillations about the x and y axes of the subsatellite. It is ineffective against components of angular velocity that are parallel to the wire. This type of motion which is a spin of the subsatellite can be controlled by the z-axis attitude thruster.

Figure 12

Lever Arm Attached to the Subsatellite with a Damping Joint.

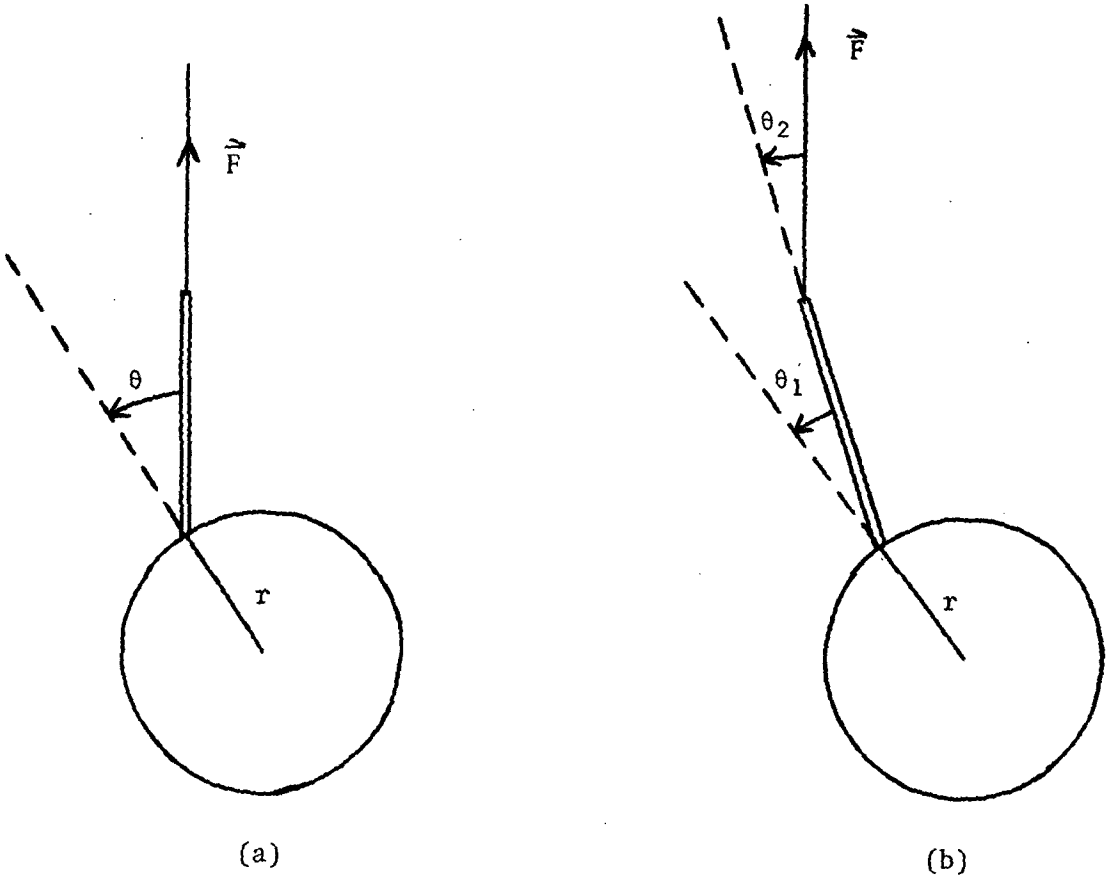

This system is capable of damping a circular wobble which cannot be damped by any of the other damping systems described in this report. A circular wobble consists of oscillations about the x and y axes of the subsatellite that are 90° out of phase with each other. The component of angular velocity along the body z-axis is assumed to be zero since it can be eliminated by the z'-axis attitude control thrusters. Under this assumption, the damping joint must constantly rotate in order for the subsatellite to wobble regardless of the phase of the x and y components of the oscillation.

For the sake of analysis, let us assume that the joint connecting the lever to the subsatellite consists of two axes, one of which is parallel to the body x-axis, and the other of which is parallel to the body y-axis. Let us assume that the wobble is described approximately by the equations

$$\theta_x = A_x \sin \omega_x t \tag{25}$$

and

$$\theta_y = A_y \cos \omega_y t \tag{26}$$

where θ_x is the rotation angle about the x-axis and θ_y is the angle about the y-axis. For small amplitude oscillations equations (25) and (26) are a good description of the motion. The frequencies of the oscillations are:

$$\omega_x = \sqrt{rF/I_x} \tag{27}$$

and

$$\omega_y = \sqrt{rF/I_y} \tag{28}$$

where r is the distance from the center of mass to the attachment point, F is the wire tension, and I_x and I_y are the moments of inertia about the x and y axes respectively. The critical damping coefficients are:

$$b_x = 2\ I_x\omega_x \tag{29}$$

and

$$b_y = 2\ I_y\omega_y \tag{30}$$

If $I_x = I_y$ and $A_x = A_y$ then the motion is a circular wobble. If the moments of inertia are unequal, the motion will alternate between circular or oval and linear wobble. The damping joints are effective against the x and y components individually and there is no requirement that the angle θ between r and F be changing as long as the motion is not a pure spin.

The lever arm may remain aligned with the wire either as a result of being long or as a result of the damping coefficient being low enough that the torque exerted on the lever by the subsatellite is small. The lever does not need to remain aligned with the wire for the system to provide damping. The configuration shown in Figure 12b will work also, but is somewhat more complicated to analyze. The only requirement for damping is that the joints rotate and thereby dissipate energy.

The effect of a lever arm with damping joints is very similar to that of attitude damping thrusters about the body x and y axes. Some simulations of the effect of x and y attitude thrusters are given in Section 2.3.10 of Quarterly Report #5, December, 1985.

2.1.8 Comparison Of MMC And SAO Simulations Of Retrieval With Rotation Of The Subsatellite -

As a further test of equation (18) comparison runs have been done using the simulation programs at MMC and SAO. The two programs were developed independently and each contains features not available in the other. Both model rotation of the subsatellite and retrieval with a tension control algorithm. The MMC program contains a model of the response of the reel control mechanism which is not available in the SAO version. In order to establish common ground for the comparison it was agreed to use as simple a case as possible that would show retrieval with rotation of the subsatellite. More complicated comparisons could be done later if needed once agreement was obtained on a basic reference case. Two or three runs were done with each program before establishing a common case for comparison. The final result was a retrieval run which treates the Shuttle as a point mass, and includes no model of the reel mechanism, a one dimensional rotation of the subsatellite, and a retrieval tension control law containing three terms involving damping, gravity gradient compensation, and a prescribed length vs. time profile.

The runs done at SAO, in addition to being useful for comparison, are also useful for completing the analysis of an earlier case that needed to be rerun because of a program bug. Three simulations have been done at SAO for the comparison of the MMC and SAO analysis programs. The tension control law normally used in the SAO simulation program is given by equation (2.1.16) on page 8 of Quarterly Report No. 3, June 1985, for this contract. In the first simulation the program was modified to use the equation:

$$f_c = m^*\left[3\Omega^2\ell + 2\varsigma\omega_c(\dot{\ell} - \dot{\ell}_c)\right] \qquad (31)$$

where:

$m^* = \frac{m_1 m_2}{m_1+m_2}$ = reduced mass

Ω = orbital angular velocity

ℓ = distance between mass centers

ζ = .9 = damping ratio

$\omega_c = \sqrt{3}\ \Omega$ = control frequency

$\dot{\ell}_c = -\frac{3}{2}\ \ell\ \Omega \cos\theta_c \sin\theta_c \quad (\theta_c = 12°)$

The parameters for the run are:

Tether length ℓ_o	=	20 km (deployed upward)
Shuttle mass m_1	=	101,614 kg
Subsatellite mass m_2	=	550 kg
Shuttle altitude	=	296 km
Subsatellite radius	=	80 cm
Moment of inertia	=	124 kg-m^2

The initial conditions for the run have the tether aligned with the local vertical and the subsatellite rotated 2^0 toward the forward direction (the direction of motion). There is no initial angular velocity of the subsatellite (except for the orbital angular velocity) and no initial retrieval rate or tether libration velocity.

The control law given by equation (31) differs from the control law cited in Quarterly Report No. 3 in that the factors accounting for deceleration of the subsatellite and the reduced gravity gradient for non-vertical tethers have been omitted. The effect of omitting these terms is to give a larger control ten-

sion, and more rapid retrieval at a larger retrieval angle. The control frequency ω_c for the damping term is taken as the in-plane frequency rather than the out-of-plane frequency as in Quarterly Report No. 3.

A simulation has been done for 10,000 seconds of orbital time with output at 1 second intervals. The frequent sampling is necessary because the rotational period of the subsatellite is on the order of 10 seconds. The in-line thruster is never turned on in the SAO. Figure 13 shows the results of the first simulation. Part (a) is the tether length vs. time. The final tether length at 10,000 seconds is 117 meters. Part (b) shows the in-plane angle of the tether vs. time. The angle is larger than the commanded angle of 12° because the tension is somewhat larger than required in this simplified control law. The effect of the subsatellite rotation can be seen as the tether length becomes shorter near the end of the run. Part (c) shows the tension vs. time and part (d) shows the rotation angle of the subsatellite. The amplitude is almost 8° at the end because of the large tension ratio between the first and last points. In the current mission plan, the in-line thruster would be activated to maintain adequate tension during the final stages of retrieval so that the growth of the oscillation amplitude would be halted before it reaches the levels shown in Figure 13d. This run provides an opportunity to test equation (18) for the case of retrieval from a length of 20 km with a single-axis rotation of the subsatellite (no coning). Table 11 shows the results of the comparison. The amplitudes of the oscillation shown in the second column are obtained by quadratic interpolation between the output points at 1 second intervals, and the tension values are crudely interpolated between output points. The amplitudes in the fourth column calculated using equation (18) show good agreement at

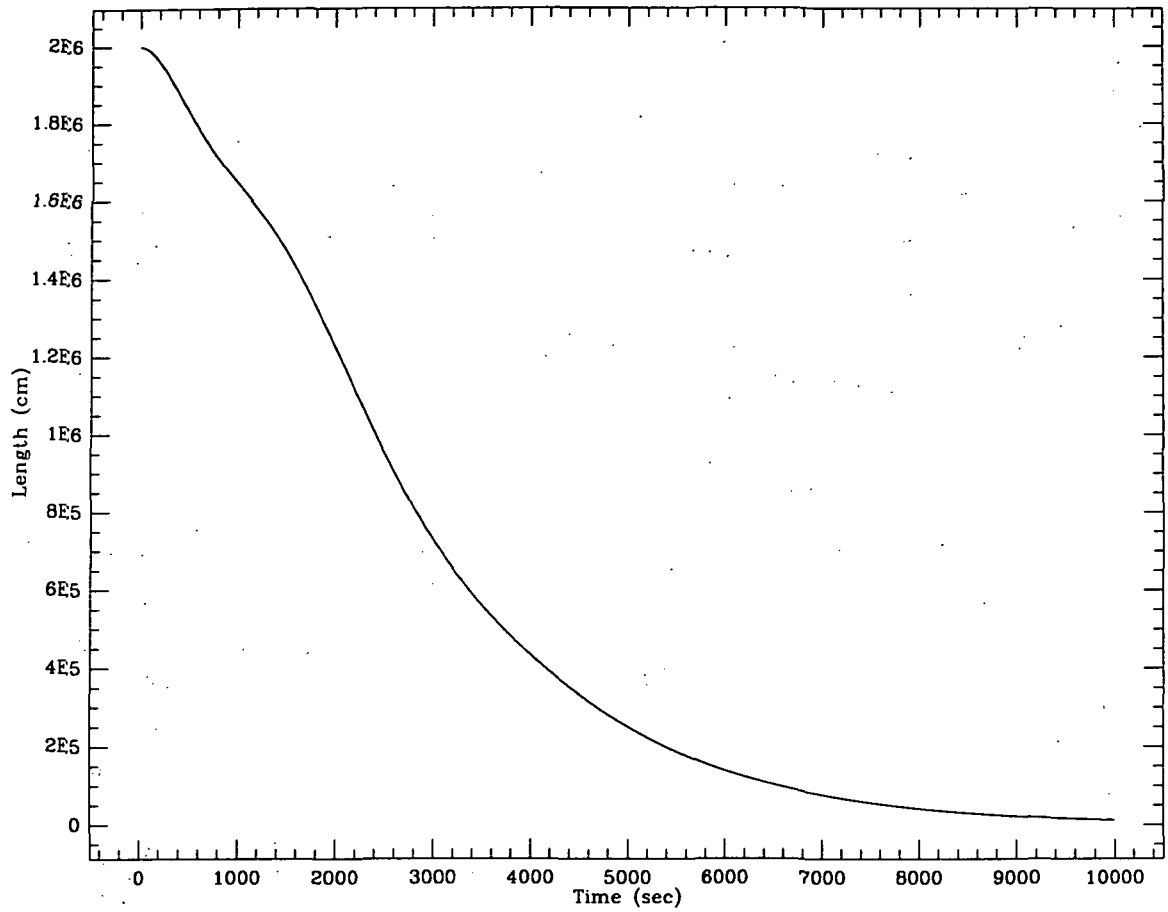

Figure 13a↑

Figure 13b↓

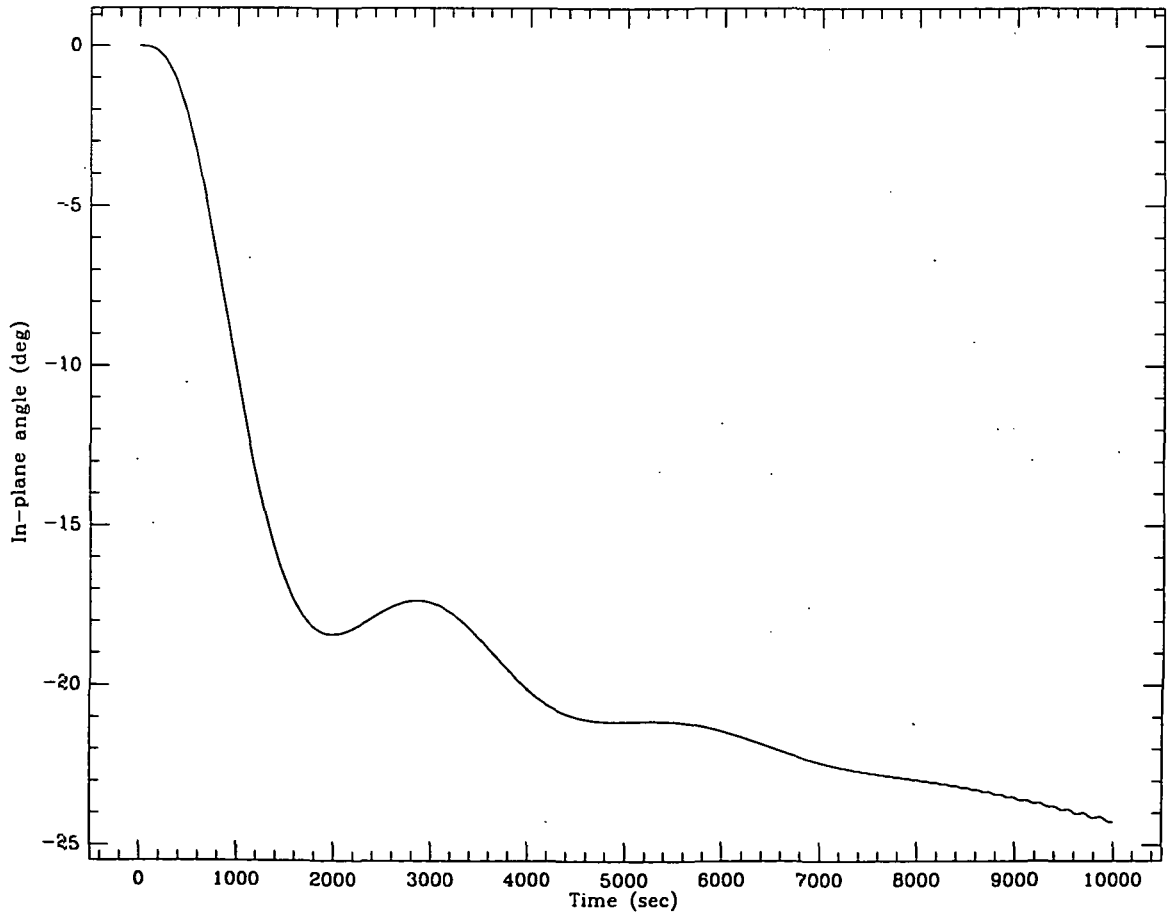

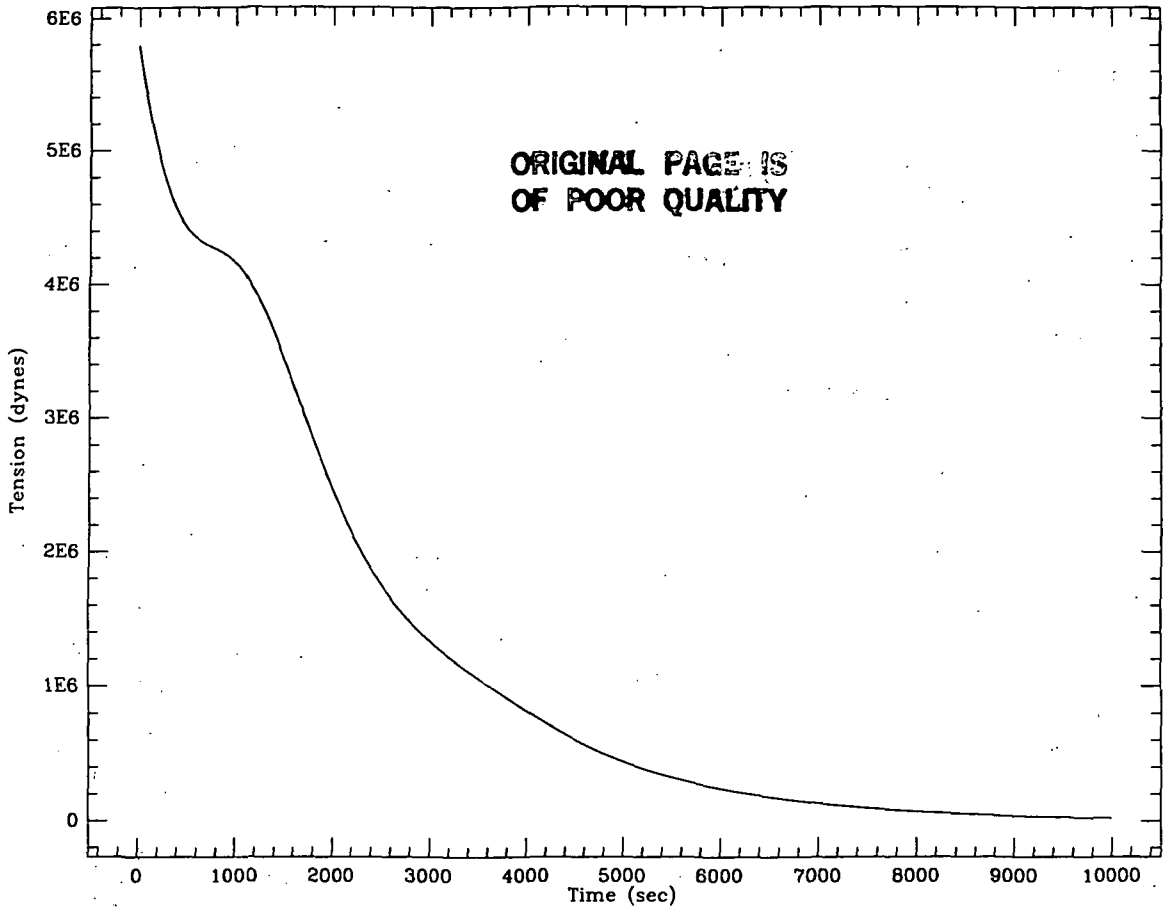

Figure 13c↑

Figure 13d↓

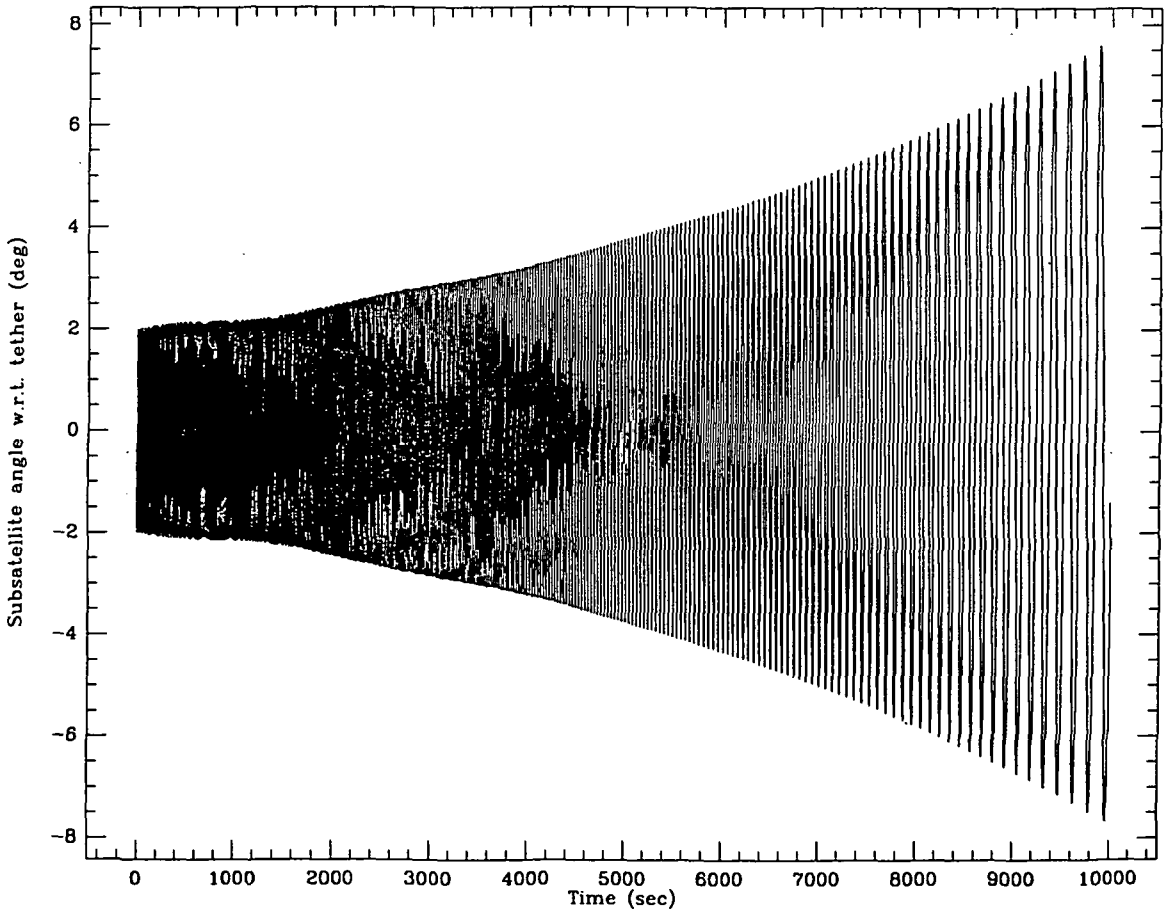

the beginning of the run with the percentage error increasing with time. The energy losses have been shown to be within the limits expected from the damping in the control law.

Table 11

t (sec)	θ (deg)	Tension (dynes x 10^6)	$\theta_o(T_o/T)^{1/4}$ (deg)	%Error	ℓ (km)
0	2.0000	5.79590			20.000
5.1	2.0016	5.77063	2.0022	-.03	19.999
105.0	2.0428	5.3209	2.0432	-.02	19.874
203.2	2.0756	4.9779	2.0775	-.09	19.587
402.3	2.1234	4.5366	2.1263	-.14	18.752
1003.9	2.1692	4.1563	2.1734	-.19	16.439
2000.5	2.4665	2.4633	2.4770	-.43	12.243
3009.4	2.8691	1.3327	2.8882	-.67	7.241
4009.7	3.2370	.8111	3.2700	-1.02	4.320
5014.5	3.7649	.4346	3.8220	-1.52	2.484
6015.4	4.3465	.2385	4.4406	-2.16	1.376
7010.3	5.0073	.1309	5.1591	-3.03	.763
8006.9	5.7997	.0695	6.0439	-4.21	.415
8990.0	6.6805	.0371	7.0708	-5.84	.224
9961.0	7.6694	.0197	8.2831	-8.00	.120

The first run, although useful as a test of equation (18) cannot be compared to any of the MMC runs since the MMC tension control law contains an additional term. In order to make sure that the retrieval profile is correct before doing any further rotational dynamics runs (which consume a lot of computer time), a test has been done for retrieval without rotation modelled. The tension control law used for this run is:

$$f_c = m^*\left[3\Omega^2\ell + 2\varsigma\omega_c(\dot{\ell} - \dot{\ell}_c) + \omega_c^2(\ell - \ell_c)\right] \qquad (32)$$

where:

$$\ell_c = \ell_o e^{-\alpha t} = \text{commanded length}$$

$$\ell_o = 20 \text{ km}$$

$$\alpha = \frac{3}{2} \Omega \cos \theta_c \sin\theta_c \quad (\theta_c = 12°)$$

and the other parameters are the same as in equation (31). The orbital parameters and initial conditions are the same as before except that the subsatellite is treated as a point mass. Since there is no rotational dynamics, the integration proceeds rapidly because there are no other short period effects to be followed. The integration has been run for 10,000 seconds of orbital time with output at 100 second intervals. Figure 14 shows the results of the simulation. Part (a) is the length vs. time. The final length is 446.6 m at 10,000 seconds. The tether stops retrieving at around 5600 seconds at a length of 2.227 km and redeploys slightly to a length of about 2.257 km at around 6000 seconds before resuming the retrieval. This is presumably because the retrieval was running ahead of the commanded profile specified by the variable ℓ_c. Figure 14b shows the in-plane angle vs. time. The behavior here differs markedly from that seen in Figure 13b. The initial overshoot to about 30° is counteracted by the slow down in the retrieval rate and the tether swings to about 10° in the opposite direction. Figure 14c shows the behavior of the tension vs. time. The tension does not decrease monotonically with time.

The results in Figure 14 look closer to the results shown in the first MMC simulation. However, differences remained. The MMC simulation contained a model of the response of the reel mechanism which is not included in the SAO model. When the reel effects were removed from the MMC simulation, agreement was achieved between the shapes of the curves from the SAO and MMC simulation programs.

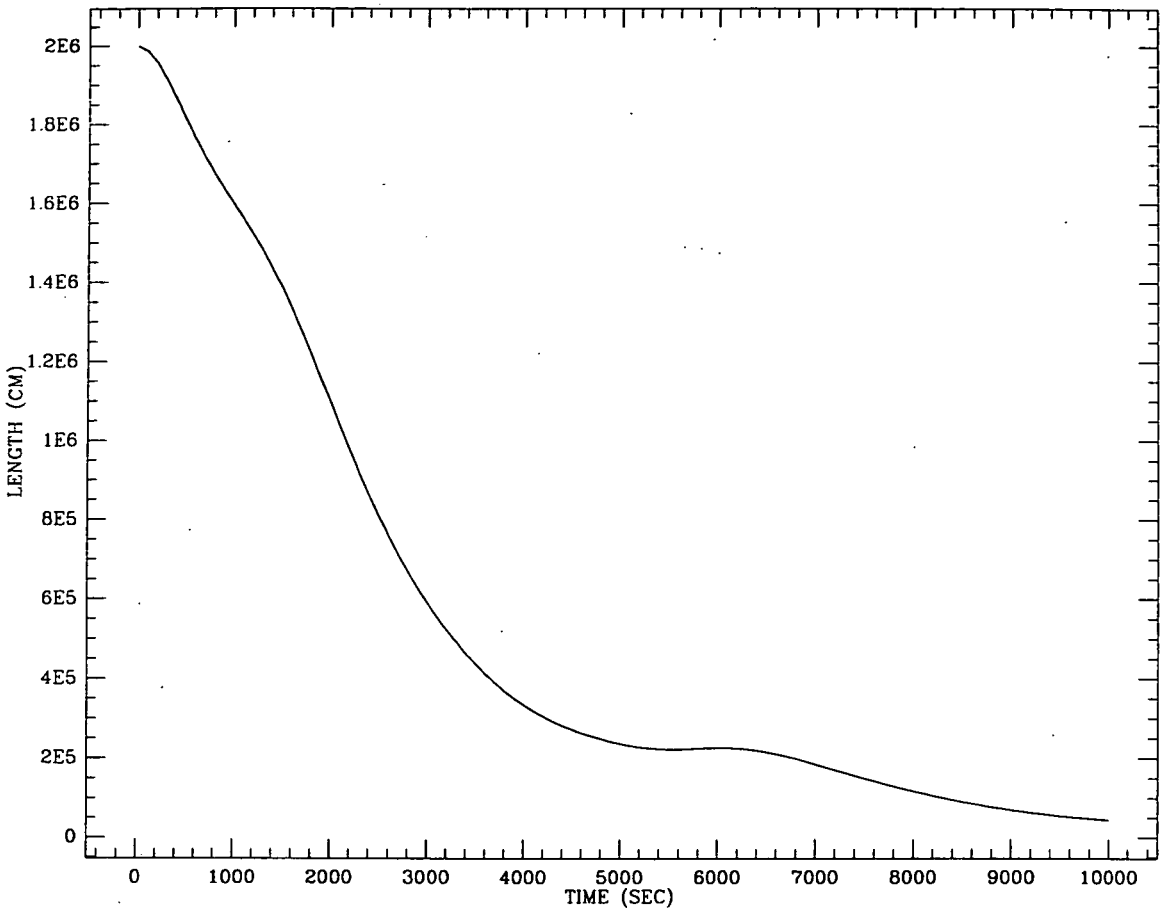

Figure 14a↑

Figure 14b↓

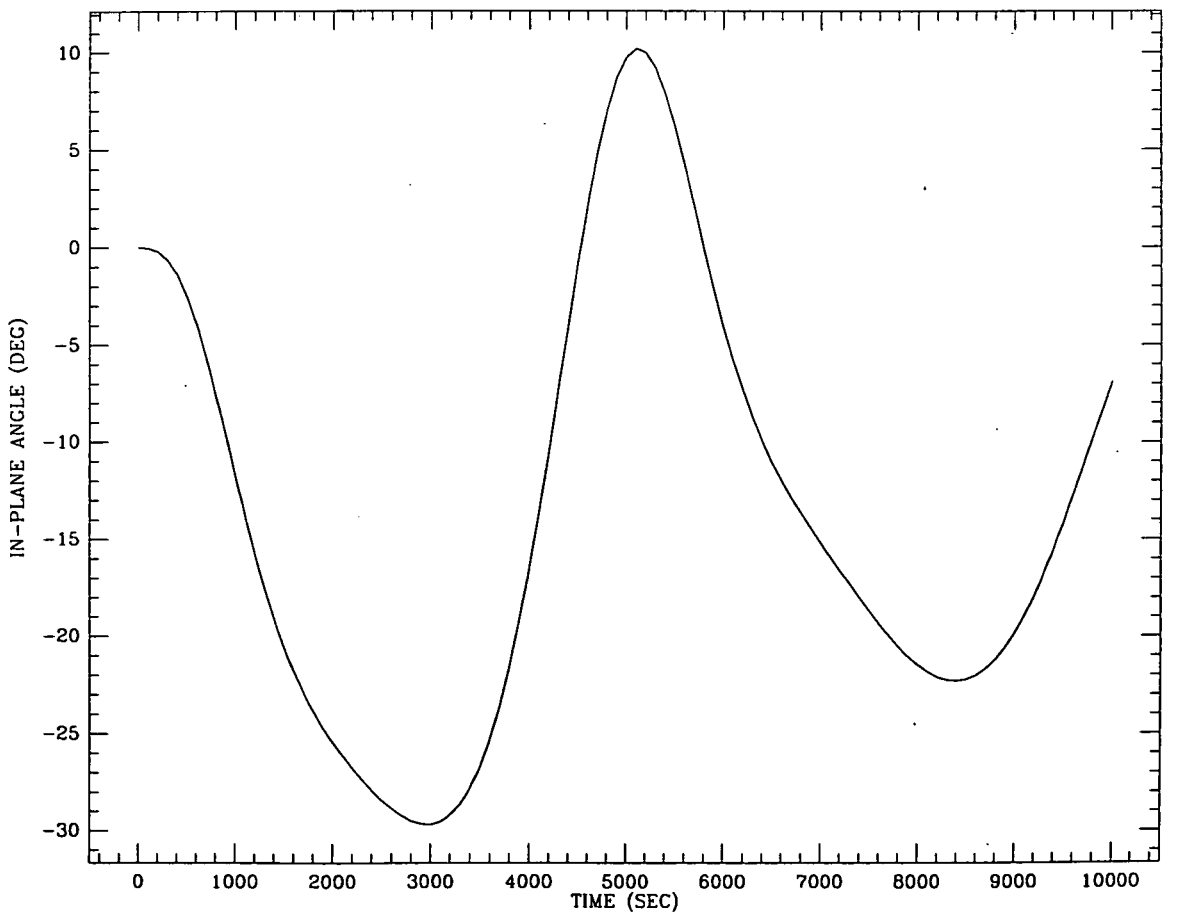

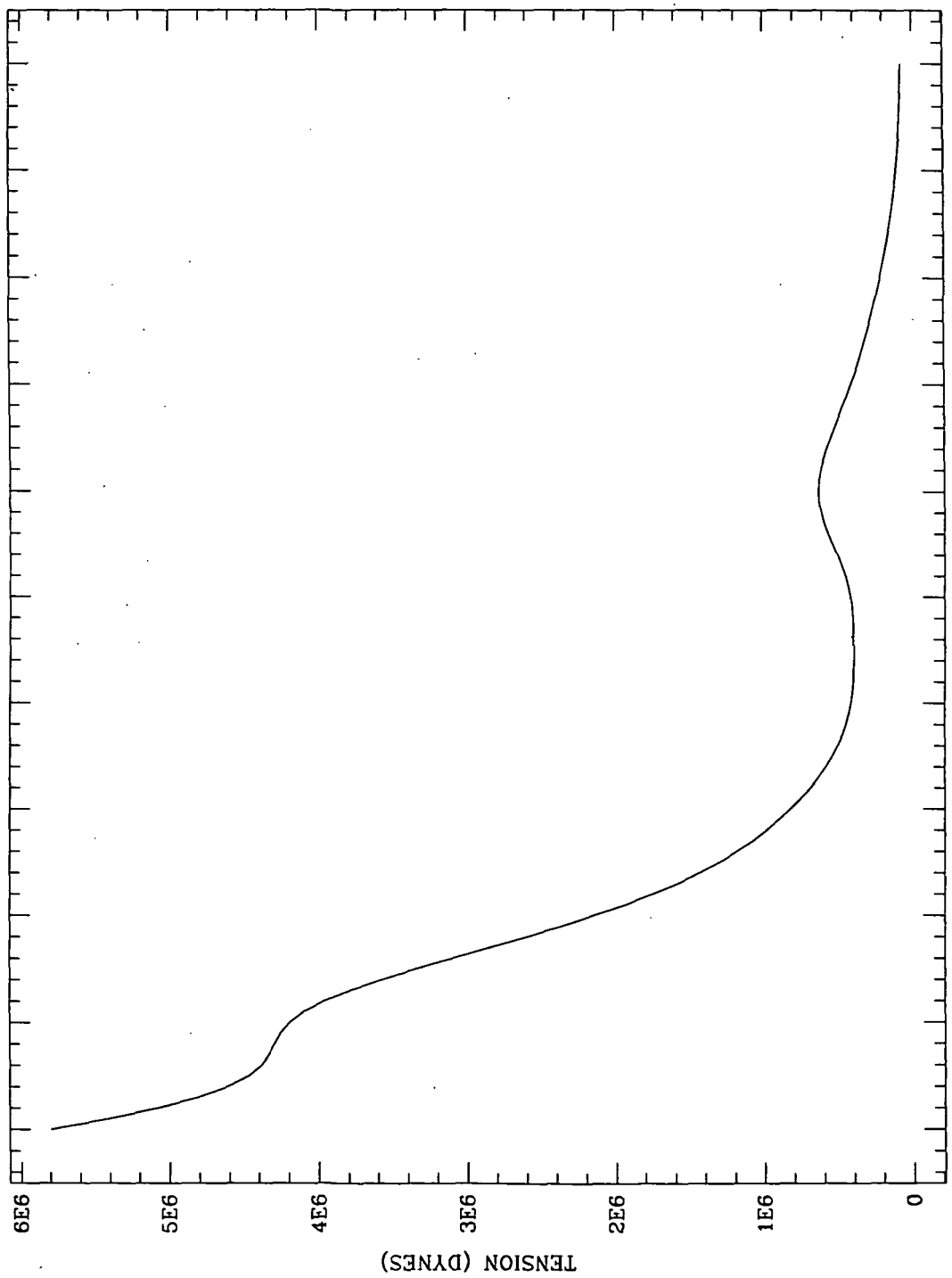
TENSION (DYNES)
6E6
5E6
4E6
3E6
2E6
1E6
0
0
1000
2000
3000
4000
5000
6000
7000
8000
9000
10000
TIME (SEC)

Figure 14c

Having achieved satisfactory agreement on the control laws the retrieval run has been repeated with the rotation of the subsatellite included. Figure 15 shows the results. Part (a) is the length vs. time. The final tether length is 445.8 meters (446.6 m between mass centers with r = 80 cm). Part (b) is the in-plane angle vs. time, and part (c) is the tension. As expected, Figures 15a, b, and c, are virtually identical to Figures 14a, b, and c. Figure 15d is the rotation angle vs. time. The shapes of the curve seems to agree with that of the MMC simulation at least up to the point where the in-line thruster comes on it the MMC simulation. Figure 15e shows the rotation angle during the first 500 seconds, and Figure 15f shows the last 500 seconds. The difference in frequency results from the decrease in tension during the run. Figure 15g shows the rotational kinetic energy as a function of time. The difference in amplitude on alternate peaks results from the fact that the rotational kinetic energy is measured in inertial space. The angular velocity of the subsatellite adds to the orbital angular velocity on the forward swing and subtracts from it on the backward swing.

The rotation amplitude has been analyzed using equation (18) the results are shown in Table 12. The agreement is good at the beginning, and the energy losses are within what can be expected from the damping in the tension control law.

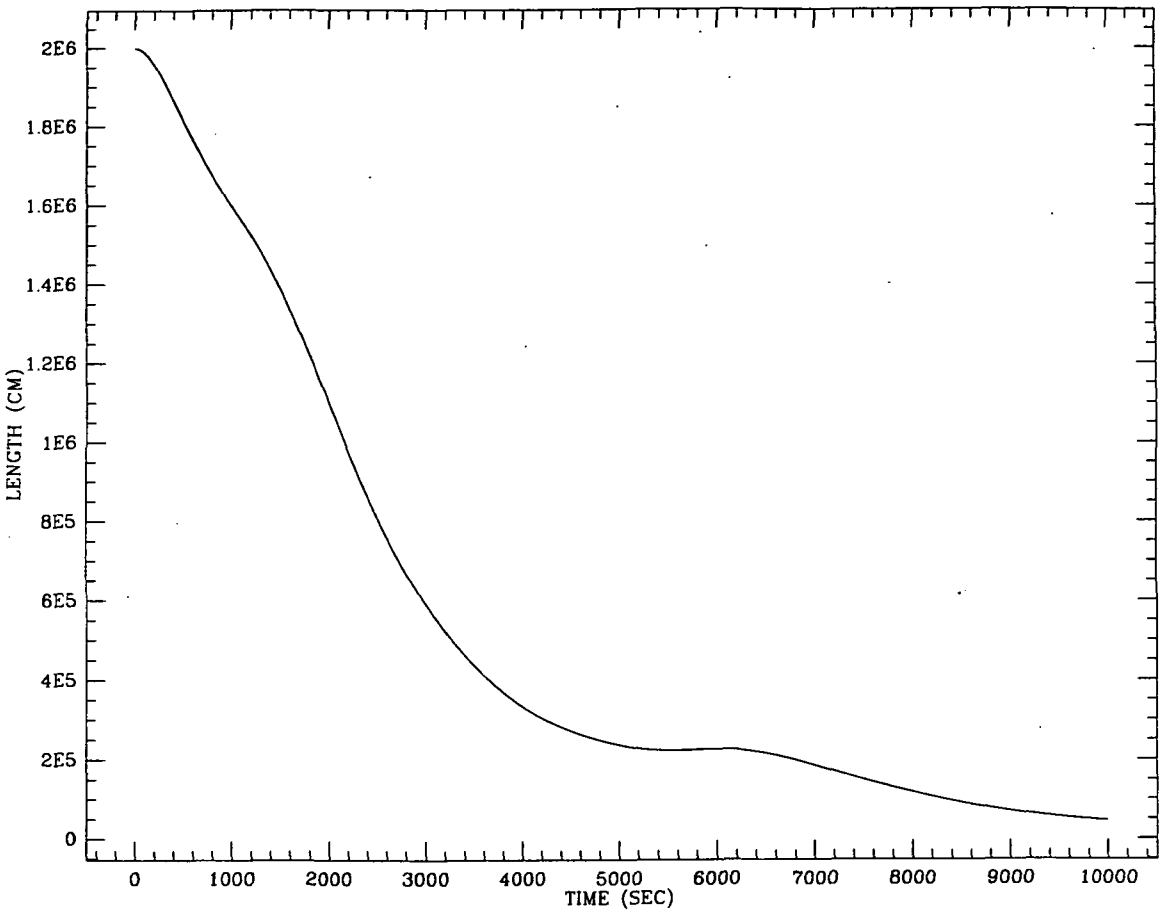

Figure 15a↑

Figure 15b↓

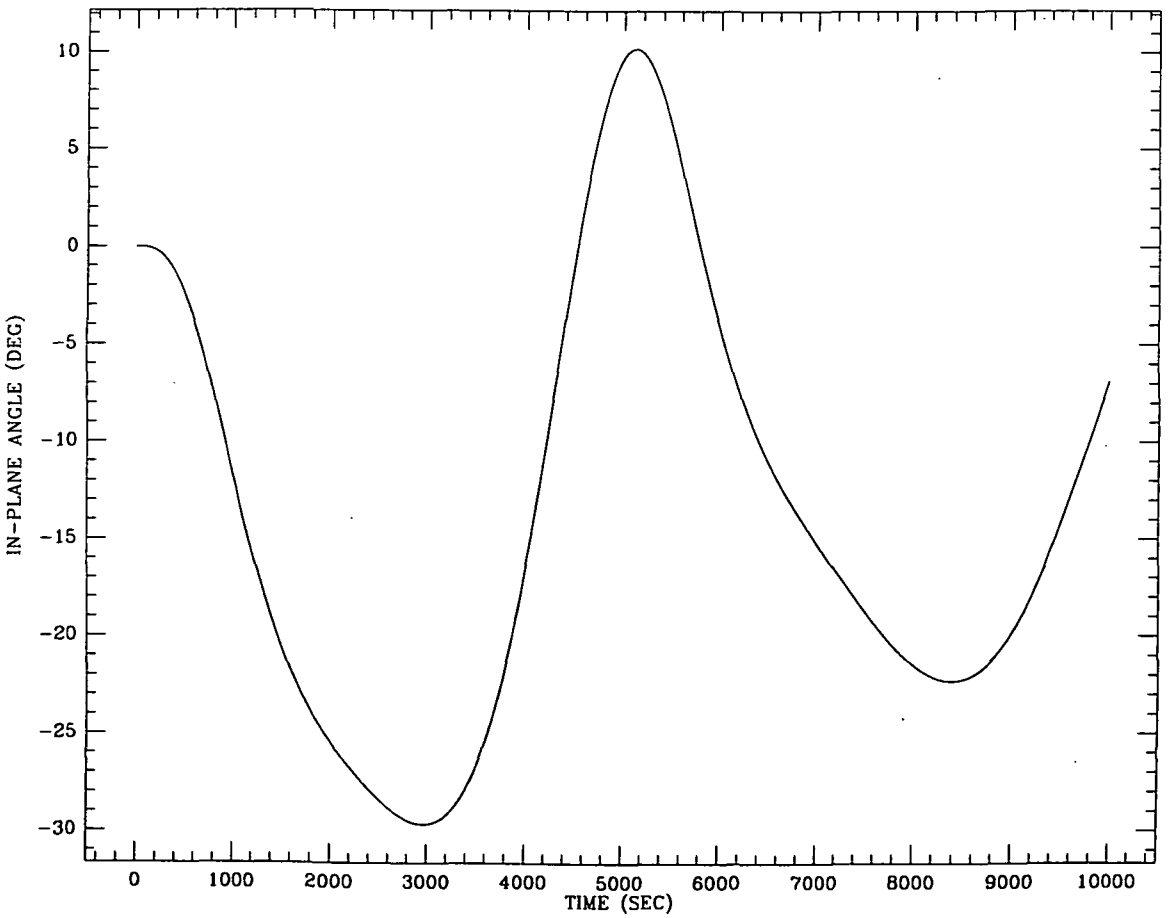

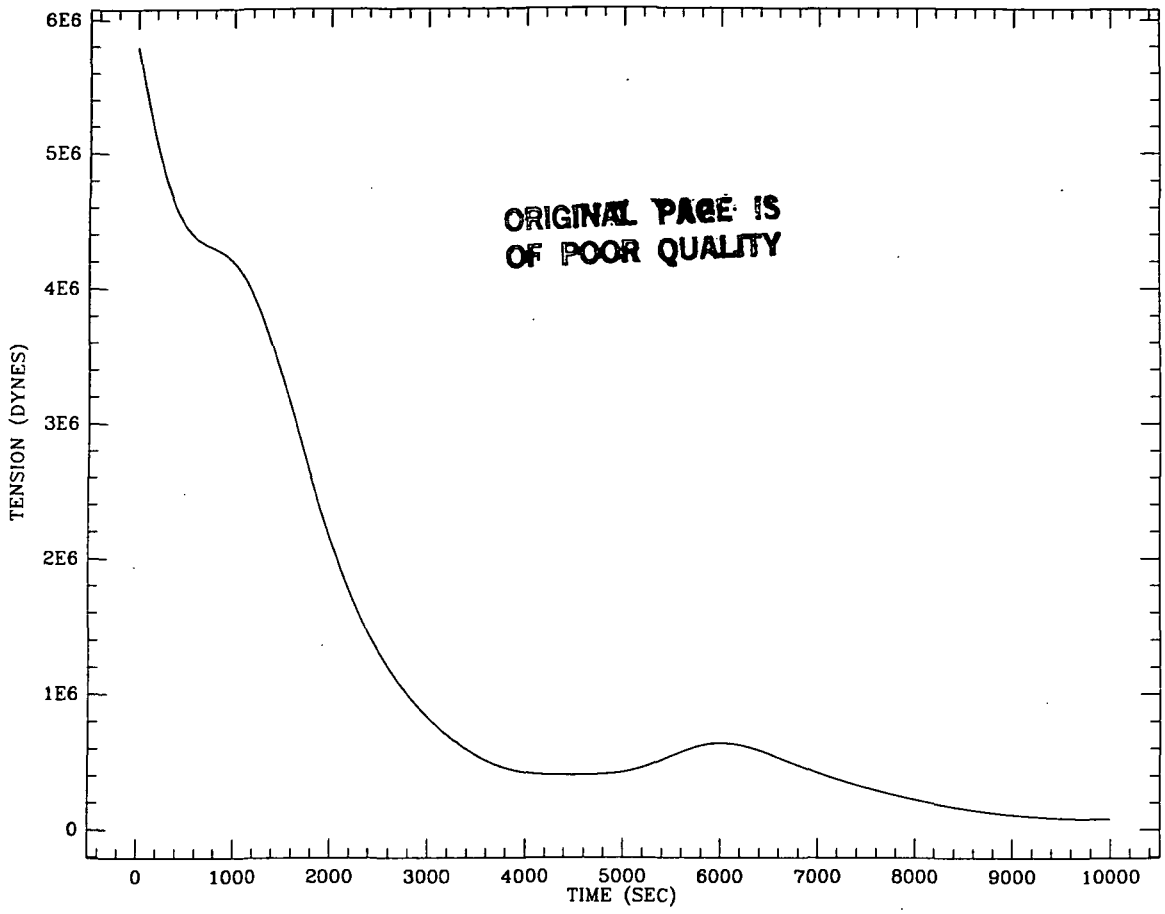

Figure 15c↑

Figure 15d↓

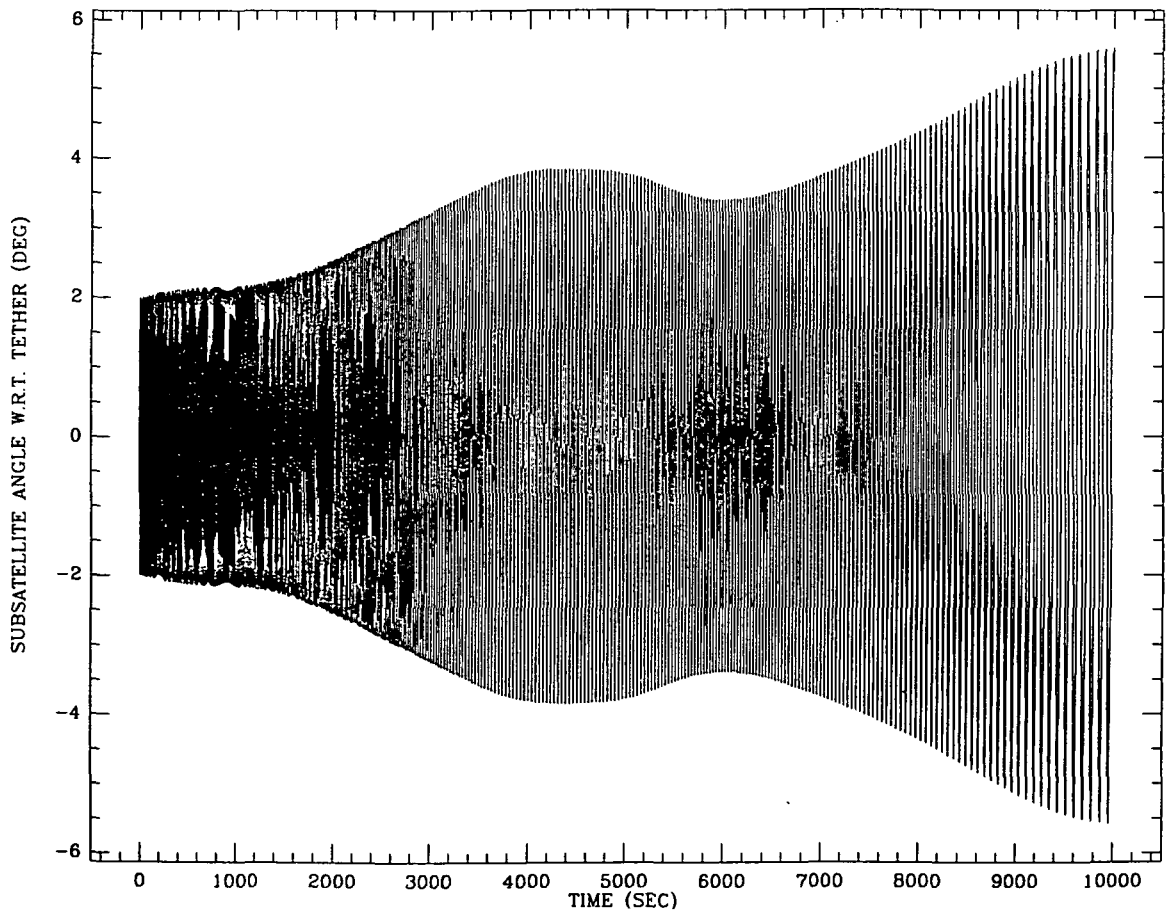

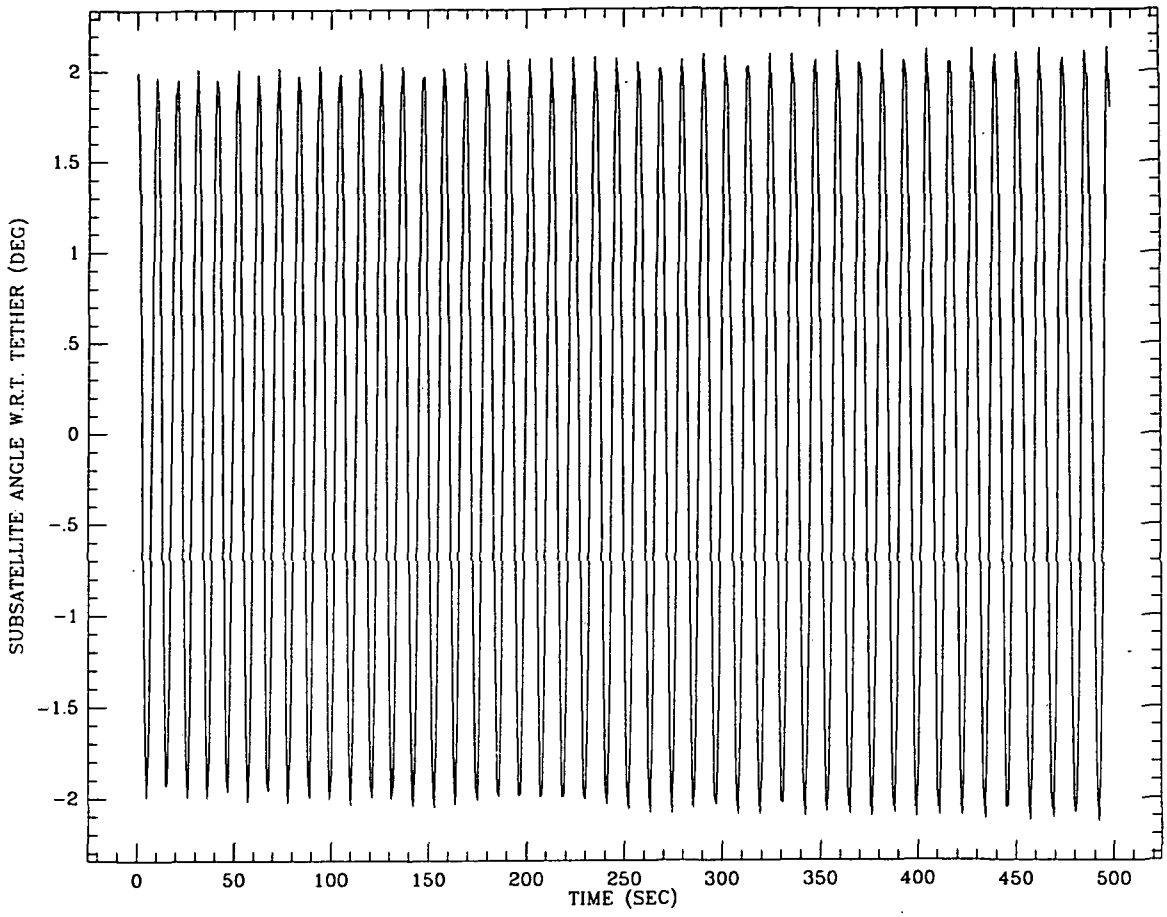

Figure 15e↑

Figure 15f↓

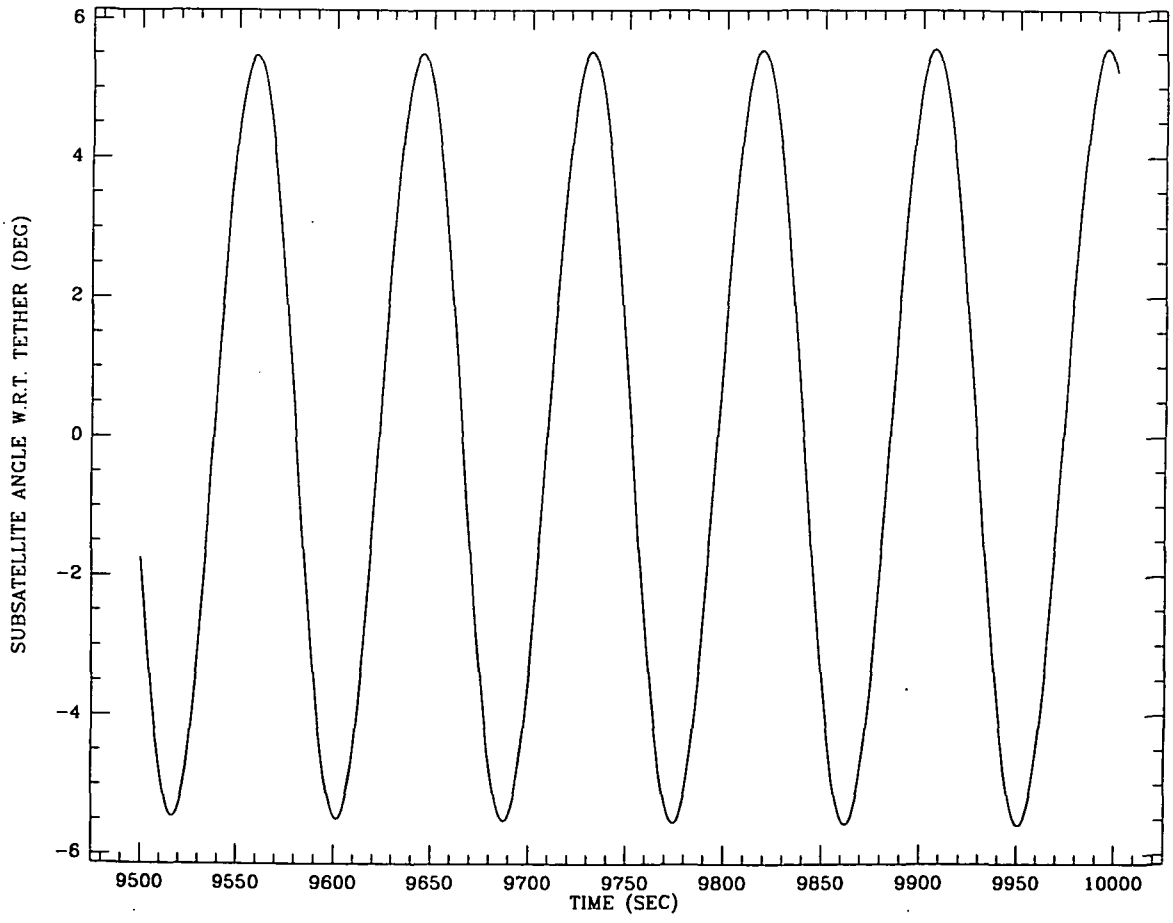

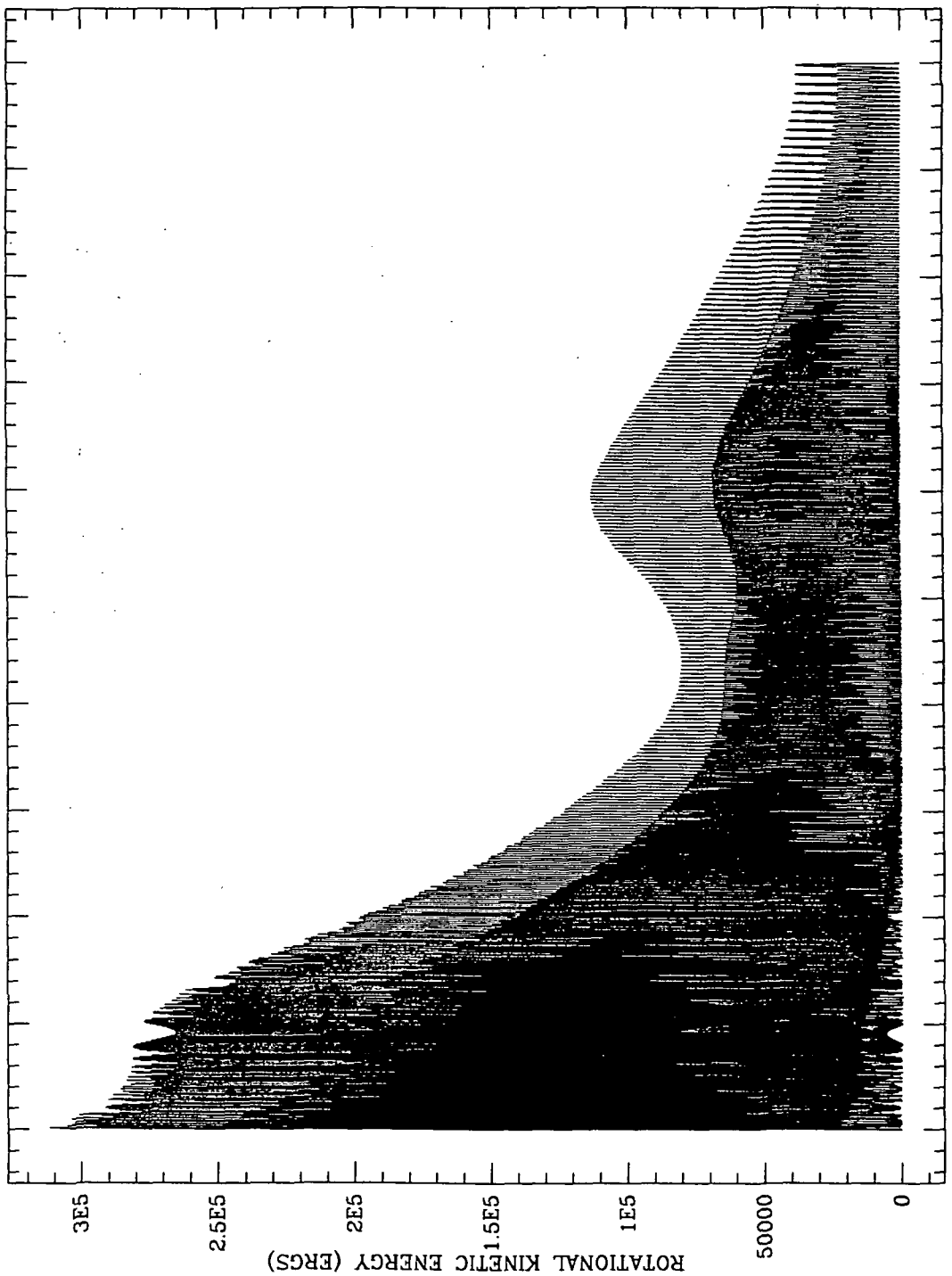

Figure 15g

Table 12

t (sec)	θ (deg)	Tension (dynes x 10^6)	$\theta_o(T_o/T)^{1/4}$ (deg)	%Error	ℓ (km)
0	2.0000	5.79590			
5.14	2.0011	5.776	2.0017	-.03	19.999
104.62	2.0319	5.395	2.0362	-.21	19.872
201.97	2.0669	5.074	2.0676	-.04	19.572
404.96	2.1175	4.599	2.1191	-.07	18.641
1003.84	2.1646	4.191	2.1689	-.20	15.971
2006.70	2.5593	2.126	2.5699	-.41	10.950
3004.40	3.2368	.822	3.2591	-.69	5.880
4010.40	3.8100	.4190	3.8571	-1.24	3.319
5017.58	3.7785	.4247	3.8441	-1.73	2.357
6011.75	3.3976	.6358	3.4752	-2.28	2.257
7001.66	3.7532	.4187	3.8578	-2.79	1.845
8003.43	4.3739	.2213	4.5244	-3.44	2.268
9000.72	5.1518	.1111	5.3750	-4.33	.697
9995.02	5.5797	.0769	5.8929	-5.61	.447

2.2 Slack Tether Studies

During the reporting period SAO has studied the situation in which the deployer reel jams during the retrieval maneuver, leading to loss of tension with the tether and satellite moving toward the Shuttle. Specifically, SAO has:

- Studied, in considerable detail, the dynamics of the tether following reel jam up to loss of tension; the tether velocity on loss of tension is derived.
- Implemented the results of this study as initial conditions for the fully slack tether simulator SLACK3, and made sample runs.
- Calculated the closest approach of the satellite to the Shuttle on a free-orbit assumption, and hence the maximum amount of tether available to impact on the Shuttle.

More detailed study of specific cases is planned for the next reporting period.

2.2.1 Reel Jam: Dynamics Up To Loss Of Tension -

The dynamics of the system in the reel jam case are trivially different from the model in the simulation program SLACK3 -- the only major difference is that the free end tether segment is replaced by a massive satellite. However, SLACK3 (as detailed in previous reports) of necessity deals only with fully slack tethers. It cannot follow the process from the initial impulse (tether break or reel jam) up to the time tension is lost, since elastic forces are dealt with only indirectly. Thus, we need to determine separately what happens during the initial loss of tension process, so that we may prepare "initial conditions" to start the simulation in SLACK3.

In this section we apply general wave propagation techniques to the problem of the initial dynamics following reel jam, and derive an explicit algorithm for

computing the tether velocity upon loss of tension. Generally (though see Section 2.2.3), the reel jam will generate an impulsive wave (step function profile of strain) which propagates up and down the tether decreasing strain further at each pass and reflecting off the end masses until tension is lost.

In Section 2.2.2 we apply separation of variables to assist in the above examination; unfortunately separation of variables breaks down at the moment of loss of tension, and we must combine the two approaches. In Section 2.2.3 we make an approximate calculation which shows that for the given reel control law and typical system parameters, we will be in the simplest regime, where the tether loses tension on the first pass of the impulse, and hence we need not be too concerned with the fact that we have greatly simplified the end reflections.

2.2.1.1 Pre-Jam Assumptions -

To facilitate obtaining a solution we make the following explicit assumptions:

- Uniform Tether Velocity V
- Uniform Tether Strain ϵ
- At $t = t_J = 0$, the reel/Shuttle turns into an infinite mass at rest, and the satellite becomes an infinite mass moving at velocity V.

The tether velocity V, due to the reel motion under the retrieval control law, we also call the "reel velocity".

These assumptions ignore several potentially important factors:

- V, ϵ variations due to gravity gradient forces on a finite mass tether
- V, ϵ variations due to reel acceleration
- structure of attachment at Shuttle

The V and ϵ variations probably do not strongly effect the overall result we shall obtain. For short tethers, one or even twenty kilometers, the satellite mass dominates the tether mass, and the gravity gradient induced variations will

be small. The time scale of the retrieval law is long enough (hours) compared to the tether dynamical time scales that any variations in V or ϵ due to reel motion will rapid equalize along the tether. The attachment at the Shuttle is more problematical; any reflections will clearly not be clean. Our simplification of the attachment is partly due to practicality: the structure is not adequately defined, and its inclusion would greatly complicate the analysis. Also, we show in Section 2.2.3 that the retrieval law is such that we will almost always be in a regime where no reflections of loading waves off the ends will be expected.

2.2.1.2 Problem Parameters And Variables -

Throughout the analysis we shall use the following notation:

V, ϵ	:	initial (uniform) velocity, strain
EA, μ	:	tether properties, typically 10^5 kg m/s^2, 10^{-2} kg/m
E'A($\equiv C_v$)	:	tether damping; use = 0, actually $\sim$ 200 kg m/s
L	:	tether natural length deployed at $t_J = 0$
m	:	subsatellite mass
s	:	tether natural coordinate
Ω	:	orbital angular velocity, typically 10^{-3} s^{-1}

2.2.1.3 Velocity Scales -

We may define several velocities in the problem, all of which will be of importance:

c : speed of sound in the tether; speed of wave propagation

V : initial velocity (reel velocity)

V_{REC} : Recoil velocity of cut tether; a function of ϵ.

We can estimate the range of these velocities, information which will be useful later. The simplest is the sound speed c, which depends only on the tether mass properties:

$$c = \sqrt{EA/\mu}$$

Typically, $c \sim 3 \times 10^3$ m/s.

The recoil velocity is simply $V_{REC} = \epsilon c$. To estimate this we need an estimate of ϵ at the moment of reel jam. From the retrieval law in the next section with $\theta \simeq 10°$, $T \simeq 2.7\ \Omega^2 mL$. Take $\Omega \sim 10^{-3}$ s^{-1}, m ~ 500 kg, and $L \sim 10^3$ m. Then T ~ 1.35 kg m/s^2 (Newtons) and hence $\epsilon = T/EA \sim 10^{-5}$. Then the typical c ~ 3×10^3 m/sec implies $V_{REC} \sim 3 \times 10^{-2}$ m/sec. Similarly if we take $L \sim 2 \times 10^4$ m (20 km) we get T ~ 39 kg m/s^2, $\epsilon \sim 4 \times 10^{-4}$, and $V_{REC} \sim 1.2$ m/sec.

The control law gives a reel velocity depending on the retrieval angle and the current length, $V = (3/4)L\Omega\sin(2\theta)$. With $\theta = 13°$, $V \approx 0.3$ L (km).
In summary:

L = 1 km, $V_{REC} \sim 0.03$ m/sec V ~ 0.3 m/sec

L = 20 km, $V_{REC} \sim 1$ m/sec V ~ 6 m/sec

Note that the reel velocity V is greater than the recoil velocity V_{REC} by about an order of magnitude, and the sound speed c is some three orders of magnitude higher still.

2.2.1.4 Retrieval Law -

The control law assumed for retrieval is

$$\dot{L} = -\alpha L$$

where

$$\alpha \equiv \frac{3}{4} \Omega \sin (2\theta)$$

The equilibrium behavior generated by this law is retrieval at a constant angle θ ahead of the vertical (for an upward deployed tether).

The tether tension is given (essentially) by two factors, (1) gravity gradient force on the satellite, and (2) reel acceleration/deceleration by the control law. We have

$$T_{gg} = (3\ m\ \Omega^2 \cos\theta)\ L$$

and

$$T_{CL} = -m\ \ddot{L} = -m \frac{d}{dt} (\dot{L}) = -m \frac{d}{dt} (-\alpha L) = \alpha\ m\ \dot{L} = -\alpha^2 mL.$$

Note that these have the same variation with L and Ω. The total tension is then

$$T = [3\Omega^2 \cos\theta - \frac{9}{16} \Omega^2 \sin^2 (2\theta)]\ mL = 3\ \Omega^2\ mL\ [\cos\theta - 3\sin^2\theta\cos^2\theta]$$

For a typical value of θ, 13°,

$$T_{gg}/T_{CL} = \frac{3\cos\theta}{9/16\ \sin^2(2\theta)} \approx 25$$

In this case, the gravity gradient induced tension strongly dominates. However, if we take θ = 45°, then T_{gg}/T_{CL} is only 3.77.

2.2.1.5 Gedanken Experiment $V = V_{rec}$ -

Energy considerations can specify the magnitude of the tether velocity change (by conversion of elastic into kinetic energy) but do not tell us the direction of the increment. This simple energy balance also does not apply after the loading wave reflects from the ends since energy will then be transferred to the Shuttle or satellite. To resolve these ambiguities and to pave the way for further analysis, we perform a simple thought experiment:

First, transform the reference frame so that tether is at rest.

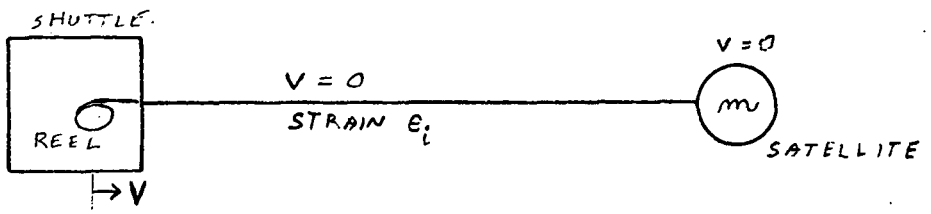

We refer to this frame of reference as the "Tether Frame", and the frame in which the Shuttle is at rest as the "Shuttle Frame." Now, cut the tether at the moment the reel jams.

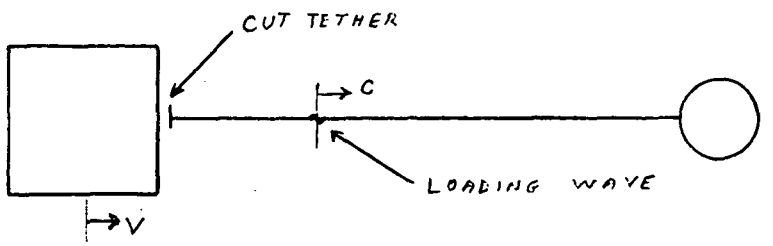

The free tether is now the familiar cut-end case. A wave of loading will propagate down the tether at velocity $\lambda = c$, and the tether in its wake will be moving to the right at velocity

$$V_{REC} = \epsilon\, c'$$

If the Shuttle is moving at precisely this speed, $V = V_{REC}$, it makes no difference if we have cut the tether or not; i.e., we have found the solution for

reel-jam in the case $V = V_{REC}$.

In this case, $V = V_{REC}$, the tether will relax to $\epsilon = 0$ and be hanging dead in space -- except that the satellite m is still coming in at V and will collect tether as it comes.

This special case, $V = V_{REC}$, divides reel jam cases into two regimes, $V > V_{REC}$ and $V < V_{REC}$. The two cases each have unique features and will be treated separately.

2.2.1.6 Fast Retrieval, $V > V_{rec}$ -

The only difference from the $V = V_{REC}$ case is that the Shuttle is moving faster than the tether which has gone slack and catches up with a portion of it before the slackening wave reaches the satellite. We are left, at $t = t_J + L/c$ with:

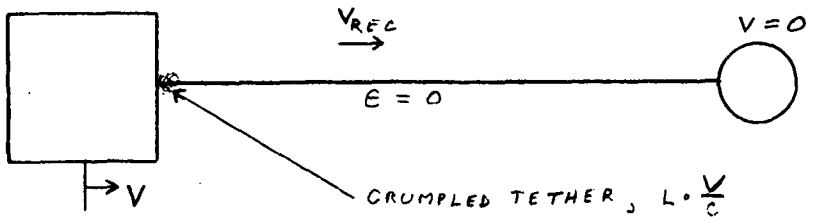

or, transferring to the original reference frame:

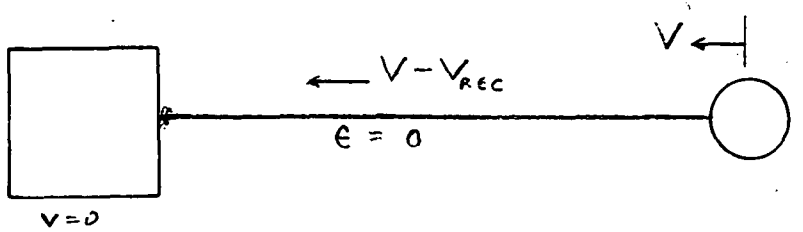

Note that there might be some change in the velocity of the mass m during the time L/c that the wave takes to release tension, but:

- This time is short.
- We are supposing that the tether tension basically balances the gravity gradient force.
- If we worry about this then we should also take into account Coriolis and drag.

2.2.1.7 Slow Retrieval, $V < V_{rec}$ -

In this case, our cut tether analogy soon leads to:

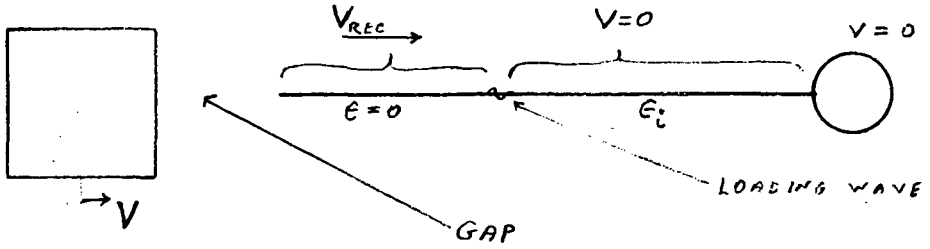

I.e., the tether separates from the Shuttle. Of course, in the actual reel-jam the tether remains fixed to the Shuttle which moves inexorably at V. We will have

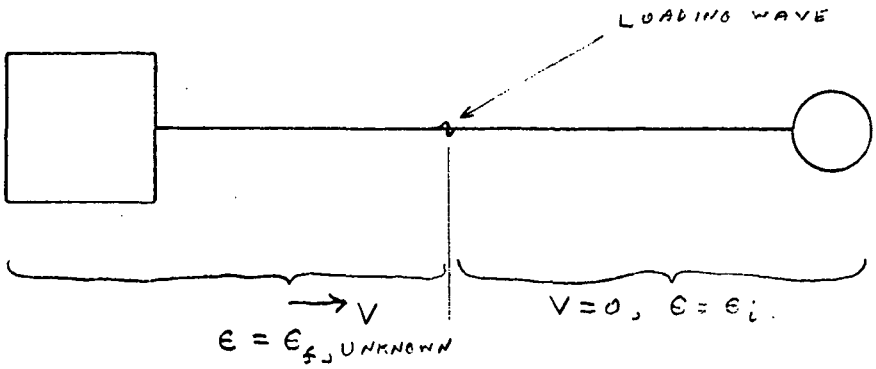

2.2.1.7.1 Jump Conditions -

In Gullahorn and Hohlfeld (1986) we derived jump conditions across the boundary between slack and taut regions. We now need the analogous conditions when the tension is positive in both regions. Following Appendix J of Gullahorn and Hohlfeld:

Mass Conservation: No forces are involved in this derivation, so it is unchanged from slack case:

$$\mu_1 \ (\Lambda - v_1) = \mu_2 \ (\Lambda - v_2)$$

Momentum Conservation: The derivation in Gullahorn and Hohlfeld is unchanged up to:

$$-\mu_o \ \lambda \ (v_2 - v_1) = T_2 - T_1$$

Here the μ's are linear densities, $\mu_o = \mu_1(1+\epsilon_1) = \mu_2(1+\epsilon_2)$ is the "natural" density. Λ is the physical velocity of the boundary; $\lambda = (\Lambda - v_1)/(1+\epsilon_1) = (\Lambda - v_2)/(1+\epsilon_2)$, the velocity in "natural" coordinates. Using

$$v_1 = 0 \qquad v_2 = V$$

$$\epsilon_1 = \epsilon_i \qquad \epsilon_2 = \epsilon_f$$

we get, with Hooke's law ($EA\epsilon = T$),

$$\mu_i \ \Lambda = \mu_f \ (\Lambda - V)$$

$$-\mu_i \ \Lambda \ V = EA \ (\epsilon_f - \epsilon_i)$$

The first of these equations gives:

$$(\mu_i - \mu_f)\Lambda = -\mu_f V$$

leading to

$$\Lambda = + \frac{\mu_f}{\mu_f - \mu_i} V = \frac{1/(1+\epsilon_f)}{1/(1+\epsilon_f) - 1/(1+\epsilon_i)} V$$

$$= \frac{1+\epsilon_i}{\epsilon_i - \epsilon_f} V$$

Then the second equation becomes

$$-\frac{\mu_o}{1+\epsilon_i} \cdot \left[\frac{1+\epsilon_i}{\epsilon_i-\epsilon_f} V\right] V = E A (\epsilon_f-\epsilon_i)$$

$$(\epsilon_f-\epsilon_i)^2 = \frac{\mu_o}{EA} V^2 = \frac{V^2}{c^2}$$

Noting that the tether undergoes compression, $\epsilon_f < \epsilon_i$, and that $V > 0$,

$$\epsilon_i - \epsilon_f = V/c$$

or

$$\boxed{\epsilon_f = \epsilon_i \left[1 - \frac{V}{\epsilon_i c}\right] = \epsilon_i \left[1 - \frac{V}{V_{REC}}\right]}$$

Also note

$$\Lambda = \frac{1+\epsilon_i}{\epsilon_i-\epsilon_f} \cdot c(\epsilon_i-\epsilon_f) = (1+\epsilon_i)c \approx c$$

or

$$\lambda = \frac{\Lambda - V_i}{1+\epsilon_i} \equiv c$$

I.e., the boundary propagates as expected, at the speed of sound.

In summary, up to t + L/c we have

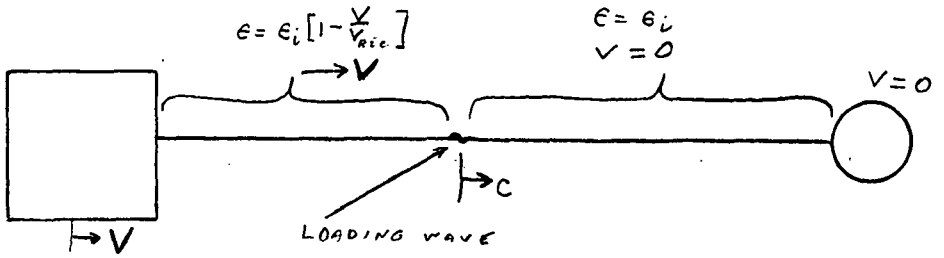

As a check, note that we can obtain the same result for ϵ_f from a kinematic argument. If $X_i = \epsilon_i L$ and $X_f = \epsilon_f L$ are the physical lengths of the tether before and after the loading wave passes (L is the natural length) then at t = L/c, when the wave has just reached the satellite, we know the distance between the Shuttle and satellite has closed by Vt, giving:

$$X_f = X_i - V\frac{L}{c}$$

$$\Rightarrow \quad \epsilon_f L = \epsilon_i L - \frac{L}{c} V$$

$$\Rightarrow \quad \epsilon_f = \epsilon_i - \frac{V}{c} = \epsilon_i \left[1 - \frac{V}{V_{REC}}\right]$$

as above.

Note that

- The tether is still taut.
- Therefore, the stress wave can reflect from the subsatellite.
- The Shuttle and satellite are still closing at velocity v = V.

These imply:

A. We need to look at reflection of stress waves. Note that (assuming clean reflections and no damping) the stress profile will always be a step function with one step.

B. The Shuttle and satellite will eventually close to a distance allowing complete slackness at $t_s = (\epsilon\ L)/V$. The time to propagate a wave along the tether, i.e., the time per bounce, is $\delta t = L/c$. Thence, the number of bounces before the tether goes slack is about

$$N_s = \frac{t}{\delta t} = \frac{\epsilon L/v}{L/c} = \frac{\epsilon c}{V} = \frac{V_{REC}}{V}.$$

Of course, pending analysis:

- there may be slack regions before t_s
- even after t_s there is no guarantee that one will achieve uniform slackness.

2.2.1.7.2 Impulse Reflection And Evolution Past T = L/C -

Attempts to apply general reflection considerations lead to some confusing subtleties.

Instead, we have solved explicitly a sample problem using separation of variables, and evaluated the (series) solution with a simple computer program. The derivation is below in Section 2.2.2. One can scale the problem so that the only free parameter is V/V_{REC} (or simply V, since V_{REC} is scaled to 1).

Sample results for $V/V_{REC} = -0.3$ are on the next page. In general, we may induce

1. The wave front propagates at c, reflecting instantaneously and continuing at c.
2. The wave is always compressive by the amount $\delta\epsilon = V/C$ $(= \epsilon_i)$. I.e., nothing unexpected happens at the reflections.
3. The velocity is
   $v = 0$ to the left of wavefront
   V to the right of wavefront
   Alternately, when the wavefront passes a mass element there is an increment in its velocity of magnitude
   $$\delta v = |V|$$
   The increment is in the direction the wavefront travels.

Everything is clear-cut up to loss-of-tension. Now we must consider the final pass of the wave through the tether, during which tension is lost.

First, consider a case where the wave is about to reflect from the left (fixed) end, and would thereafter have negative tension:

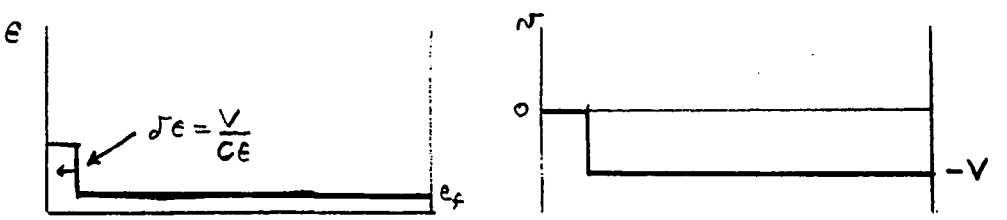

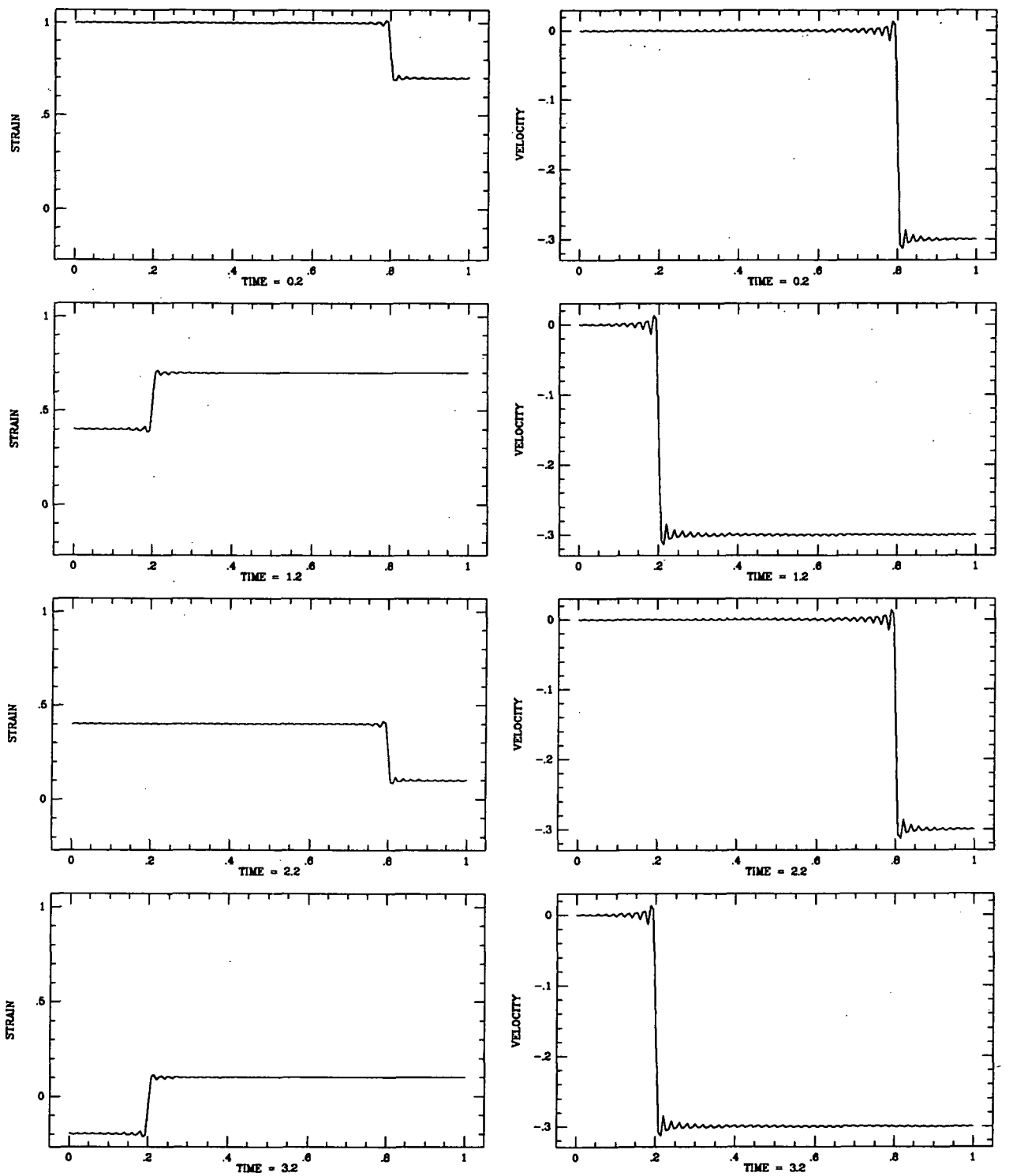

Figure 16. Snapshots of the strain and velocity profiles following a reel jam. These are derived from the separation of variables solution in Section 2.2.2.

After reflection we will have a situation similar to the $V < V_{REC}$ treated above:

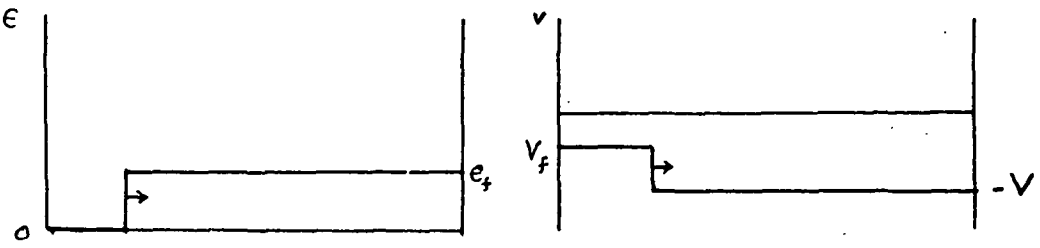

The velocity jump, as before, will be "V_{REC}," but in this case the V_{REC} appropriate to the remnant strain,

$$v_f = -V + \text{"}V_{REC}\text{"} = -V + \epsilon_f c$$

Noting that $\epsilon_f < \delta\epsilon$ by definition, and that $\delta\epsilon = \frac{V}{c}$ (= initial V_{REC}), we confirm that

$$v_f < -V + \frac{V}{c}\, c = 0.$$

All we can (generally) say is

$$-V < v_f < 0$$

The above conclusions are for the situation with the moving boundary at the right:

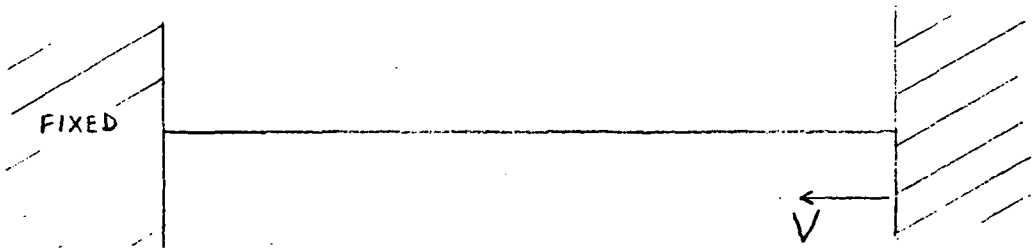

Our reel-jam situation has the moving boundary on the left:

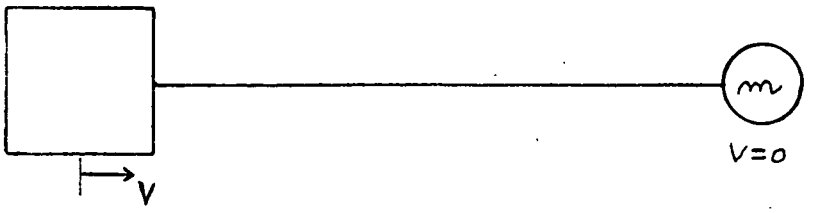

in which case the above results translate to

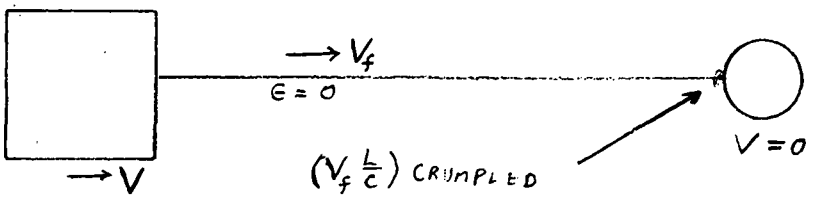

where now $v_r \equiv V - \epsilon_f c > 0$, the opposite sign from v_r in the separation of variables derivation.

Transforming to the original problem in Shuttle based coordinates:

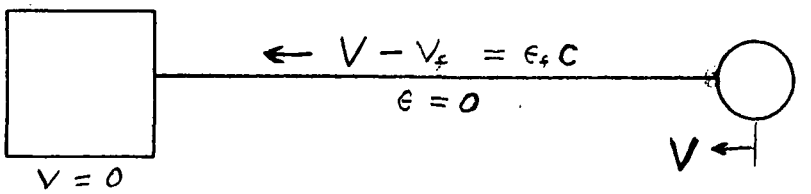

<u>Second</u> consider a case which goes slack after right end reflection:

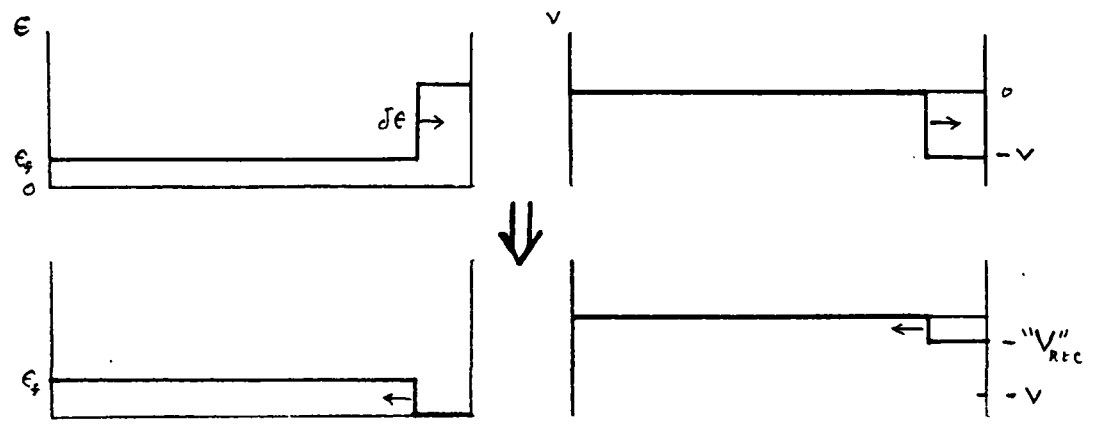

and we get

$$|v_f| = \text{"}V_{REC}\text{"} = \epsilon_f c$$

looking like (flipped to the original reel-jam case)

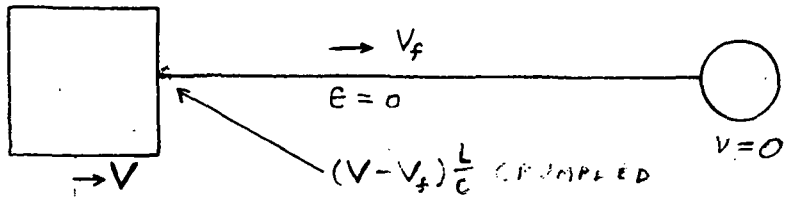

or, transferring to the desired Shuttle coordinates:

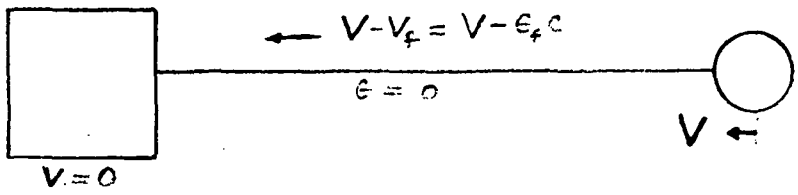

2.2.1.7.3 Enumeration Of Final States For Decreasing Reel Velocities -

As we decrease the initial (reel) velocity from some value larger than V_{REC}, the loss-of-tension problem passes through distinct regimes as the number of reflections of the compressive wave before complete loss of tension increases. We shall examine explicitly the first few of these regimes to seek easily encapsulated regularity. Define a parameter

$$\nu = \frac{V}{\epsilon c} = \frac{V}{V_{REC}}.$$

The initial configuration is:

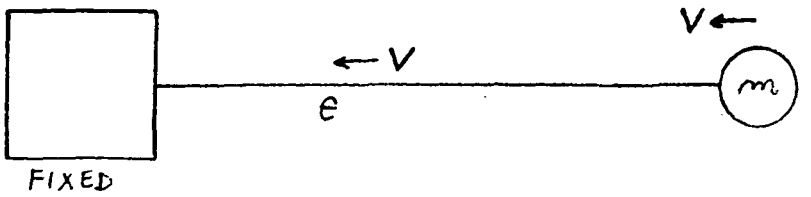

$\boxed{\nu > 1}$ i.e. $V > V_{REC}$. In this case the tether loses tension on the initial pass of the compressive wave. No reflections need be considered.

$$V_f = V - \epsilon c = V - V_{REC} = \left[1 - \frac{1}{\nu}\right]V$$

$$= [\nu - 1]\epsilon c$$

An amount $V \bullet \frac{L}{C}$ of tether will be left crumpled on the Shuttle.

$\boxed{\frac{1}{2} < \nu < 1}$ The loading wave will reflect once, off the satellite.

Here, as in all cases below,

$$\delta\epsilon = \frac{V}{c} = \nu\epsilon$$

For the single reflection case,

$$\epsilon_f = \epsilon - \delta\epsilon = \left[1 - \frac{V}{\epsilon c}\right]\epsilon = [1 - \nu]\epsilon$$

Note that $0 < \epsilon_f < \frac{1}{2}\epsilon$. In particular, $\epsilon_f(\nu=1)=0$, and $\epsilon_f(1/2) = \epsilon/2$. The final velocity is:

$$V_f = V - v_f = \epsilon_f c = [1 - \nu]\epsilon c$$

In this case, a portion of tether will be crumpled onto the satellite.

$\boxed{\frac{1}{3} < \nu < \frac{1}{2}}$ There are two reflections, the final one off the Shuttle.

$$\epsilon_t = \epsilon - 2\delta\epsilon = [1-2\nu]\epsilon$$

$$\epsilon_t\left(\frac{1}{2}\right) = 0, \quad \epsilon_t\left(\frac{1}{3}\right) = \frac{1}{3}\epsilon$$

$$V_t = V - \epsilon_t c = \nu\epsilon c - [1-2\nu]\epsilon c = [3\nu-1]\epsilon c$$

Note that $V_t(\nu = 1/2) = \epsilon c/2$, and $V_t(1/3) = 0$.

$\boxed{\frac{1}{4} < \nu < \frac{1}{3}}$ There are three reflections, the final one off the satellite.

$$\epsilon_t = [1-3\nu]\epsilon \qquad \epsilon_t\left(\frac{1}{3}\right) = 0 \qquad \epsilon_t\left(\frac{1}{4}\right) = \frac{1}{4}\epsilon$$

$$V_t = \epsilon_t c = [1-3\nu]\epsilon c$$

$$V_t\left(\frac{1}{4}\right) = \frac{1}{4}\epsilon c \qquad V_t\left(\frac{1}{3}\right) = 0$$

The trend is clear, and is plotted on the next page.

Summary: The result is cleaner if we use $\frac{1}{\nu}$ instead of ν.

$1/\nu < 1$	$V_t = (\nu\text{-}1)\ \epsilon c$
$1 < 1/\nu < 2$	$V_t = (1\text{-}\nu)\ \epsilon c$
$2 < 1/\nu < 3$	$V_t = (3\nu\text{-}1)\ \epsilon c$
$3 < 1/\nu < 4$	$V_t = (1\text{-}3\nu)\ \epsilon c$

C-2

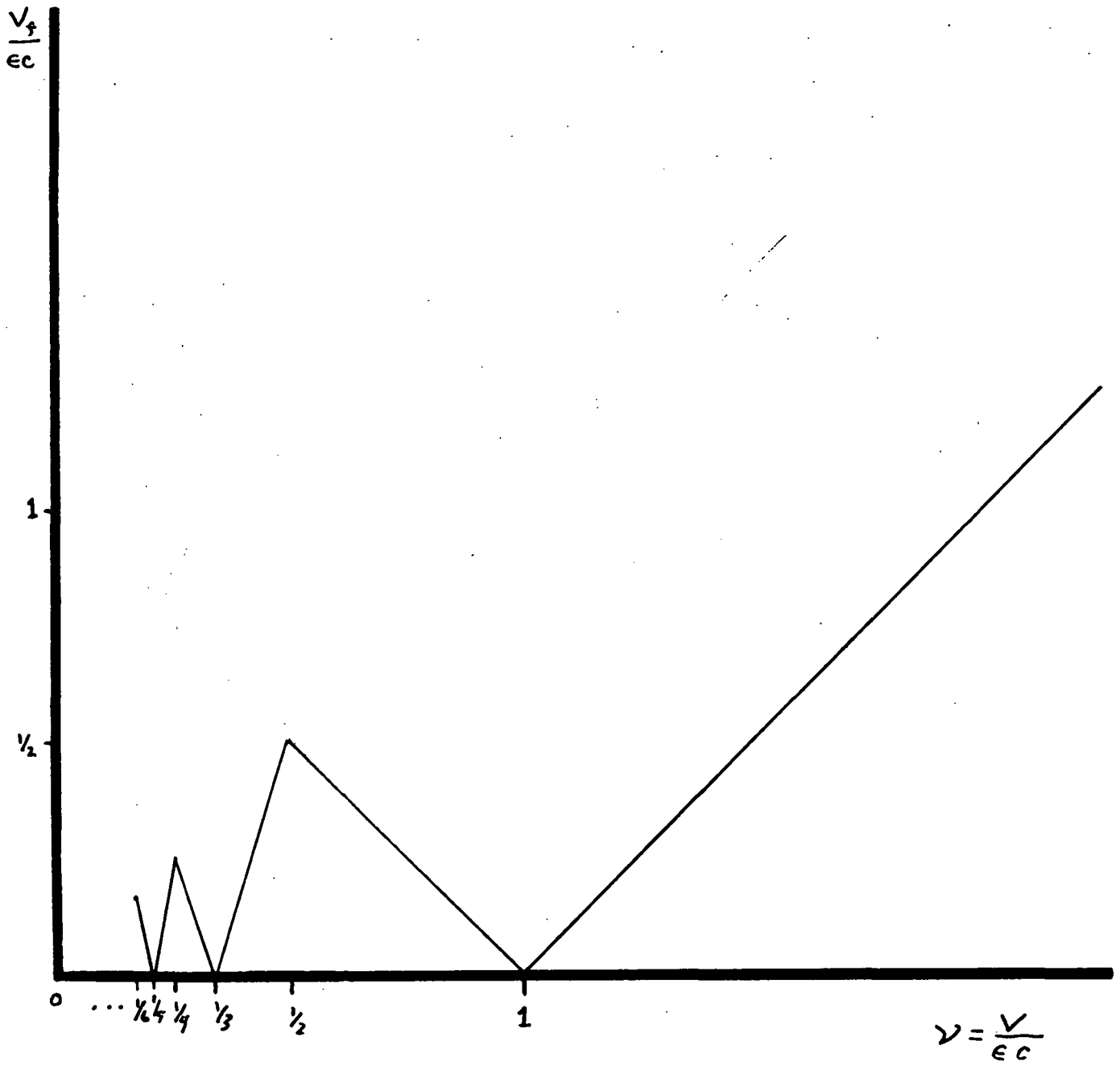

Figure 17. The final tether velocity V_f as a function of the reel velocity at the moment of jam, V. When scaled by the elastic recoil velocity $V_{REC} = \epsilon c$ (the recoil velocity of a cut tether), this simple functional relation results. This result ignores gravity gradient effects (small during the few seconds of recoil); any initial tension variations due, for instance, to variations in reel velocity prior to jam; and assumes an undamped Hooke's law tether.

This generalizes to:

$$2n < \frac{1}{\nu} < 2n+1 \qquad V_t = \left\{(2n+1)\nu - 1\right\} \epsilon c$$

$$2n+1 < \frac{1}{\nu} < 2n+2 \qquad V_t = \left\{1-(2n+1)\nu\right\} \epsilon c$$

$$V_t\left(\frac{1}{2n}\right) = \frac{\epsilon c}{2n}, \quad V_t\left(\frac{1}{2n+1}\right) = 0, \quad V_t\left(\frac{1}{2n+2}\right) = \frac{\epsilon c}{2n+2}$$

2.2.1.8 An Algorithm For The Initial Velocity -

From the above discussion we can now write down an explicit algorithm for computing the final tether velocity upon loss of tension after the loading wave has finished propagating up and down the tether reflecting at either end. As input data we need only the initial reel velocity, the initial strain, and the tether properties.

1. Compute $\nu = V/\epsilon c$, where:
   V = initial velocity, at reel-jam
   ϵ = initial strain, $\epsilon = T/EA$
   c = speed of sound, $c^2 = EA/\mu$

2. Compute $n = \left[\frac{1}{2\nu}\right]$ where $[\bullet]$ is the greatest integer function.

3. IF $2n < \frac{1}{\nu} < 2n+1$ THEN

   $$V_t = \left\{(2n+1)\nu - 1\right\} \epsilon c$$

   ELSE

   $$V_t = \left\{1-(2n+1)\nu\right\} \epsilon c$$

2.2.2 Separation Of Variables Applied To Reel Jam -

We apply standard separation of variable techniques to provide an explicit series solution of the reel jam problem. This solution applies only up to the first loss of tension since it relies on the wave equation being satisfied in the body of the tether; as soon as tension is lost, the wave equation does not apply uniformly. It appears that the series could be evaluated in closed form, but to reduce both effort and possibility of error we have chosen simply to evaluate it directly.

We consider the problem in the coordinate system comoving with the tether and satellite at the moment of the jam (t=0). The physical coordinate is x, and the natural coordinate along the tether is s. The satellite is fixed at x = s = 0. (Note that we are reversing the ends from the convention used in Section 2.2.1.) The Shuttle, with s = L, is initially at x = $(1+\epsilon_i)L$, where L is the tether deployed natural length at the moment of reel jam and ϵ_i is the initial strain. We ultimately seek the strain and velocity profiles $\epsilon(s,t)$ and $v(s,t)$, but we shall work with the displacement $u(s,t) \equiv x(s,t) - s$. Then the tether wave equation (EQ), initial conditions (IC) and boundary conditions (BC) are:

EQ	$u_{tt} - c^2 u_{ss} = 0$	$0 < s < L,\ t > 0$
IC	$u(s,0) = \epsilon_i s$	$0 < s < L$
	$u_t(s,0) = 0$	
BC	$u(0,t) = 0$	$t > 0$
	$u(L,t) = \epsilon_i L - Vt = q(t)$, say	

The first step in solving these equations is to make the BC homogeneous, i.e. with zero right hand side. Introduce

$$\psi(s,t) \equiv (s/L)\ q(t)$$

and then transform to a new dependent variable $\hat{u}$,

$$\hat{u}(s,t) \equiv u(s,t) - \psi(s,t)$$

The system then becomes:

EQ	$\hat{u}_{tt} - c^2 \hat{u}_{ss} = 0$	$0 < s < L,\ t > 0$
IC	$\hat{u}(s,0) = 0$	$0 < s < L$
	$\hat{u}_t(s,0) = (V/L)\ s$	
BC	$\hat{u}(0,t) = 0$	$t > 0$
	$\hat{u}(L,t) = 0$	

Note that in general EQ would now be inhomogeneous, with right hand side $-(s/L)q''(t)$, which would lead to further complications. We have this simple system because the 'forcing' motion of the end point (Shuttle) is at constant velocity.

The above is now a simple textbook exercise, and separation of variables gives a solution of the form:

$$\hat{u}(s,t) = \sum_{n=1}^{\infty} \left[A_n \sin\left(\frac{n\pi ct}{L} \right) + B_n \cos\left(\frac{n\pi ct}{L} \right) \right] \sin\left(\frac{n\pi s}{L} \right)$$

This formula incorporates the BC. We must use the IC to determine the coefficients A_n and B_n, completing the solution.

The first IC gives $0 \equiv \hat{u}(s,0) = \sum_{n=1}^{\infty} B_n \sin(n\pi s/L)$. This can only be true for all $s \in [0,L]$ if $B_n = 0$ for each n.

The second IC gives $(V/L)s = \hat{u}_t(s,0) = \sum_{n=1}^{\infty} A_n\ (n\pi c/L)\ \sin(n\pi s/L)$, $0 < s < L$. The standard trick of multiplying by $\sin(m\pi s/L)$ and integrating from 0 to L gives, after some algebra, $A_m = 2\ (VL/c)\ (-1)^{m+1} / (m\pi)^2$.

The solution is then:

$$\hat{u}(s,t) = \left[\frac{2VL}{c} \right] \sum_{n=1}^{\infty} \frac{(-1)^{n+1}}{(n\pi)^2} \sin\left(\frac{n\pi ct}{L} \right) \sin\left(\frac{n\pi s}{L} \right)$$

and the physical displacement

$$u(s,t) = \hat{u}(s,t) + \psi(s,t)$$
$$= \hat{u}(s,t) + \{ \epsilon_i s - (V/L)st \}.$$

We ultimately want the strain, $\epsilon = \partial u/\partial s$, and the physical velocity $v(s,t) = \partial x/\partial t = \partial(s+u)/\partial t = \partial u/\partial t$. These are

$$\epsilon(s,t) = \epsilon_i - \frac{V}{L}t + \left[\frac{2V}{c} \right] \sum_{n=1}^{\infty} \frac{(-1)^{n+1}}{n\pi} \sin\left(\frac{n\pi ct}{L} \right) \cos\left(\frac{n\pi s}{L} \right)$$

and

$$v(s,t) = 2VL \sum_{n=1}^{\infty} \frac{(-1)^{n+1}}{n\pi} \cos\left(\frac{n\pi ct}{L} \right) \sin\left(\frac{n\pi s}{L} \right) - V\frac{s}{L}$$

We have written a simple program to evaluate the above expressions for $\epsilon(s,t)$ and $v(s,t)$. One inputs the problem parameters V, L, c, and some run parameters such as the number of terms to sum in the series. The output is examined (although it could be plotted) and with 100 terms the result is quite clear: a step function in ϵ and v propagating at c, reflecting at the boundaries. Sample results are shown above in Figure 16 and discussed in Section 2.2.1.7.

The problem can always be scaled to leave just one parameter.

First scale s so that L=1.

Then scale t so that c=1.

Then scale u so that ϵ_i=1.

Noting that the second and third scalings imply $V_{REC} = 1$, we are left with only one essential parameter that we can choose, the boundary (reel) velocity V/V_{REC} ($\equiv$ V under the above scaling).

2.2.3 Implications Of The Control Law For Reel Jam Initial Conditions -

It was seen in the above that, at least under reasonable simplifying conditions, the motion of the tether upon final loss of tension is dependent upon only one parameter, $\nu \equiv V/\epsilon c$, where V is the tether's velocity at the moment of the jam (reel velocity), ϵ is the tether's strain at that moment, and c is the axial speed of sound in the tether, $c^2 = EA/\mu$.

Given the particular form of the retrieval control law in Section 2.2.1.4, we can compute this factor ν as a function of the system parameters (tether properties and satellite mass) and of one variable, the retrieval angle θ. In particular, ν does not depend on the length at reel jam. For typical system parameters, ν is comfortably greater than 1 for retrieval angles greater than about 2°; thus, in practical cases, we avoid the complexities of the poorly known reflection properties from the satellite and deployer.

The reel velocity will be given directly by the control law. We also need the tether strain ϵ. In computing this we ignore the reel acceleration and the tether mass. We may do the first because we have seen above that the gravity gradient tension dominates, strongly at moderate and small angles. It will turn out that it is at a quite small angle that the transition to the high velocity, $\nu > 1$, regime takes place. The tether mass will be dominated by the satellite mass for the short tethers (say 1 km) of interest.

The gravity gradient force is then simply

$$T_{gg} = (3\ m\ \Omega^2 \cos\theta)\ L$$

leading to initial strain

$$\epsilon = T_{gg}/EA = \left(\frac{3\ m\ \Omega^2 \cos\theta}{EA} \right) L.$$

The velocity is given directly by the control law:

$$V \equiv |\dot{L}| = \alpha L$$

where

$$\alpha \equiv (3/4)\,\Omega \sin(2\theta)$$

Here, L is the length at reel jam, Ω is the orbital angular velocity, and θ is the retrieval angle.

Combining the above expressions:

$$\nu = \frac{V}{\epsilon c} = \frac{\frac{3}{4}\,\Omega \sin(2\theta)}{\sqrt{\frac{EA}{\mu}}\;\frac{3\ m\ \Omega^2 \cos\theta}{EA}}$$

or

$$\boxed{\nu = \left\{ \frac{\sqrt{\mu EA}}{2\ m\ \Omega} \right\} \sin(\theta)}$$

Note that this does not depend on L. **That is, as long as we are in steady state retrieval (that is the actual tether angle is equal to the control law angle), the basic form of the loading after the reel jam does not depend on how close the satellite is at jam.** The actual velocity at loss of tension will vary with L, but this will be a simple scaling; since the distance to be covered by the recoiling tether is similarly scaled, **the time scale for impact on the Shuttle is also independent of the length at jam.**

We can evaluate the above expression for ν with typical parameter values $\Omega \approx 10^{-3}\ s^{-1}$, $m \approx 500$ kg, $\mu \approx 10^{-2}$ kg/m, $AE \approx 10^{5}$ kg m s^{-2}. This gives

$$\nu \approx 30 \sin(\theta).$$

Thus, for sin θ > 0.03, or θ > about 2°, ν > 1 and we are in the "slack on first pass" region. That is, the tether will go slack during the initial propagation of the wave of compression without waiting for reflections from the satellite and/or Shuttle and the complications they introduce. Thus, in practical cases, the end result does not depend on the simplifying reflection assumptions

made in Section 2.2.1.7.2, and the analysis is more secure than if it did.

2.2.4 Satellite Orbit After Reel Jam -

At the moment of reel-jam, or more precisely at the moment the tether loses tension, the satellite becomes a freely orbiting object. In examining the early behavior of the system, that is up until the tether is brought into full tension again, this free orbit will provide a good approximation to the actual satellite motion. While the tether is slack at the satellite end, it will obviously not effect the satellite motion, and even if a portion of the tether is affecting the satellite the influence will not be great since the tether mass is so small; it will only be when the tether acts simply as a taut link with the relatively immovable Shuttle that the approximation breaks down.

In particular, we may compute the closest approach of the satellite to the Shuttle in its free orbit. This will give us an estimate of the amount of tether (tether length - closest distance) available to entangle the Shuttle and deployment mechanisms.

We define our standard corotating coordinate system centered on the Shuttle with the x axis radially outward and the y axis along-orbit. The retrieval law from Section 2.2.1.3 will then specify the initial values of the satellite position and velocity in terms of the length at reel jam and the retrieval angle:

$$x = L\cos\theta$$

$$y = L\sin\theta$$

$$\dot{x} = -(3/4)\Omega\sin(2\theta)L\cos\theta$$

$$\dot{y} = -(3/4)\Omega\sin(2\theta)L\sin\theta$$

The equations of free body motion are

$$\ddot{x} = 3\Omega^2 x + 2\,\Omega\,\dot{y}$$

$$\ddot{y} = -2\,\Omega\,\dot{x} - \tilde{D}$$

where the drag is represented by

$$\tilde{D} \equiv C_D \frac{A}{m} \rho_a\, v_a^2.$$

Here, C_D is the coefficient of drag, typically taken as 2; A and m are the satellite area and mass; ρ_a is the ambient atmospheric density; and v_a is the velocity through the atmosphere.

Scale distance by the tether length L, $\xi \equiv x/L$ and $\eta \equiv y/L$, and time by the orbital angular velocity, $\tau \equiv \Omega\, t$, and denote the τ-derivative by $()'$. Then we obtain the following **scaled equations:**

Initial conditions:

$$\xi = \cos\theta$$

$$\eta = \sin\theta$$

$$\xi' = -(3/4)\sin(2\theta)\cos\theta$$

$$\eta' = -(3/4)\sin(2\theta)\sin\theta$$

Equations of motion:

$$\xi'' = 3\,\xi + 2\,\eta'$$

$$\eta'' = -2\,\xi' - (D/L)$$

where $D \equiv \tilde{D} / \Omega^2$.

We see that there are only two fundamental parameters left:

θ -- The retrieval angle.

D/L -- Drag / Length at reel jam.

Note that θ only appears in the initial conditions, and D/L only appears in the equations of motion. Also, if drag is negligible, the length does not enter into the solution and the only available parameter is θ.

We can evaluate a typical drag for 295 km altitude. Using $C_D = 2$, $\rho_a = 3 \times 10^{-14}$ g/cm^3, $\Omega = 1.2 \times 10^{-3}$ sec^{-1}, $v_a = R\Omega = 8 \times 10^5$ cm/sec, m = 500 kg = 5×10^5 g, $A = \pi$ (80 cm)^2 = 2×10^4 cm^2, we get $D \approx 0.01$ km. Thus, even for L quite small, say 100 meters, D/L is small.

We have written a brief program to solve the equations of motion using a simple Runge-Kutta integrator. One inputs the retrieval angle θ and the drag/length parameter D/L. The program then tabulates (on the terminal) the position and velocity, and also the distance to the Shuttle, as a function of time. We have exercised the program and noted the closest approach (in dimensionless radius, $\rho^2 \equiv \xi^2 + \eta^2$) for various θ and D/L.

D/L:	0.01	0.1	0.5
θ			
5°	0.9972	0.9972	0.9971
15°	0.9744	0.9741	0.9726
30°	0.8983	0.8950	0.8766
45°	0.7699	0.7493	0.6089
60°	0.5691	0.4675	0.0580

If we assume D = 0.01, then the D/L value tells us L. We can then scale the above dimensionless minimum approach distances to get actual closest approach and subtract from L to get the amount of tether available to entangle the deployer (given in meters):

L:	1 km	100 m	20 m
θ			
5°	3	0.3	0.1
15°	26	3	0.6
30°	102	11	3
45°	230	25	8
60°	421	53	19

We should point out that not all of the above tabulated tether will actually impact on the Shuttle. These values simply represent the maximum amount that the satellite's orbit will allow in the region of the Shuttle under "optimal" circumstances. The results tabulated above encourage the use of smaller retrieval angles. The time scales to closest approach are also of interest. With

D/L = 0.01 (i.e. for a 1 km tether) these are, at 5°, 33 seconds; at 15°, 120 s; at 30°, 270 s; at 45°, 575 s; at 60°, 1200 s. For larger D/L these numbers increase, but not very substantially.

These results have also helped us in interpreting the results of simulations reported below.

2.2.5 Implementation Of Reel Jam In SLACK3 -

We have added an option to the SLACK3 program for running simulations of reel jam cases (as well as the previous cut tether cases). The only modifications required are in the routine SPECIFY which sets up the initial state, that is the state at the moment the tether completely loses tension (SLACK3, to allow high resolution models, assumes all tether segments are slack, with instantaneous "hard" bounces when a segment goes taut). Recalling that SLACK3 uses a menu system (with defaults) for selecting many parameters, the apparent differences to the user are:

- The reel jam option must be chosen (the default run type is still a tether break case, but this could easily be changed).
- If the reel jam option is chosen, the program attempts to force the user to choose reasonable deployment angles, e.g. in the orbital plane and with the proper sign for retrieval (forward if deployed up, backward if deployed down). Out-of-plane or wrong-sign deployment could be chosen by specifying the angles before specifying the reel jam option.
- If the reel jam option is chosen, the program asks for the length at jam, rather than the cut length.

The choice of other parameters and options remains basically unchanged; thus, one could, for instance, have a reel jam case with Shuttle rotation and acceleration.

The assumptions made and internal mechanics of the modification are:

- We assume that the actual deployment angle is the angle in the retrieval control law of Section 2.2.1.4. That is, the retrieval maneuver has reached the steady state. Thus, reel velocity does not need to be input separately. (This could be changed if desired.)

- The internal tether masses are each given a velocity computed with the algorithm of Section 2.2.1.8.

    •First, the retrieval angle and the tether length give the reel velocity. See Section 2.2.1.4.

    •The angle and length also give the tether tension (which is assumed to be the gravity gradient tension only, ignoring the reel acceleration) using the tension calculation already in the program.

    •Combined with tether properties, we now get the strain ϵ and sound speed c, and hence the dimensionless parameter ν.

    •$v_\ell/\epsilon c$, and hence v_ℓ, are now calculated as in Section 2.2.1.8.

- The final mass point, formerly the free end,

    •has the satellite mass added to it,

    •is given the original reel velocity.

- As previously, we make the tether slightly slack to begin with, with some randomization of segment lengths and directions. This was originally done to avoid sudden uniform tensionings and simultaneous bounce problems, and in the reel jam case obviates having to deal with the (very small) amount of tether already swept up by the Shuttle or satellite while the final slackening wave propagates along the tether.

In addition to these changes specific to the reel jam option we have taken the opportunity to fix a bug in the boom motion routine (it could no longer deal with the case of no Shuttle thruster firings), and to change some of the parameter defaults. The default altitude and ambient atmospheric density are now 295 km and 2.7×10^{-14} g/cm^3 (appropriate to 295 km and 1000°). The default tether properties are now ρ = 0.1 g/cm, AE = 10^{10} dynes, C_v ($\equiv$ AE') = 2×10^7 dyne-sec (see Lorenzini, et al., 1985, Section 2.3.2 for these values).

Two sample runs were made, both with reel jam at one kilometer. They confirm, in general, the satellite orbit considerations of Section 2.2.4.

(Those calculations were actually made in response to the SLACK3 runs.) The retrieval angles were 13° and 45°.

In the 13° case, the progress of the tether toward the Shuttle is only barely visible on the plots, and the satellite turns around and draws the tether taut at about 300 seconds. (As noted in previous reports this generally causes the program to fail.) Note that the time to closest approach at 15° given in Section 2.2.4 is 120 seconds; since the SLACK3 simulation starts out with the tether slack by a few percent, it is not surprising that the time to full tension is somewhat more than the expected value of twice the time to closest approach.

The 45° case is more interesting. In Figure 18 we see a substantial amount of tether impacting on the Shuttle in the first 200 seconds or so, followed by avoidance as the infalling tether is carried along orbit by Coriolis force. The tether seems to avoid wrap-around of the Shuttle. Although at the initial tether speed of 0.8 m/sec some 160 meters could have impacted on the Shuttle in that time span, visual inspection indicates that a smaller portion of the available 230 meters did so. Note that the total time up to re-tension is 1225 seconds, about twice the 575 seconds to closest approach from Section 2.2.4.

More information could be obtained from the 45° case by rerunning it with more tether segments, and by modifying the plot program to show only the near-Shuttle segments.

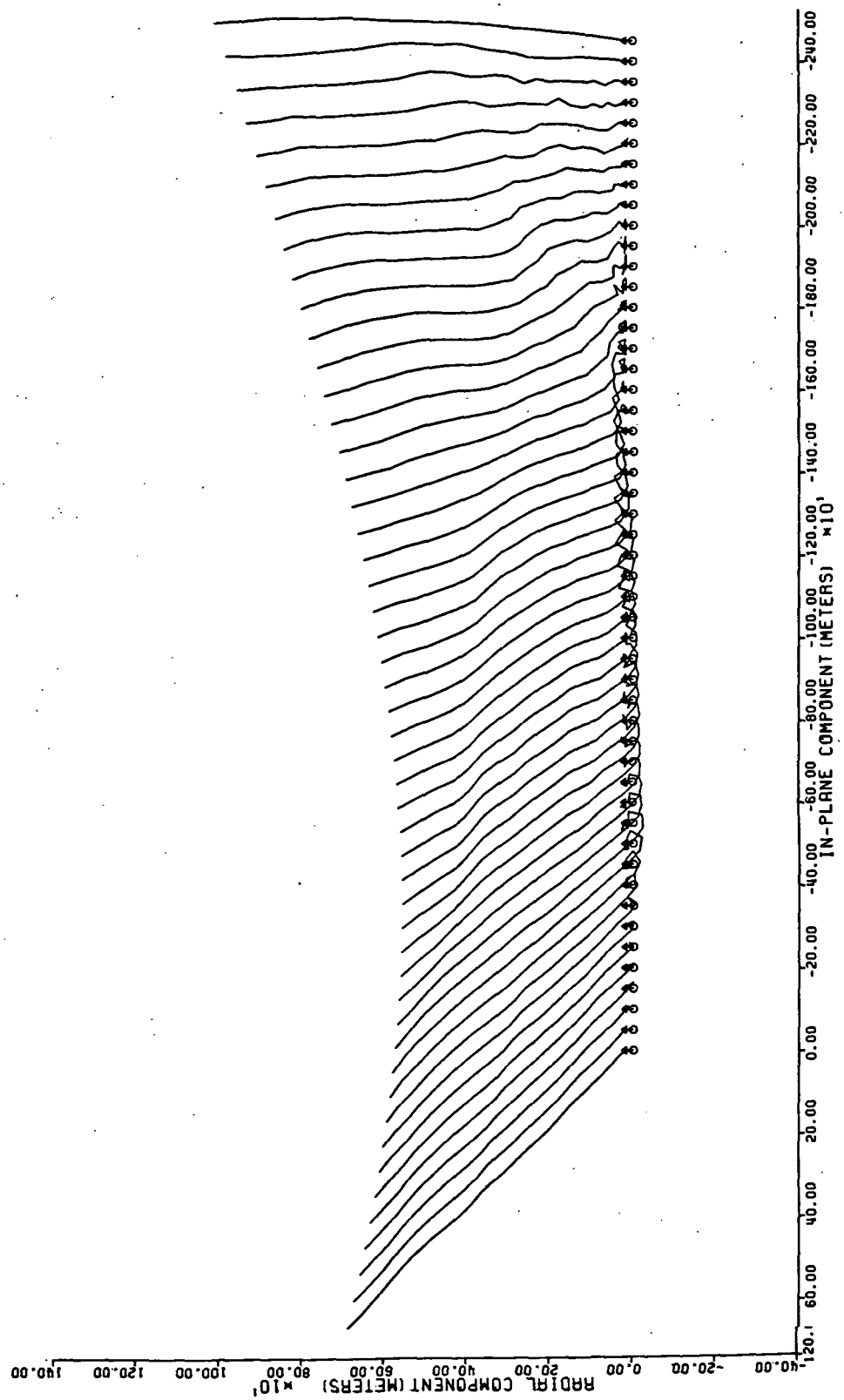

Figure 18. SLACK3 simulation of reel jam. Retrieval angle 45°, 1 kilometer deployed at jam. Model has 25 segments, with output every 25 seconds. Total time span shown 1225 seconds, up until re-tensioning of the tether.

2.2.6 References To Section 2.2 -

Gullahorn, Gordon E., and Hohlfeld, Robert G., 1986. Analytical Investigation and Simulation of Partially Tensioned Tethered Systems, Contract RH5-394202 (Martin Marietta Corporation), Final Report, March.

Lorenzini, Enrico, Arnold, David A., Grossi, Mario D., Gullahorn, Gordon E., Harrold, William and Hohlfeld, Robert G., 1985. The Investigation of Tethered Satellite System Dynamics, Contract NAS8-36160, Quarterly Report 3, June.

3.0 PROBLEMS ENCOUNTERED DURING REPORTING PERIOD

The analysis of the string-like dynamics of the tether following a thruster activation was one of the items planned to be started during the current reporting period. Because of a rearrangement of the priorities, the above mentioned item has been replaced by the comparison simulations between SAO and MMA computer codes during retrieval and by extra analysis of the damping of the satellite rotational oscillations by means of reel control.

4.0 ACTIVITY PLANNED FOR THE NEXT REPORTING PERIOD

In the next reporting period we will investigate the effect of the wire intrinsical damping on the satellite rotational dynamics. A reasonable model of the tether damping as a function of tether length will be implemented into our comptuer code and retrieval simulations will be performed.

The simulation activity of the tether dynamics following a reel jam will also be continued. Simulations of some of the most critical situations, during the retrieval phase, will be run by making use of the SLACK2/3 computer code.